Raman and Infrared Absorption Spectroscopy for Tissue Diagnostics

Diploma Paper
by
Joakim Bood & Hugo Carlsson

Lund Reports on Atomic Physics, LRAP-168
Lund, March 1995

1 Abstract

This report surveys initial Raman and infrared absorption spectroscopic measurements with the purpose to investigate the potential of these methods for tissue characterization.

By using an equipment basically consisting of a Ti:Sapphire laser, a fibre optic probe, a single stage spectrometer, and a CCD detector high quality Raman spectra have been recorded of the solvents: nitrobenzol, 1,2-dichlorbenzol, 1,4-dioxane, and toluene. Spectra have also been recorded of the purified tissue constituents cholesterol and NADH, but also of an aorta tissue specimen. All spectra have been recorded in the region 350-1800 cm^{-1}.

With the commercially available Bomem DA8 FTIR spectrometer infrared absorption spectroscopic measurements in the region 3000-10000 cm^{-1} have been recorded of collagen, elastin, cholesterol, NADH, and also of tissue specimens of fat, muscle, and aorta.

The results suggests that Raman and infrared absorption spectroscopy might be useful for tissue characterization.

Contents

2 Introduction

2.1 Introduction

From Planck´s equation E = hν, where h is the Planck constant and ν is the frequency, it can be seen that the highest energy radiation in the electromagnetic spectrum corresponds to the γ-ray/X-ray region. In this region the energy may be great enough to break up bonds in molecules. At the other end of the spectrum, radiowaves have very low energy, only enough to cause nuclear or electron spin transitions within molecules. The regions of the electromagnetic spectrum and the types of energy transitions and phenomena observed are summarized in Table 2.1. These regions, including the infrared, give vital information about the structure of molecules and hence of different substances.

Table 2.1. *The electromagnetic spectrum.*

Region	Energy[1]	Spectroscopic phenomena	Energy transitions
γ-ray/X-ray	100 - 10^7 eV	Inner electron transitions	Bond breaking
UV/Visible	1 - 100 eV	Outer electron transitions	Electronic
IR	10^{-3} - 1 eV	Molecular vibrations Fine structure	Vibrational
Microwave	10^{-6} - 10^{-3} eV	Molecular rotations	Rotational
Radiowave	10^{-12} - 10^{-6} eV	Hyperfine structure Isotopic shifts	Nuclear and electron spin

[1] $1\text{eV} = 1.60219 \cdot 10^{-19}\,\text{J}$

From a medical point of view, it would be of great interest to establish a non-intrusive method for *in vivo* discrimination between normal and diseased tissue, thus providing an alternative to conventional biopsy. Optical spectroscopy provides much information about the chemical composition of substances and can therefore in different ways be utilized for the purpose of tissue characterization.

2.2 Spectroscopic techniques for tissue characterization

Laser-induced fluorescence. In laser-induced fluorescence (LIF) a laser is tuned to a transition from a lower to a higher electronic state in the molecule, and the fluorescence light that is released upon the subsequent decay is observed. Since different types of tissue exhibit different fluorescence signals, LIF is a proper technique for tissue characterization and diagnostics. In fluorescence diagnostics one normally evaluates either the information from the natural tissue fluorescence (autofluorescence) or the fluorescence spectrum due to any exogenous fluorophore. Autofluorescence has been used for tumour characterization [1,2,3] as well as for caries studies in teeth [4,5] and for localization of atherosclerotic lesions in blood vessels [6,7]. Another powerful application of LIF is photodynamic therapy (PDT). Prior to PDT the induced fluorescence spectrum can be utilized for establishing the spread of tissue disease. Furthermore PDT provides a selective therapy, since the injected photosensitizer is accumulated in the tumour. PDT has been used for therapy of malignant tumours [8,9].

Time-resolved laser-induced fluorescence. Time-resolved fluorescence technique is another valuable tool in biophysical studies [10]. In time-resolved LIF one utilizes the different temporal behavior of the fluorescence decay of different types of tissues. With this approach it is feasible to discriminate diseased tissue from normal by evaluating the difference in the fluorescence decay curves. Since the lifetimes involved are normally short, picosecond spectroscopy is most often required. Time-resolved LIF has been used in the diagnosis of atherosclerotic plaque [11,12] and for tumour demarcation [12].

Transillumination. Another technique for tissue characterization is optical transillumination. This method is based on the characteristic attenuation in tissue when transilluminated by visible laser light. However, multiple scattering of light prohibits detailed visual observation inside turbid media, such as tissue. The multiple scattering causes a decreased contrast in the transmitted light. The effect of light scattering can, however, be reduced by time gating. In this approach the tissue is transilluminated with picosecond laser pulses, and the transmitted light is detected with a high time resolution. The photons that leaves the tissue first have covered the shortest path length in the tissue. Thus, the intensity of this early light will depend on the optical properties of a volume close to a straight line through the tissue, yielding spatially resolved information about the tissue optical property. Time-resolved transillumination has been demonstrated to work for breast cancer detection *in vitro* [13,14,15,]. A related alternative method is to irradiate the tissue with an intensity modulated laser beam and measure the demodulation and the phase shift (phase-resolved transillumination).

Raman spectroscopy. Raman spectroscopy is a technique based on the so-called Raman scattering. The physical origin of Raman scattering lies in inelastic collisions between the molecules composing the sample and photons of an irradiating laser beam. An inelastic collision means that there is an exchange of energy between the photon and the molecule with a consequent change in energy, and hence frequency, of the emitted light. Furthermore, due to the law of energy conservation, the energy gained or lost by the photon during the scattering process must equal an energy change within the molecule. It follows that by measuring the energy gained or lost by the photon, one can probe changes in molecular energy. Raman spectroscopy is concerned essentially with the vibrational

energy levels of the molecule. Thus, by monitoring the Raman scattered light, one can probe molecular vibrations, and the Raman spectrum is a *vibrational spectrum of a molecule*. Since the vibrational spectrum of a molecule is a sensitive indicator of chemical properties, Raman spectroscopy has become a very attractive approach for tissue characterization.

Infrared spectroscopy. Infrared (IR) spectroscopy is a technique in many ways very similar to Raman spectroscopy. Both of the methods probe the vibrational or rotational energy levels of molecules, and hence they belong under *vibrational spectroscopy*. In IR spectroscopy, in contrast to Raman spectroscopy, it is the absorbed or reflected light, instead of the scattered, that is measured. Thus IR spectroscopy is divided into two different approaches: IR absorption spectroscopy and IR reflection spectroscopy, of which the former one is more commonly used. Another difference of IR spectroscopy compared to all of the previously discussed techniques is that a polychromatic light source, instead of a monochromatic one (laser), is used. When using IR spectroscopy for tissue characterization one generally operates in the near-infrared (NIR) to mid-infrared region.

Infrared spectroscopy and, in particular, Raman spectroscopy provides much more detailed information about a tissue sample than laser-induced fluorescence, since sharp spectral lines result rather than broad fluorescence features. Moreover, Raman and IR spectroscopy are, as has been mentioned above, very closely related to each other, but they are however not duplicates. Both of the techniques seems to have some very interesting features that are proper in tissue characterization. Therefore we have chosen to evaluate the potential of these methods for tissue characterization.

2.3 Human tissue

2.3.1 Collagen and elastin

Collagen. The collagens are a family of highly characteristic fibrous proteins found in all multicellular animals. The collagens of tendon, cartilage, and bone are the single most abundant proteins of the body. Individual collagen molecules are linear structures built up from three *polypeptide* chains. The individual chains, the *α-chains*, wind in a shallow so-called *α-helix*. α-helices are secondary structures formed in order to get a hydrophobic core and a hydrophilic surface (hydrophobic=water assimilating, hydrophilic=water resisting). Three of the α-chains twist together into a comparatively rigid triple helix that forms about 95% of the central portion of the collagen molecule. The triple helix is responsible for the fibrous nature of collagen. At the tips of the central triple helix, the amino acid chains fold into globular segments that cap the ends of the molecule. The entire structure is held together by hydrogen bonds between the α-chains in both the triple helix and globular caps. There are also OH-groups added to the aminoacids. These groups are very important as hydrogen-bonding features that stabilize the triple helix. There are at least 14 distinct types of collagen molecules designated types I to XIV. Fig. 2.1 illustrates a collagen molecule in diagrammatic form.

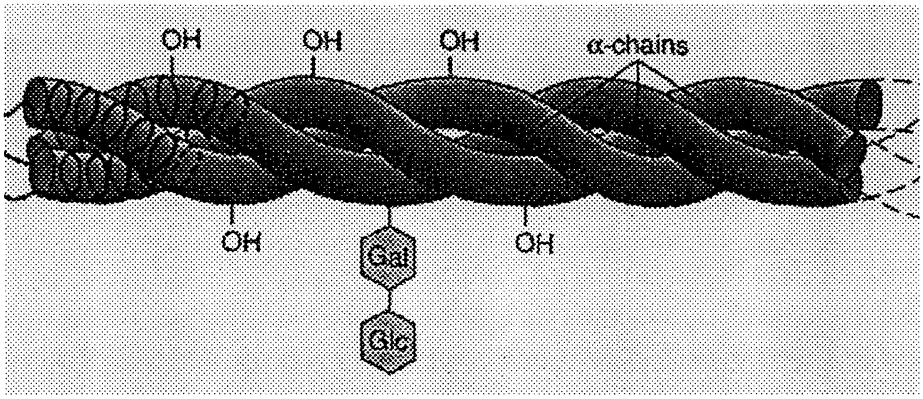

Fig 2.1 *A collagen molecule in diagrammatic form. The carbohydrate portion of collagens consists almost completely of short two-sugar galactose-glucose (Gal-Glu) units attached to the protein component of the molecule. From Ref. [16].*

Elastin. Many tissues, such as skin, blood vessels, and lungs, need to be both strong and elastic in order to function. A network of elastic fibers in these tissues gives them the required resilience so that they can recoil after transient stretch. Long, inelastic collagen fibrils are interwoven with the elastic fibers to limit the extent of stretching and prevent the tissue from tearing. The main component of elastic fibers is elastin, a highly hydrophobic protein, which, like collagen, is exceptionally rich in proline and glycine but, unlike collagen, is not glycosylated. Elastin molecules are secreted into the extracellular space and gather into elastic fibers to the plasma membrane, generally in cell-surface infoldings. The elastin protein is composed largely of two types of short segments that alternate along the polypeptide chain. These segments are: hydrophobic segments that are responsible for the elastic properties of the molecule, and α-helical segments, which form cross-links between adjacent molecules.

2.3.2 Cholesterol

Cholesterol ($C_{27}H_{46}O$) belongs to the category of *lipids*. Lipids, and especially phospholipids, are important structural factors in biological membranes. The lipid bilayers of these membranes are not composed exclusively of phospholipids, they often also contain cholesterol and glycolipids. Eucaryotic plasma membranes contain especially large amounts of cholesterol. Furthermore cholesterol is a *steroid* lipid, which means that the molecule is based on a framework of four interconnected carbon rings. The category of steroids can be divided in several subgroups, among which cholesterol belongs to the *sterols*. Sterols are characterized of a hydroxyl group (-OH) linked to one end and a complex, nonpolar carbon chain at the opposite end of the ring structure. This may be verified in Fig 2.2, in which the structural formula of cholesterol is shown. Cholesterol occurs in biological tissues under pathological conditions, e.g. in advanced *atherosclerotic plaques*.

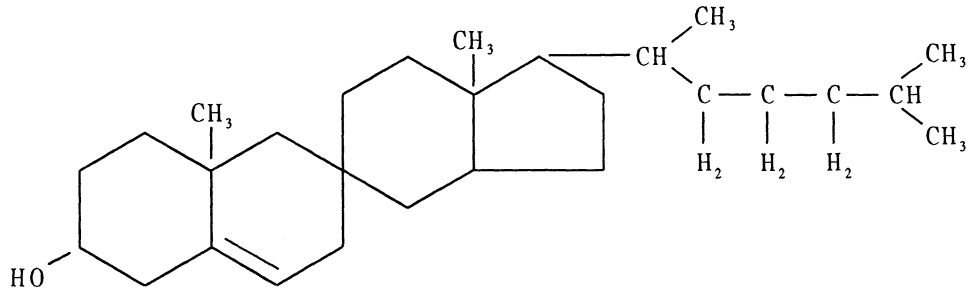

Fig.2.2 *The structure formula of cholesterol. The polar hydroxyl group appears at the extreme left, while the nonpolar hydrocarbon chain comes into view at the right hand side. The steroid ring structure is located between these two groups.*

2.3.3 NADH

NADH is the reduced form of NAD^+ (nicotinamide adenine dinucleotide). The structure formula of NADH is shown in Fig. 2.3.

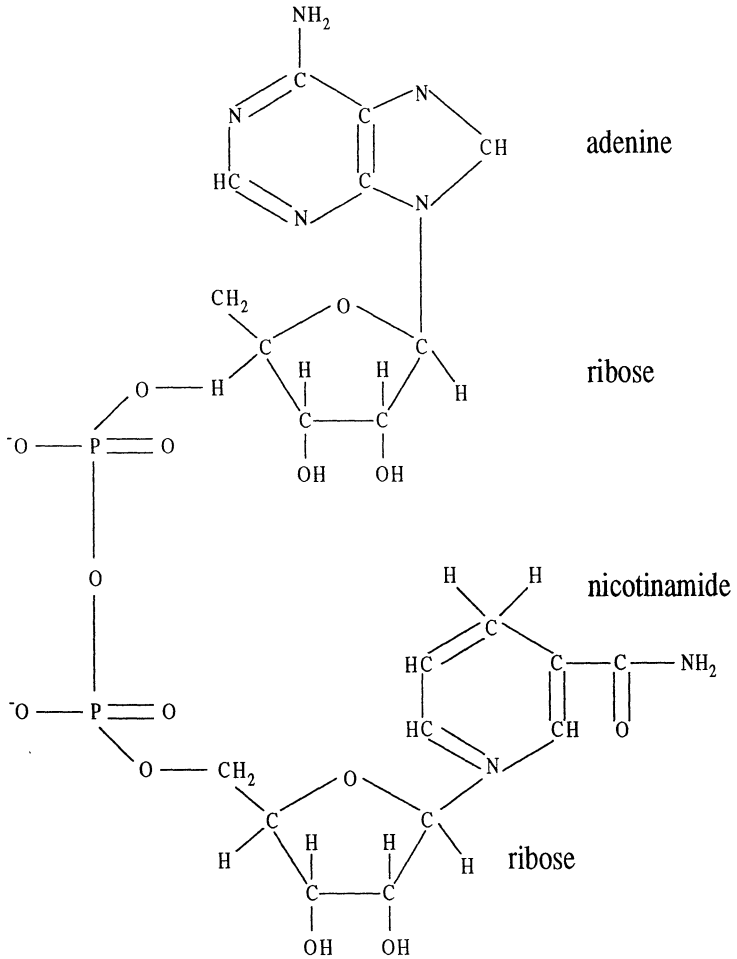

Fig. 2.3 *The structure formula of NADH. The molecule consists of two ribose complex linked together by a diphosphate group, one adenine ring, and one nicotinamide ring.*

NADH is an important substance in the cell *catabolism.* Catabolism is the enzymatic breakdown of the proteins, lipids, and polysaccharides that make up the major part of the food. The catabolism may be regarded as proceeding in three stages. Fig. 2.4 shows a simplified diagram of the catabolism. NADH plays a central role in the last stage of the catabolism, that is the energy *metabolism.* This stage includes a series of reactions called *the citric acid cycle* and the oxidative *phosphorylation.* Both of these processes occur in aerobic bacteria and the mitochondria of eucaryotic cells (Eucaryotic cells do have a nucleus, which procaryotic cells do not). All human cells are eucaryotic. NADH serves as a central intermediate molecule in the above processes in the manner of oxidation of acetyl groups to carbondioxide (CO_2) and water (H_2O). NADH is formed by the addition of a hydrogen nucleus and two electrons (i.e. a hydride ion, H^-) to NAD^+, that is: $NAD^+ + H^+ \rightarrow$ NADH. Thus, NADH acts as a convenient source of readily transferable electrons in cells. As mentioned previously, NADH is present in the cytoplasma and especially (80%) in the mitochondria of cells. Thus, malignant tissue with an increased energy metabolism may exhibit elevated levels of NADH.

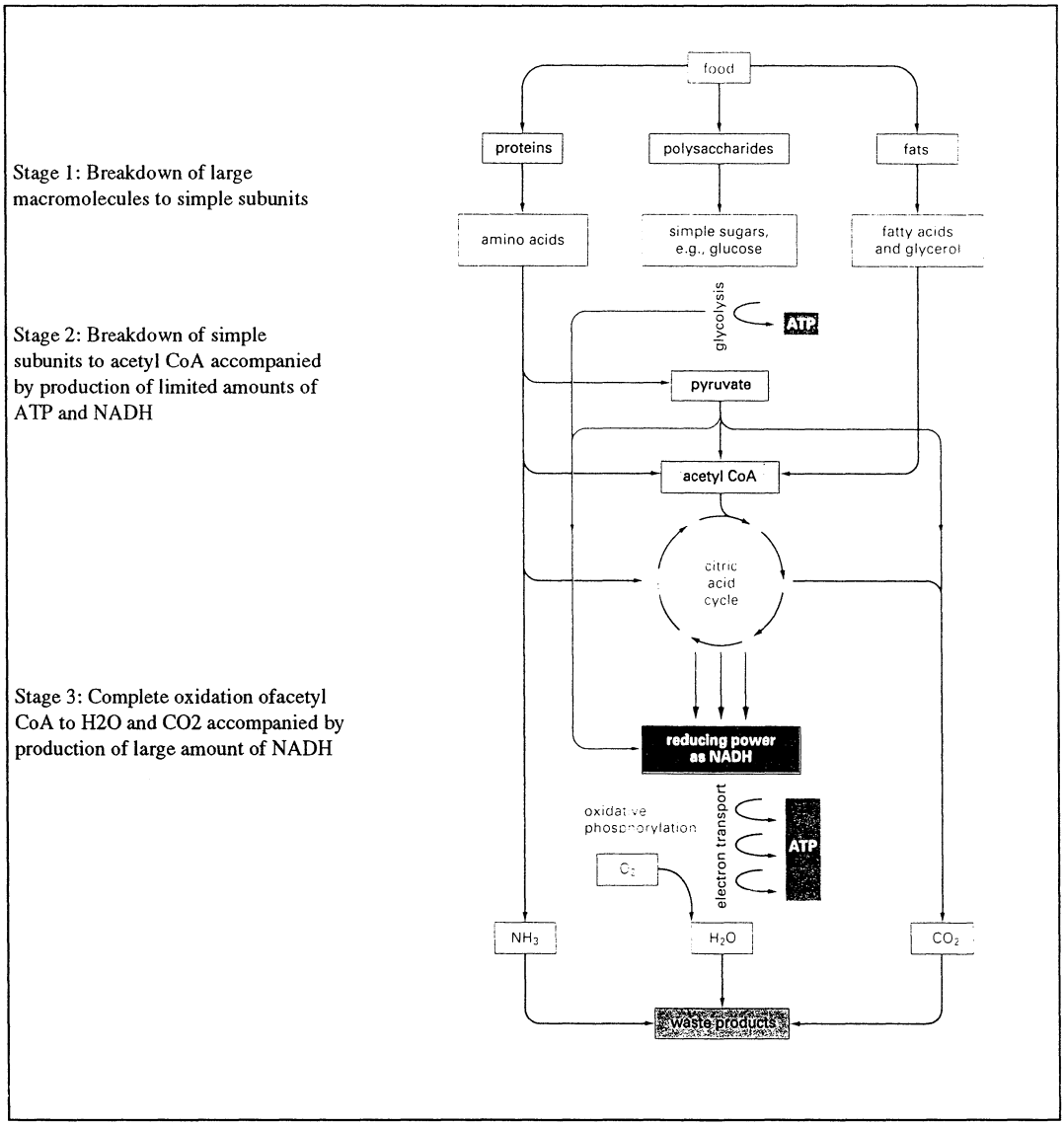

Fig.2.4 *A simplified diagram of the cell catabolism. NADH is particularly important in stage 3, that is in the citric acid cycle and the phosphorylation. From Ref. [17].*

2.3.4 Tissues of the heart and blood vessels

The heart, *cor*, is mainly a large muscle by which the blood is pumped around in the circulatory system. The heart is symmetrically built and consists of a left and a right half. Each half contains two chambers: an *atrium*, and a *ventriculus*. In the right atrium the superior and inferior vena cava emerges. From the right ventriculus the pulmonary artery proceeds. In the left atrium four pulmonary veins emerges (two from each lung) and from the left ventriculus the aorta diverts.

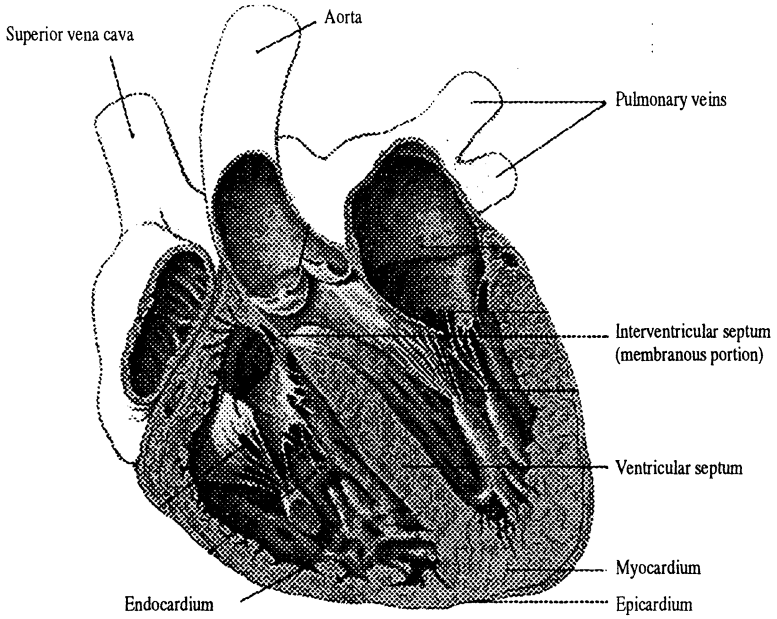

Fig. 2.5 *Frontal cut through the heart with the pulmonary artery removed. From Ref. [18].*

The heart is surrounded by the *pericardium* whichs outermost section is composed of a membrane of connective tissue with a thin serous membrane on the inside. The innermost section of the pericardium is connected to the heart and hence forming the heartwalls outermost section, *epicardium.* The epicardium consists of a lining of mesothelial cells and an underlying layer of connective tissue. The cardiac muscle tissue, *myocardium*, is forming the middlemost and thickest layer of the heart wall. The myocardium of the ventricles is substantially thicker than that of the atria. The cardiac muscle consists of long fibers that are cross-striated. The fibers are branched and connected to each other, thus forming a three-dimensional network. Cardiac muscle cells do not divide and thus destroyed cells are not replaced by new cells. An injury to cardiac muscle tissue is repaired by the formation of fibrous connective tissue. The heartwalls innermost section, *endocardium*, can be divided into three layers: an inner layer of of endothelium and subendothelial connective tissue; a middle layer comprised of connective tissue and smooth muscle cells; and an outer layer which is continuous with the connective tissue of the myocardium. The heartwall also include a fibrous "skeleton" This fibrous skeleton, which consists of dense connective tissue, is situated around the openings of the two arteries leaving the heart and around the openings between the atria and the ventricles. Each annular arrangement of fibrous tissue serves for the attachment of valves that allows blood to flow in only one direction through the openings.

The interventricular septum serves as the wall between the right and left ventricles. It contains cardiac muscle except in the so called membranous portion where it consists of the fibrous skeleton. The endocardium lines each surface of the interventricular septum. The interatrial septum is much thinner than the interventricular septum. Except for certain small areas that contain fibrous tissue, it has a center layer of cardiac muscle with a lining of endocardium facing each chamber. The valves of the heart have a center sheet of fibrous tissue and on all surfaces exposed to blood they are covered by endothelium. Fibrous thread-like cords extend from the free edge of the atrioventricular valves to muscular projections from the wall of the ventricles called papillary muscles.

Arteries and veins have the same principally build-up. Arteries are traditionally divided into three types: large or elastic arteries; medium or muscular arteries; and small arteries or arterioles. Likewise, veins are traditionally classified as large, medium, and small. The small veins, or venules, are further subclassified as postcapillary and muscular. In both arteries and veins, the wall is divided into three major components: a *tunica intima*, a *tunica media*, and a *tunica adventitia*. Histologically, arteries and veins (and also their subclasses) are distinguished from each other on the basis of thickness and differences in the composition of the various layers, especially the tunica media. However, veins generally have thinner walls than arteries.

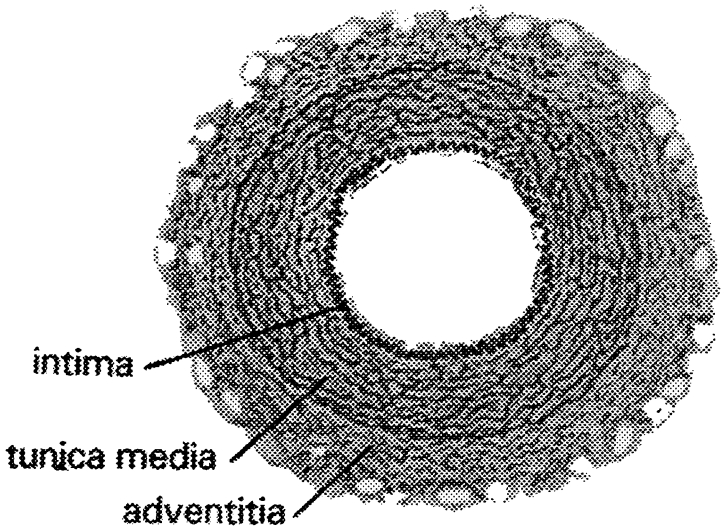

Fig. 2.6 *Cross-section of an artery. From Ref. [18].*

The tunica intima consists of a lining endothelium with its basal lamina, a subendothelial layer of connective tissue, and a layer of elastic material (the internal elastic membrane). The tunica media of elastic arteries consists of sheets of elastic material with intervening layers comprised of smooth muscle cells, collagenous fibers, and ground substance. In muscular arteries the tunica media contains smooth muscle cells, collagenous fibers, and relatively little elastic material. The smooth muscle cells are arranged in a spiral fashion. The tunica adventitia is a connective tissue layer. The main extracellular component is collagenous fibers, but there is also a loose network of elastic fibers. In veins, the tunica adventitia also contains bundles of longitudinally disposed smooth muscle cells. More about different tissues of the heart and blood vessels can be read in Ref. [18,19].

2.4 The purpose of this project

The medical group at the Department of Atomic Physics prosecute research in a wide range of laser applications in medicine. However, until now the research on Raman spectroscopy for medical applications is limited to an initial investigation of the potential of near infrared Raman spectroscopy in tissue diagnostics presented in a Diploma work by Ulf Gustafsson [20]. No research at all has been performed on infrared spectroscopy in tissue characterization at the department.

This project consists of two parts:

1. A study of the potential for near infrared Raman spectroscopy in tissue characterization.

2. A study of the potential for near infrared absorption spectroscopy in tissue characterization.

Part one of the project is focused on the following items:

- To give an introduction to the theory and practice of Raman spectroscopy with the focus on tissue Raman spectroscopy.

- To assemble a Raman spectroscopy arrangement based on a Ti:Sapphire laser, a single-stage spectrometer, and a charge coupled device detector.

- To use the Raman spectroscopy arrangement for measurements on pure tissue constituents, such as cholesterol and NADH, and to test the arrangement for measurements on a biological tissue sample.

Part two of the project concern about the following main subjects:

- To give an introduction to the theory and practice of infrared spectroscopy.

- To use an equipment based on a Fourier transform spectrometer and an InSb detector in studies of pure tissue constituents and tissue samples.

3 Theory of Raman and Infrared spectroscopy

3.1 Introduction

Both Raman and infrared spectroscopy are techniques based on interaction between electromagnetic radiation and matter. The physical processes of the two techniques are, however, quite different. Raman spectroscopy is based on scattering, the so-called Raman scattering, which will be discussed later. In Infrared (IR) spectroscopy, on the other hand, light absorption is measured. Both Raman and IR spectroscopy may be summed up as vibrational spectroscopy, since molecular vibrations are the physical base in both of the techniques.

In vibrational spectroscopy the energy splitting, and transition probabilities, between vibrational energy levels of molecules are measured. With this information one can determine concentrations of molecules present, and in some cases their chemical microenvironment. The determining factor for which vibrational frequencies one might be able to measure with the different techniques is the symmetry of the actual molecule.

3.2 Theory of molecular vibrations

3.2.1 Molecular oscillations

For simplicity we consider a diatomic molecule. Imagine the two atoms as two point masses m_1 and m_2 connected by an elastic spring. Fig 3.1 shows our simple model for a diatomic molecule.

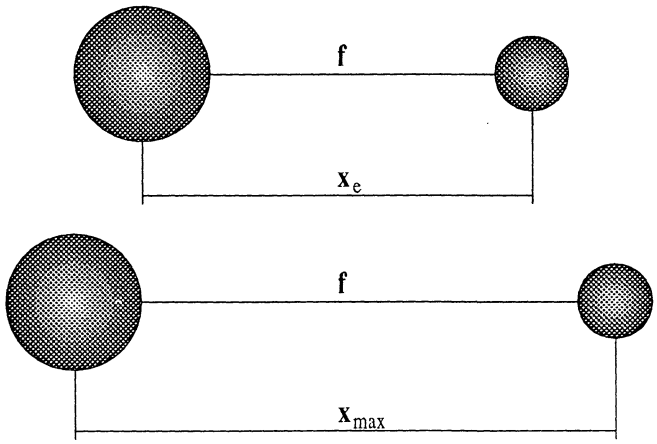

Fig 3.1 *Model of an oscillating diatomic molecule. m_1 and m_2 are the masses of the atoms, f is the force constant, x_e is the equilibrium separation and x_{max} is the maximum separation.*

The simplest assumption for vibration of a diatomic molecule is that each atom moves towards or away from each other. The system will oscillate around its equilibrium separation x_e. The oscillation is caused by a restoring force K. In an approximation of the first order K is proportional to and opposed to the distortion Δx (Hooke's law), such that

$$K = -f\Delta x = -f\left(x - x_e\right) \tag{3.1}$$

The proportionality factor f, which in the model corresponds to the spring constant, is called the force constant in the case of molecular vibrations. The calculating of f, which is a measure of the bond strength, is one of the most important theoretical applications of vibration spectroscopy. The calculation of f is necessary for theoretically calculation of the vibrational frequencies of a molecule.

The molecule as a one-dimensional harmonic oscillator. The atoms moves towards or away from each other. The Hamiltonian may in this case be expressed as

$$\mathbf{H} = \sum_{i=1}^{2} -\frac{\hbar^2}{2m_i} \cdot \frac{\partial^2}{\partial x_i^2} + V(x_1, x_2) \tag{3.2}$$

The potential energy as a function of the distance between the atoms may be evaluated by integration of Equation (3.1). Then

$$V(x) = \int_0^{x-x_e} f x dx = \frac{1}{2} f\left(x - x_e\right)^2 \tag{3.3}$$

This function has a parabolic shape. The potential curve is shown in fig 3.2. The potential V and the vibrational motion are said to be *harmonic*, since they depend on a force linearly proportional to the displacement (Eq. (3.1)).

The energy levels are obtained by the quantum mechanical treatment of the harmonic oscillator, i.e. the energy levels are the eigenvalues E to the time-independent Schrödinger equation:

$$\mathbf{H}\psi(x_1, x_2) = E\psi(x_1, x_2) \tag{3.4}$$

where $\psi(x_1, x_2)$ are the corresponding eigenfunctions and x_1 and x_2 are the positions of the atoms, respectively.

Before solving the Schrödinger equation (Eq. (3.4)) we introduce two new variables:

$$X = \frac{m_1 x_1 + m_2 x_2}{m_1 + m_2} \tag{3.5}$$

$$x = x_2 - x_1 \tag{3.6}$$

X is thus the position of the centre of gravity and x is the distance between the atoms.

With these new variables the Schrödinger equation transforms to:

$$-\frac{\hbar^2}{2\mu}\frac{\partial^2}{\partial x^2}\psi+\frac{1}{2}f(x-x_e)^2\psi=E\psi \tag{3.7}$$

where μ is the so-called reduced mass, which is defined as:

$$\mu=\frac{m_1\cdot m_2}{m_1+m_2} \tag{3.8}$$

The solutions to equation (3.7) are:

$$E=\hbar\omega_0\left(v+\frac{1}{2}\right) \tag{3.9}$$

where $\omega_0=\sqrt{\frac{f}{\mu}}$ is the frequency of the oscillation and $v=0,1,2,\ldots\ldots$, is the vibrational quantum number.

The corresponding eigenfunctions can be expressed as:

$$\psi=\text{const}\cdot\exp\left[\frac{\sqrt{mf}}{2\hbar}(x-x_e)^2\right]\cdot H_v\left[\sqrt{\frac{\sqrt{mf}}{\hbar}}(x-x_e)\right] \tag{3.10}$$

where H_v are Hermite polynomials of degree v. The Hermite polynomials may be found in any textbook of quantum mechanics, for instance in Ref. [21].

The vibrational spectrum thus contains an infinite number of equidistant energy levels with a separation ΔE, where

$$\Delta E=\hbar\omega_0 \tag{3.11}$$

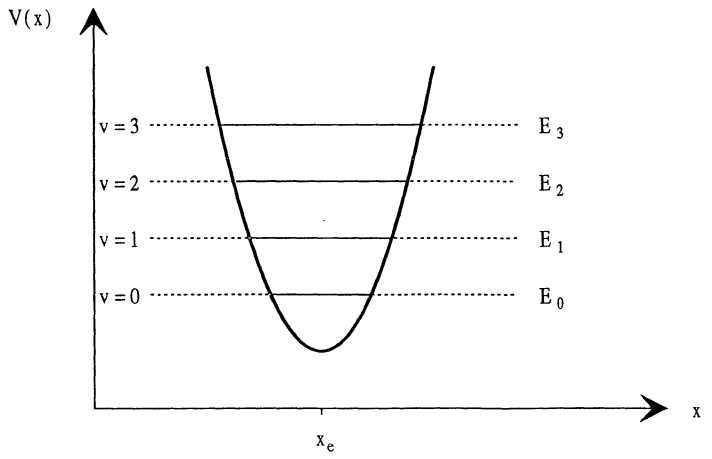

Fig 3.2 *Potential energy curve for the harmonic oscillator. E_v is the energy and v is the vibrational quantum number.*

Which transitions that may occur between different energy levels of a molecule (i.e. allowed transitions) are determined by the quantum mechanical selection rule for a harmonic oscillator. This selection rule is written:

$$\Delta v = v' - v'' = \pm 1 \tag{3.12}$$

where v'= vibrational quantum number for the upper vibrational state
v''= vibrational quantum number for the lower vibrational state

The molecule as a one-dimensional anharmonic oscillator. The harmonic oscillator is, as we already have seen, described by a parabolic potential curve. However it is quite obvious that the attractive force in a real molecule will be zero at very long distances, hence the potential will be constant in that region. Furthermore there are some phenomena in a real molecule, such as the dissociation of a molecule if a sufficient amount of energy is supplied, or the appearance of combination and overtone transitions, that cannot be explained with the harmonic approach. A more realistic treatment uses the anharmonic oscillator model. In this case the potential energy is approximated by the so-called Morse potential [19]:

$$V(x) = D\left[1 - \exp\left(-a(x - x_e)\right)\right]^2 \tag{3.13}$$

This potential is shown in fig. 3.3. This potential is asymmetric with a curvature character constant, a, and a scaling parameter, D, equal to the sum of the zero point energy E_0 and the dissociation energy E_D.

The energy eigenvalues may be calculated by quantum mechanical perturbation theory [21]:

$$E = \hbar\omega_0\left(v + \frac{1}{2} - q\left(v + \frac{1}{2}\right)^2\right) \tag{3.14}$$

where v = the vibrational quantum number
q = anharmonic constant

The anharmonic constant, q, is a measure of the deviation compared to the real harmonic case. In real systems q is positive, which means that the energy levels are not equidistant (as they are according to the harmonic oscillator model). In this case the separation between the levels decreases with increasing vibrational quantum number up to the dissociation energy level. At this level the potential is flat.

The selection rule for the anharmonic oscillator may be evaluated in much the same way as in the harmonic model, then one obtains:

$$\Delta v = \pm 1, \pm 2, \pm 3 \ldots \tag{3.15}$$

The transitions $\Delta v = \pm 1$ are commonly called fundamentals while the higher orders are called overtones or harmonics.

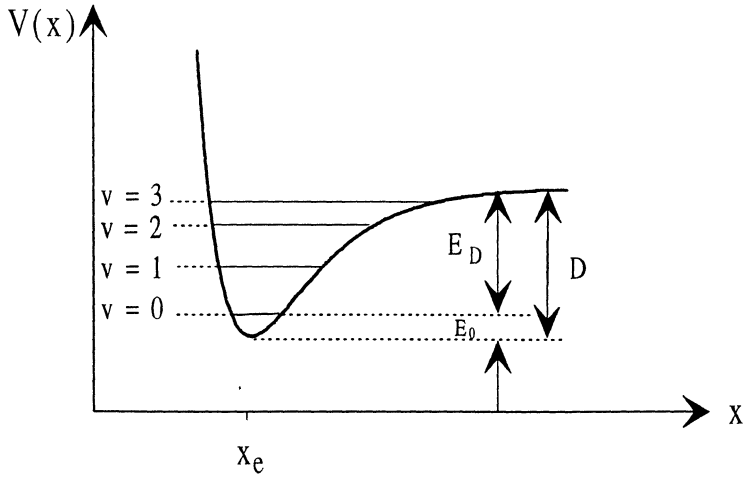

Fig 3.3 *Potential energy curve for the anharmonic oscillator. E_0 is the zero point energy, E_D is the dissociation energy, and v are vibrational quantum numbers.*

For a more rigorous quantum mechanical treatment one may consult Refs. [21], [23] or [24].

3.2.2 Molecular modes of vibration

A molecular motion may occur in essentially three different ways:

- Translation, when the molecule moves as a whole, i.e. the co-ordinates for its centre of gravity changes.
- Rotation about the principal axis.
- Vibration, during which bond distances and/or angles changes periodically.

In this paper we are only focusing on the vibrational motions, since these are the only once contributing to energy splitting in the region that is interesting for this project (in the order of 0.1 eV).

Normal modes of vibration. Until now we have only considered a diatomic molecule. In the case of polyatomic molecules the situation is much more complicated. Such molecules have several nuclear distances, several force constants, several dissociation energies etc.

The vibrational motion of a polyatomic molecule is described by fundamental frequencies or normal modes, corresponding to different types of vibration. These normal modes of vibration are defined by the following conditions:

- All atoms of the molecule move with the same frequency and usually the same phase. It means that they pass the zero crossings and turning points at the same time. The amplitudes, however, depend on the masses.

- The vibrational motion does not cause a translation or a rotation of the molecule as a whole.

- Each normal mode of vibration can be excited independently.

A normal vibration is usually not localized at a single bond in a molecule, but includes several atoms. The vibrational motion is described by a so-called normal co-ordinate Q, which is derived from the masses and relative movements of the atoms involved. Q is a measure of the amplitude of a specific normal mode of vibration.

The number of normal modes of vibration follows from simple considerations. Every atom has three degrees of freedom (the three dimensions of space) and thus there are 3N degrees of freedom for a molecule consisting of N atoms. Of these degrees of freedom, three describe rotation around a centre of gravity, which does not correspond to any vibrational motion. A further three degrees of freedom describe a translation motion which does neither give rise to any vibrational motion. Linear molecules have only two rotational degrees of freedom because the moment of inertia along the molecular axis is zero.

The number of remaining vibrational degrees of freedom n is identical to the number of normal modes, that is:

$$n = 3N - 6 \quad \text{for a non-linear molecule} \tag{3.16}$$

$$n = 3N - 5 \quad \text{for a linear molecule} \tag{3.17}$$

Classification of normal modes of vibration. There are principally two types of normal mode classification:

(A) Classification by type.

Four main types of vibration can be distinguished:

(a) **Stretching vibrations** (symbol ν); one or several of the bond lengths change.

(b) **Planar bending vibrations** (symbol δ); one ore more of the bond angles change, while bond lengths remain constant.

(c) **Out-of-plane bending vibrations** (symbol γ);one atom oscillates through a plane defined by three neighbouring atoms.

(d) **Torsion vibrations** (symbol τ); a dihedral angle (the angle between two planes, which have one bond in common) is changed.

The frequencies or energy splittings of these types of vibration decrease in the order: $\nu \geq \delta \geq \gamma \geq \tau$.

In larger organic molecules one commonly uses a further classification into rocking ρ , twisting t, and wagging ω vibrations. The basic types of vibration is shown in Table 3.1, and the further special types of vibration are illustrated in Fig. 3.4.

(B) Classification by molecular symmetry.

(a) **Symmetric vibrations** (index s), are vibrations, for which the symmetry of the molecule is retained during the vibration.

(b) **Asymmetric vibrations** (index as), are vibrations, for which one or more of the symmetry elements of the molecules vanish during the vibration.

(c) **Degenerate vibrations** can occur in highly symmetric molecules. In this case two or more vibrations have different co-ordinates but the same energy.

Table 3.1 *The main types of vibration.*

Type	Stretching vibrations	Bending vibrations In-plane	Bending vibrations Out-of-plane	Torsion vibrations
Schematic	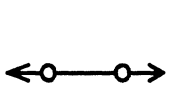	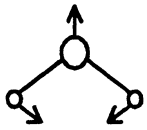	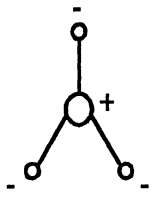	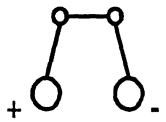
Symbol	ν	δ	γ	τ
Minimum number of bonds	1	2	3	3

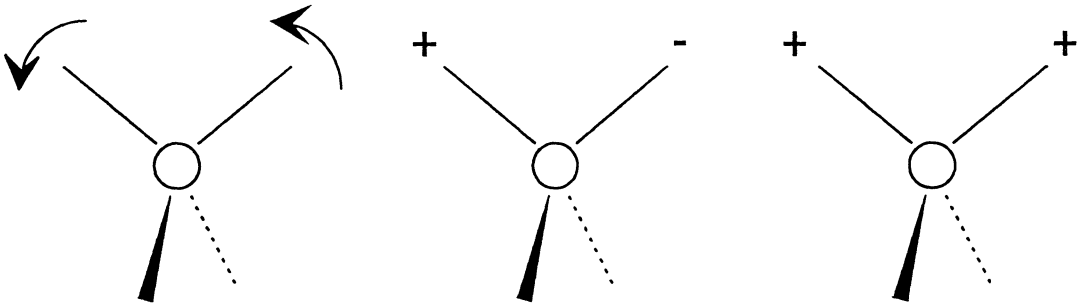

Fig. 3.4 *Special types of vibration: rocking* ρ, *twisting t, and wagging* ω.

3.3 Raman scattering

3.3.1 Introduction

Let us first very briefly discuss the interaction between light and matter. We consider a molecule irradiated by light. If the energy of the light exactly corresponds to the energy separation between two states in the molecule, the photons can be absorbed by the molecule, causing a transition from the lower to the higher energy state of the molecule, i.e. *absorption* of radiation. More about that in chapter 3.4. However, even if the light is not of a resonant frequency, i.e. the photon energy corresponds to a molecular transition, *scattering* effects can still be obtained, so-called Rayleigh and Raman scattering. In a

quantum mechanical model, light scattering is depicted as a two-photon process. The first step is the interaction between a photon and the molecule which raise the molecule to a higher energy state (virtual state). The second step is the release of another photon and the relaxation of the molecule. This will be treated more in detail in chapter 3.3.3. The difference between the absorption and scattering processes is shown in fig. 3.5.

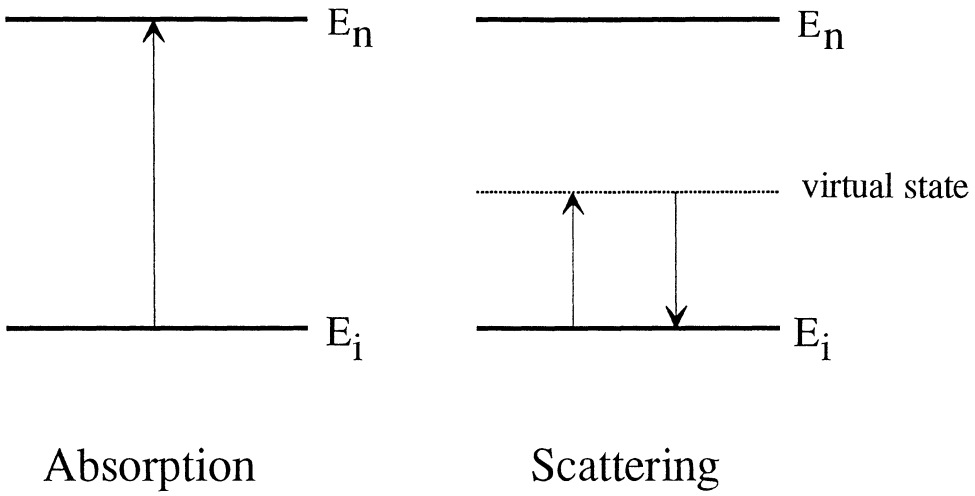

Fig 3.5 *Principal sketch of the absorption and scattering processes. E_i is the initial energy state (lower state) and E_n is a higher energy state.*

As mentioned previously there are two types of scattering processes, Rayleigh and Raman scattering. Rayleigh scattering corresponds to a molecular relaxation to the initial energy state, E_i (elastic scattering), according to the right hand side of Fig. 3.5, while Raman scattering implies a molecular relaxation to an other energy state (inelastic scattering).

The Raman shift of scattered light was first predicted in 1923 by Adolf Smekal and observed experimentally 1928 by sir Chandrasekhara Vankata Raman (1880-1970) and his co-worker K.S. Krishnan. This important discovery was recognised in 1930 when Raman was awarded the Nobel Prize in Physics [25,26,27].

Raman and Krishnan did observe a new type of scattering in addition to the well known Rayleigh scattering. This new type of scattering shows quite different characteristics compared to the Rayleigh scattering: the intensity of the Raman scattered light is several orders of magnitudes weaker than the intensity of the Rayleigh scattered light and the Raman scattered light consists of higher and lower frequencies (side bands) than the frequency of the incident light, in contrast to the frequency of the Rayleigh scattered light which has the same frequency.

3.3.2 A classical model of Raman scattering

Consider a free molecule upon which an monochromatic electromagnetic wave with amplitude E_0, frequency ω, and phase shift δ, is impinging:

$$\overline{E} = \overline{E}_0 \cos(\omega t + \delta) \qquad (3.18)$$

This wave induces a dipole moment $\overline{\mu}$ in the molecule, where

$$\overline{\mu} = \alpha \overline{E} \tag{3.19}$$

Where the induced dipole moment $\overline{\mu}$ is a function of time, and α is the polarisability of the molecule, i.e. a measure of the electronic deformation of the electron cloud by the field. Normally, $\overline{\mu}$ is not directed along $\overline{E}$ and then α is a phenomenological tensor quantity, which can be written as

$$\alpha = \begin{pmatrix} \alpha_{xx} & \alpha_{xy} & \alpha_{xz} \\ \alpha_{yx} & \alpha_{yy} & \alpha_{yz} \\ \alpha_{zx} & \alpha_{zy} & \alpha_{zz} \end{pmatrix} \tag{3.20}$$

This tensor is in almost every case symmetric i.e. $\alpha_{xy} = \alpha_{yx}, \ldots.$

The polarisability is a function of the interatomic distances in the molecule, and is hence dependent upon the vibrational modes. If Q_i is a particular vibrational normal mode of the molecule, then clearly $\alpha = \alpha(Q_i)$, and if the amplitude of motion is small, then a Taylor expansion gives:

$$\alpha(Q_i) = \alpha_0 + \left(\frac{\partial \alpha}{\partial Q_i}\right)_0 Q_i + \ldots. \tag{3.21}$$

If one assumes that the normal mode is periodic in time, then

$$Q_i = Q_i^0 \cos(\omega_i t + \delta_i) \tag{3.22}$$

where ω_i is the oscillation frequency of the vibration. Then

$$\overline{\mu} = \left[\alpha_0 + \left(\frac{\partial \alpha}{\partial Q_i}\right)_0 Q_i^0 \cos(\omega_i t + \delta_i)\right] \overline{E}_0 \cos(\omega t + \delta) =$$

$$\alpha_0 \overline{E}_0 \cos(\omega t + \delta) + \frac{Q_i^0 \overline{E}_0}{2} \left(\frac{\partial \alpha}{\partial Q_i}\right)_0 \cos\left[(\omega + \omega_i)t + \delta'\right] \tag{3.23}$$

$$+ \frac{Q_i^0 \overline{E}_0}{2} \left(\frac{\partial \alpha}{\partial Q_i}\right)_0 \cos\left[(\omega - \omega_i)t - \delta''\right] + \ldots.$$

where $\delta' = \delta_i + \delta$ and $\delta'' = \delta_i - \delta$

In this expression the trigonometrical rule $\cos A \cos B = \frac{1}{2}\left[\cos(A+B) + \cos(A-B)\right]$ is utilized.

Equation (3.23) shows that there are three types of scattered light in the linear expansion of equation (3.22):

(1) A coherent scattering term, the *Rayleigh scattering*, where light is scattered without a frequency change. This term depends directly upon the molecular polarisability.

(2) Scattering terms which contain frequencies which are the sum and differences, respectively, of the field frequency and the harmonic molecular frequency of Q_i. These last two terms are called the *anti-stokes frequency* $(\omega+\omega_i)$ (higher frequency) and the *stokes frequency* $(\omega-\omega_i)$, respectively, and refer to incoherent scattering since the phases δ' and δ'' will be different for each scattering molecule. These terms are the *Raman scattering*.

Equation (3.23) also shows that there is a requisite condition for Raman scattering to occur, which is

$$\frac{\partial\alpha}{\partial Q_i}\neq 0 \tag{3.24}$$

i.e. a vibration is said to be *Raman active* if the polarisability of the molecule changes during a vibration.

The total power radiated by an oscillating dipole $\overline{\mu}$ (see Ref. [28] page 56) in classical electromagnetics, is given by:

$$I=\frac{2}{3c^3}\overline{\left(\frac{d^2\overline{\mu}}{dt^2}\right)^2} \tag{3.25}$$

where the bar denotes time averaging, and c is the speed of light. By inserting Eq. (3.23) into Eq. (3.25), one obtains:

$$I=\frac{\omega^4\alpha_0^2E_0^2}{3c^3}\left[\frac{(\omega+\omega_i)^4}{12}\left(\frac{\partial\alpha}{\partial Q_i}\right)_0^2+\frac{(\omega-\omega_i)^4}{12}\left(\frac{\partial\alpha}{\partial Q_i}\right)_0^2\right]\left(Q_i^0\right)^2E_0^2 \tag{3.26}$$

plus cross terms which are neglected.

This intensity expression again shows that there are three main contributions to the scattering intensity:

$$I_{Rayleigh}=\frac{E_0^2}{3c^3}\omega^4\alpha_0^2 \tag{3.27}$$

$$I_{anti-Stokes}=\frac{\left(Q_i^0\right)^2E_0^2}{12}(\omega+\omega_i)^4\left(\frac{\partial\alpha}{\partial Q_i}\right)_0^2 \tag{3.28}$$

$$I_{Stokes} = \frac{\left(Q_i^0\right)^2 E_0^2}{12}(\omega - \omega_i)^4 \left(\frac{\partial \alpha}{\partial Q_i}\right)_0^2 \tag{3.29}$$

From equation (3.27) it is clear that the intensity of the Rayleigh scattered light is proportional to the fourth power of the frequency of the impinging light, while, as can be seen from Eqs. (3.28) and (3.29), the intensity of Raman light is proportional to the fourth power of the frequency of the scattered light. This implies that the scattered intensity strongly decreases with diminishing values of ω, or put in other words, the scattered intensity strongly increases with diminishing values of λ.

If one looks at Eqs. (3.28) and (3.29) one expects that the relative intensities of the anti-Stokes and Stokes components differs by the ratio of $\left[(\omega + \omega_i)/(\omega - \omega_i)\right]^4$. However, this is not consistent with experiment. To get a correct expression one has to take the occupation numbers of the actual levels into account. The ratio of the number of molecules, N, in two vibrational energy levels follows a Boltzmann distribution (at thermal equilibrium), such as

$$\frac{N_{upper}}{N_{lower}} = \exp(-\hbar\omega/kT) \tag{3.30}$$

where $\hbar$ is Planck's constant, k is Boltzmann's constant and T is the absolute temperature. According to the fact that anti-Stokes scattering starts in an upper vibrational state and Stokes scattering starts in a lower state (we will see that in the following chapter) the ratio of the anti-Stokes and the Stokes intensities may be expressed as:

$$\frac{I_{anti-Stokes}}{I_{Stokes}} = \left[\frac{\omega + \omega_i}{\omega - \omega_i}\right]^4 \exp(-\hbar\omega_i/kT) = \left[\frac{\nu + \nu_i}{\nu - \nu_i}\right]^4 \exp(-h\nu_i/kT) \tag{3.31}$$

where $\nu = \omega/2\pi$ and $\nu_i = \omega_i/2\pi$.

To form an opinion of how large this ratio is we put in some adequate numerical values in Equation (3.31). If the vibrational frequency is $\nu_i = 500$ cm^{-1} (corresponds to an energy splitting of approximately 0.06 eV), the temperature is $T = 300$ K, and the frequency of the incident light is $\nu = 12500$ cm^{-1} (corresponds to $\lambda = 800$ nm), the intensity ratio becomes $I_{anti-Stokes} \approx 0.09 I_{Stokes}$. Changing the vibrational frequency to $\nu_i = 2000$ cm^{-1} yields $I_{anti-Stokes} \approx 0.0002 I_{Stokes}$. From these examples it is obvious that the anti-Stokes scattering is weak and therefore usually ignored in conventional Raman spectroscopy.

To predict the relative intensities of the incident light, the Rayleigh scattered light and the Raman scattered light, one needs to know the values of α_0 and $\partial\alpha/\partial Q_i$. A quantum mechanical approach provides the means of calculating the different polarisabilities, but this will not be done here. Nevertheless it is expected that $\partial\alpha/\partial Q_i$ will be much smaller than α_0 and this is in fact the case. In practise there is a rule of thumb for the ratio between incident light, Rayleigh scattering and Raman scattering:

$$I_{Raman} = 10^{-5} - 10^{-3} I_{Rayleigh} = 10^{-8} - 10^{-6} I_{incident} \quad (3.32)$$

This relationship shows once again how extremely weak the Raman scattering actually is.

3.3.3 A quantum mechanical picture of Raman scattering

The classical model provides a useful conceptual model for Raman scattering. The quantum mechanical approach to the scattering process is quite different: the wave-particle duality of a light beam is incorporated by considering that the beam is composed of packets or quanta of light particles known as photons and the quantization of molecular energy levels is taken into account.

It is a reasonable approximation to write the molecular energy E_{mol} as a sum of two terms:

$$E_{mol} = E_{elec} + E_{vib} \quad (3.33)$$

where the subscripts refer to electronic and vibrational components, respectively of the total molecular energy. For present purposes the contributions due to molecular rotation and translation can be ignored. Electronic energy transitions involve much larger quantities of energy than vibrational transitions do, with values of 10000-50000 cm^{-1} for the former and 10-4000 cm^{-1} for the latter. Moreover, a good approximation for the vibrational energy E_{vib} of the ground state of a molecule is the harmonic oscillator model (compare Eq. 3.9):

$$E_{vib} = \left(v + \tfrac{1}{2}\right)h\nu_{vib} \qquad v = 0, 1, 2, \ldots\ldots \quad (3.34)$$

The vibrational levels in the ground state are thus equally spaced, quantified, by the amount ν_{vib}.

In the quantum mechanical model light scattering is depicted as a two-photon process, as illustrated in Fig. 3.7. The first step in this process is the combination of a photon and a molecule to raise the molecule to a higher energy state. This state is a so-called virtual state which mean that the state is not located in any electronic state but rather between two electronic states, i.e. a virtual state corresponds to an energy level not overlapping with any energy level of the molecule. Therefore, no absorption to this level can take place and there are no life times associated with Rayleigh and Raman scattering. Raman scattering is thus an instantaneous effect. The second step involves the release of a photon and the relaxation of the molecule. The splitting of the process in two steps can be motivated by the easily understandable picture provided, but in reality the two steps takes place simultaneously.

For Rayleigh scattering the upward and downward directed transitions have, apart from a change in sign, the same energies. Thus, in the Rayleigh process, no change in the photon energy occurs.

For Raman scattering the upward transition terminates in a virtual level as in the case of Rayleigh scattering, but the molecule relaxation terminates in a vibrational level that is either higher or lower than the initial level. If the final level is higher than the initial level a Stokes process has occurred. In this process the emitted photon has an energy $E(\nu - \nu_{vib})$, corresponding to the third term in Equation (3.23). Conversely, an anti-Stokes process results from a transition terminating in a vibrational energy level lower than the starting level. In the anti-Stokes process, the second photon has an energy $E(\nu + \nu_{vib})$, corresponding to the second term in Equation (3.23). Of course, in both Raman processes the total energy is conserved, thus for Stokes scattering the molecule gains a quantum of energy $h\nu_{vib}$ while for anti-Stokes scattering the molecule loses a corresponding amount of energy.

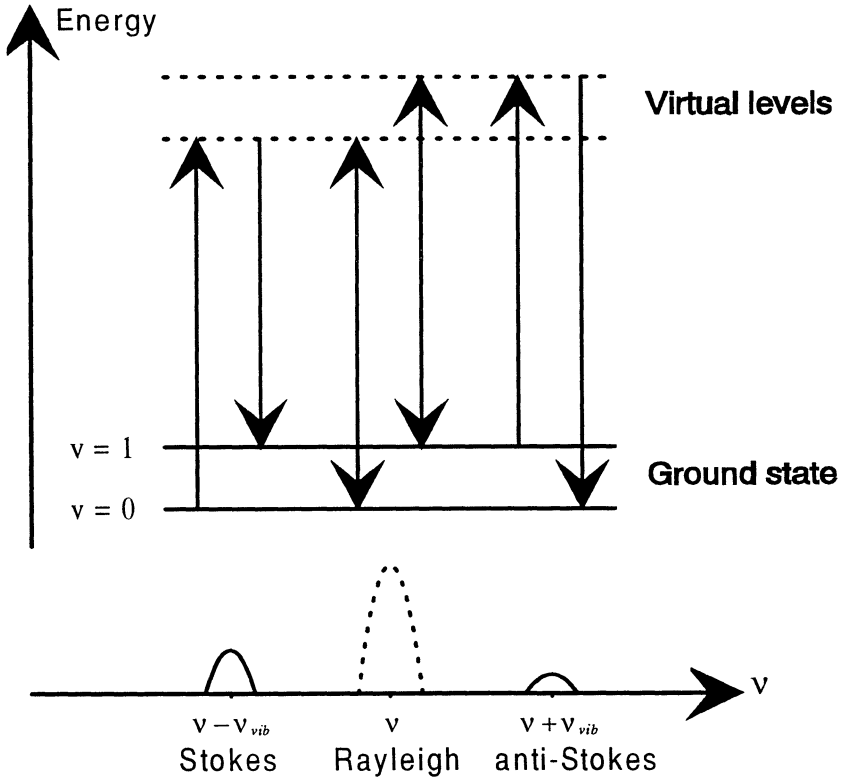

Fig. 3.7 *Rayleigh and Raman scattering.*

3.4 Raman spectroscopy

3.4.1 Introduction

Raman and Krishnan used a beam of focused and filtered sunlight in their original observation of Raman scattering. The filters were just simple coloured glass and they observed the Raman effect by the colour changes (i.e. frequency changes) that occurred in the scattered light. Rather soon they changed their experimental set-up: instead of using sun light as a light source they used a quartz mercury lamp from which all wavelengths greater than that of the indigo line (435.8 nm) was filtered out, and they changed detection system to a spectrograph and photographic plates. At almost the same time (in 1928) G. Landsberg and L. Mandelstam reported their results from a similar experiment. They were able to detect the Raman effect as well but exposure times ranging from 2 to 14 hours were required [29]. At the time of the discovery of the Raman effect the practice of experimental IR spectroscopy was very difficult, and it remained so for the next two decades. The following development in the area of Raman spectroscopy contains several improving steps among which the most important are summed up in the time schedule stated below.

1930-1950: During this period, much was being discovered about the molecule structure of many molecules.

1950-1970: Considerable development of commercial IR spectrometers with the introduction of ratio recording double-beam IR instruments were carried out.

1970-1980: The first commercial, reliable, continuos wave (CW) gas lasers were introduced, especially the Ar^+-laser, which provides a source of intense CW radiation in the blue and green regions of the spectrum was important for the development of Raman spectroscopy. This increased the intensity of the exciting radiation available for Raman spectroscopy by more than an order of magnitude. Moreover, developments in diffraction gratings, photomultiplier tubes, and photon-counting equipment made a new generation of commercial Raman spectrometers possible.

1980-: Diode array detection became possible, bringing the multiplexing advantage back to Raman spectroscopy (something that it had given up in the change from photographic to photoelectric detection). Holographic edge filters for effective suppressing of the strong Rayleigh line in the Raman spectrum has during the last couple of years been developed.

These developments have made Raman spectroscopy of today an unique and powerful analytical tool, with a wide range of applications [30,31,32,33].

3.4.2 Basic optics of a Raman experiment

The experimental set-up required for Raman spectroscopy is actually quite simple. Broken down into its basic components, a Raman experiment consists of a light source, usually a CW laser illuminating a sample, collection optics, a dispersive optical element (i.e. a spectrometer), and a detection system. Fig. 3.8 shows a conventional Raman experimental arrangement.

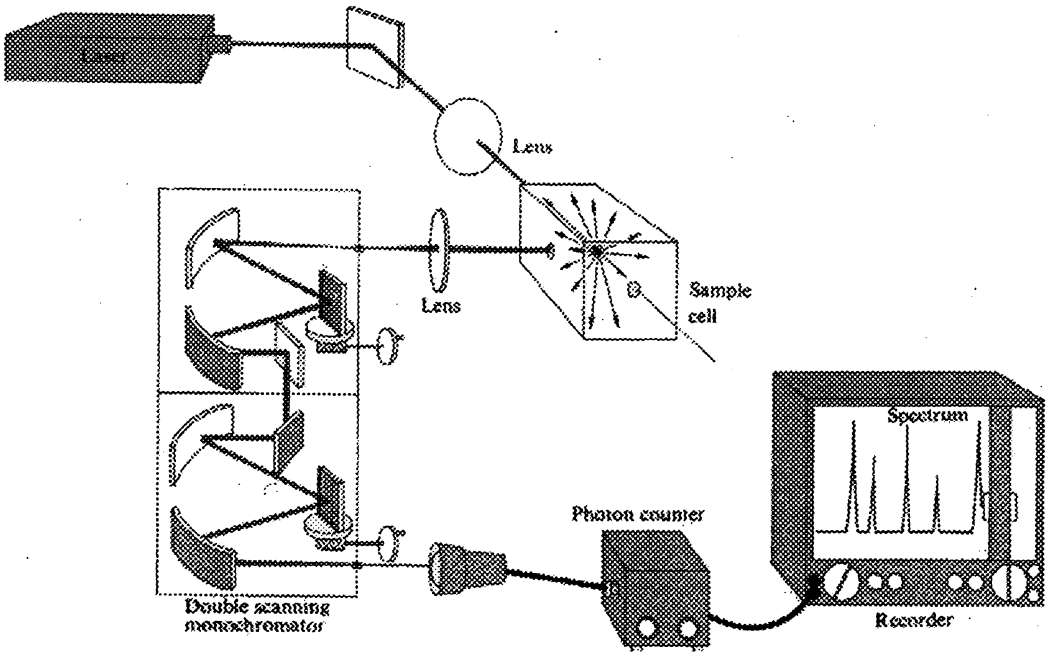

Fig. 3.8 *A laser-Raman system. From Ref. [34].*

In a standard Raman experiment, intense monochromatic radiation provided by a laser is focused onto or into the sample. Some of the resulting scattered light is gathered by collection optics and directed to a dispersing system, usually a double monochromator. The function of the monochromator is to separate spatially the scattered light on the basis of frequency (wavelength). At the exit port of the monochromator the Raman spectrum forms an image in the form of a series of very faint lines. These are detected and recorded either sequentially by a single photomultiplier used with a scanning monochromator or simultaneously by a multichannel detector, which is the modern equivalent of a photographic plate.

To get a more detailed knowledge of how a Raman experiment works we will now follow along the light path through the experiment and consider the key facets of each component in turn.

The laser. The available light sources for Raman spectroscopy are conveniently divided into pulsed and continuous wave (CW) lasers. Most of the work in analytical Raman spectroscopy today is done using a CW laser. The pulsed lasers have their primary applications in ultraviolet (UV) resonance Raman spectroscopy [35] and time-resolved Raman measurements [36,37]. In the last several years, most applications of Raman spectroscopy have involved the use of CW gas ion lasers, especially argon and krypton ion lasers. These lasers offer sufficient power levels for analytical applications, and the available lines are in the visible region of the spectrum. The wavelength of the excitation light is important, since the Raman scattering intensity varies as the fourth power of the frequency (cf. Eqs. 3.28 and 3.29), for instance Raman spectra obtained at 514.5 nm with an argon ion laser will be $(632.8/514.5)^4 \approx 2.3$ times more intense than spectra obtained at 632.8 nm with a HeNe laser operating at the same power. The available lines from both argon and krypton lasers are given in Table 3.2.

Table 3.2 *Wavelengths and corresponding relative output powers from Argon and Krypton ion lasers. Powers quoted are for lasers of a nominal total output of about 2 W. Values taken from Ref. [31].*

Argon		**Krypton**	
wavelength (nm)	output power (mW)	wavelength (nm)	output power (mW)
333.6	80	323.9	25
334.5	30	337.5	170
335.9	10	350.7	1300
351.1	600	356.4	270
351.4	10	406.7	900
363.8	700	413.1	1500
379.5	20	415.4	100
454.5	20	468.0	500
457.9	150	476.2	50
472.7	60	482.5	75
476.5	300	520.8	150
488.0	700	530.9	250
496.5	300	568.2	200
501.7	140	647.1	750
514.5	800	676.4	120
528.7	200	752.5	150
		793.1	10
		799.3	30

Alternatively, continuous tuning within a given spectral range can be achieved by using a dye laser. In essence, a dye laser consists of a light source (e.g. an argon or krypton ion laser) which pumps a dye to strongly fluorescence. A narrow spectral bandwidth, within this fluorescence output is made to lase in a dye laser cavity, and since the total fluorescence output covers a broad spectral bandwidth (typically 50 nm), the laser output can be tuned continuously within the overall fluorescence emission.

Another source that has seen limited use in analytical Raman spectroscopy is the frequency doubled Nd:YAG laser (532 nm). It is a solid state device that offers reliability and ease of operation. The Nd:YAG laser must be frequency doubled to reach the visible range. The doubling units that use potassium trihydrogen phosphate (KTP) or potassium dihydrogen phosphate (KDP) crystals are still somewhat temperature sensitive and tend to drift a bit when used at high powers.

Lenses and filters. The laser is usually focused onto the sample by using a long focal length lens that may be antireflection coated for the laser line of interest. By varying the focal length, one can change the spot size at the sample. Normally one strives for small spot size at the sample in order to make the collection process simple. In addition to the focusing lens, a polarization rotator and a laser line filter are usually incorporated. The laser line filter is either a narrow band pass interference filter or a prism monochromator. Requirements for an effective filter are high degree of transmission at the laser line and adequate rejection (more than 99.9 %) at other wavelengths. This rejection filter eliminates nonlasing emission lines that are present and can be elastically scattered by the sample producing undesired artefacts in the Raman spectrum.

Collection optics. The collection system usually consist of two lenses. The first lens should have a very short focal length and a low so-called f/Number. The f/Number is defined as the ratio between the focal length and the diameter of the lens e.g. f/5 means that f/D = 5 where f is the focal length and D is the aperture diameter of the lens. The reason why the first lens should have a low f/Number is that the lens then will collect the scattered light in the largest possible solid angle. The second lens is used to refocus the collected light onto the entrance slit of the spectrometer, matching the f/Number of the spectrometer to that of the collection optics. This ensures that the spectrometer is neither overfilled nor underfilled. If it is overfilled one loses signal and on the other hand if it is underfilled the resolving power of the spectrometer diminishes (the resolving power is defined by $R = \lambda/\delta\lambda$, where $\delta\lambda$ is the resulting line width of the spectral apparatus when using monochromatic light of wavelength λ).

Almost any collection geometry (i.e. set-up of the lenses or other optics) can be utilized in Raman spectroscopy, but specific experiments may require certain optimized collection angles. In practice, most instruments are operated in a 90° or 180° scattering geometry. The 90° system is certainly the easiest to set up, since the illumination axis and the collection axis are separated in space. One simply has to ensure that the two axis intersect at their focal points. The major advantage of the 90° system is the ease of introduction of sampling accessories. Fig. 3.9a shows a 90° scattering lens system.

The two-lens system described above can be easily converted to a 180° system by including a small mirror or prism on the front side of the first lens. A 180° back scattering lens collection system is displayed in Fig 3.9b.

One other interesting modification to the collection optics is the use of fiber optics. Properly designed, a fiber-optic illumination and collection system can incorporate both efficient illumination and a high collection efficiency [38]. Another advantage is the ease of remote sampling.

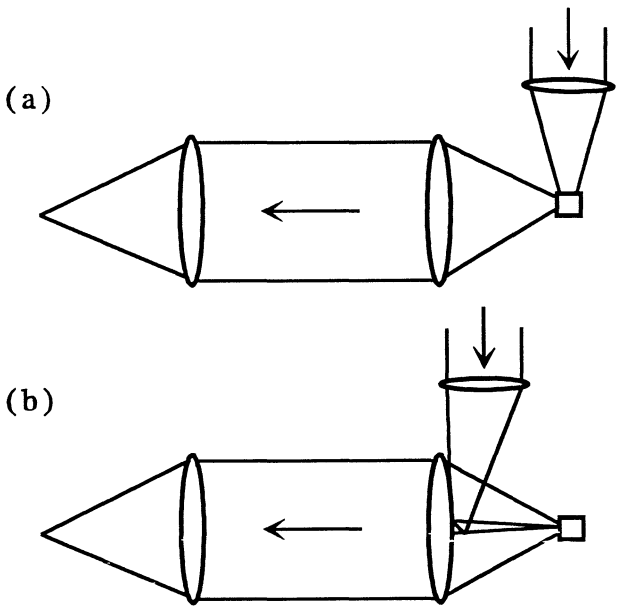

Fig 3.9 *(a) A 90° scattering lens collection system. (b) A 180° backscattering lens collection system.*

The spectrometer. A spectrometer is required to disperse the collected light for sequential presentation to a detector or to disperse it across an array detector. Since the elastically scattered component (the Rayleigh scattering) is also collected, the spectrometer must be able to discriminate efficiently against this strong signal. For analytical Raman spectroscopy the standard system is still the double monochromator, i.e. a two-grating system. Such a system is shown in Fig. 3.8. The major problem associated with that system is the high transmission losses. Since the first monochromator serves essentially to reduce the stray light level from the very strong Rayleigh scattering and it suffers by a low transmission, an alternative approach using a single monochromator might be feasible, if this intensity could be reduced with a filter. In such a system it is necessary to suppress the Rayleigh scattered light before it reaches the entrance slit of the spectrometer. Recent development in filter technology may provide the means of accomplishing this. It is thus important that the filter has very high extinction at the laser line and good transmission characteristics over the rest of the spectrum. The use of such a filter with a single monochromator could increase Raman sensitivity by a significant factor.

The detection system. There are two main methods by which the line spectrum across the exit port of the spectrometer may be detected. The first and most simple method is to use a scanning spectrometer and to place a narrow exit slit over the exit port, followed by a photomultiplier tube. By slowly turning the grating, using the accurate drive of the spectrometer, the lines of the spectrum move in succession across the slit and are detected and recorded as outlined in the upper part of Fig. 3.10. In the second method a multichannel detector is placed at the exit port of the spectrometer. A multichannel detector is similar to having several of hundred minute detectors across the port. The entire Raman spectrum is then registered simultaneously with the different elements of the detector. Thus it is possible to observe the entire Raman spectrum in real time. When using multichannel detection the grating is turned only to change the spectral region across the detector. A multichannel detection system is displayed in the lower part of Fig. 3.10. The drawback of such a system involves a resolution/bandwidth trade-off. If high bandwidth or spectral coverage is required, then resolution must be sacrificed. Continuing advances are being made in the sensitivity of array detectors. Techniques for reduction of readout noise and background noise are being developed. The introduction of charge coupled device (CCD) and charge injection device (CID) detectors will further improve the results being obtained in multichannel detection.

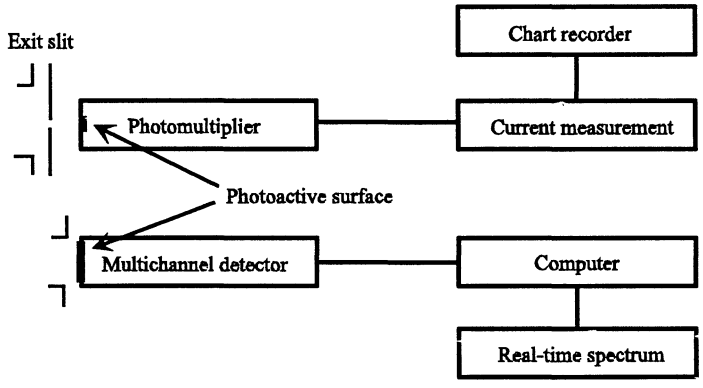

Fig. 3.10 *The principles of single-channel (scanning) and multi-channel detection.*

3.4.3 Fluorescence as a limiting factor

As mentioned previously, Raman scattering is a very weak effect and hence it is of great importance to avoid the influence of other interaction effects, i.e. Rayleigh scattering and fluorescence. Suppression of Rayleigh scattering has been briefly discussed in chapter 3.4.2 and we will in this chapter focus on the question: How to get rid of the contribution due to fluorescence in the Raman spectrum?

Let us start with a short description of the fluorescence. Consider a photon, falling within the interaction distance of a molecule in the ground state. If there is any excited state, which corresponds to the energy of the incoming photon, the photon will interact with the molecule. Either the photon may be scattered, which implies that it, within an extremely short period of time (about 1 ps), may have changed its direction and polarization but not its energy. The molecule will thus remain in its ground state. The molecule can also be excited by absorbing the photon, if its energy exactly corresponds to the energy of an excited state of the molecule. We will now discuss what will happen following the absorption. Excited states are unstable, meaning that the molecule will try to get rid of the excess energy and return to its ground state. This can be done in several different manners but the essential process in connection to Raman spectroscopy is fluorescence. Fluorescence implies that the molecule, after a rapid relaxation to the lowest vibrational state in the excited electronic state, will return to the ground state by emitting a photon. Since the transition may be terminated in any of the vibrational states of the electronic ground state, the energy of the photons will not have a distinct value, but rather a broad distribution. Fig. 3.11 shows a schematic picture illustrating the fluorescence process.

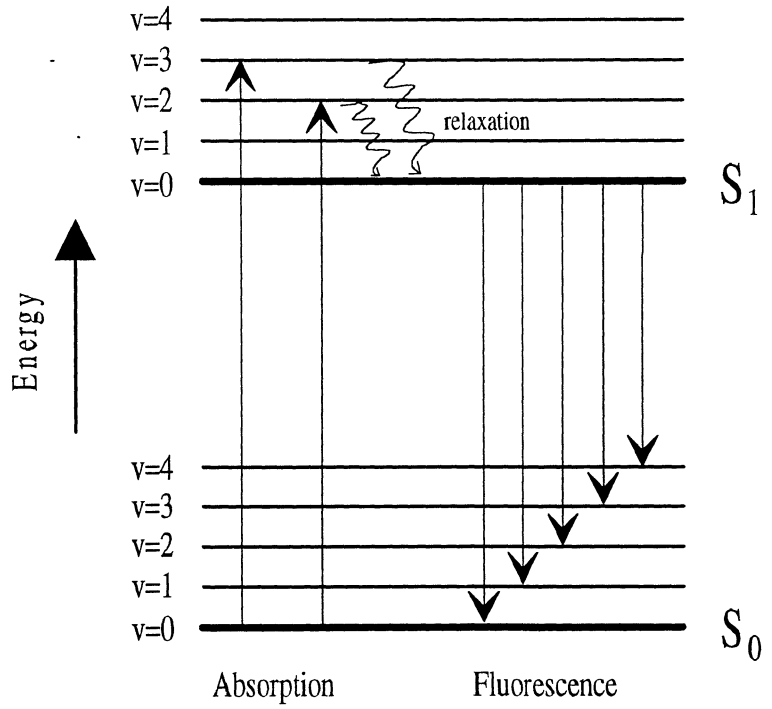

Fig 3.11 *A schematic illustration of fluorescence. S_0 and S_1 are electronic states while v is vibrational quantum number associated with the corresponding vibrational level.*

Thus the fluorescence will contribute to a broad background superimposed on the Raman signals. Since fluorescence as a phenomenon is approximately 10^3 times stronger than Raman scattering it is of vital importance to eliminate or at least to suppress the fluorescence signal in Raman spectroscopy.

There are several possible approaches, to reduce the influences of fluorescence in Raman spectroscopy. One obvious approach is to purify the sample as much as possible. This method is essential for many analytical Raman spectroscopy studies, since the fluorescence background quite often results from impurities in the sample. Another technique that may be attractive, if the sample itself is not fluorescent, is photo bleaching of the sample impurities, which implies that the sample is illuminated by a laser beam for several hours. Furthermore one can add a fluorescence quenching agent to the sample, which will suppress the fluorescence background. All of the approaches mentioned so far do often not sufficiently suppress the fluorescence or are not applicable to the actual experimental situation. But, on the other hand, these techniques do not require any changes or extra equipment in addition to a conventional Raman experimental set-up.

However, it is quite easy to understand that the previously mentioned methods can not be used in medical applications. Tissue diagnostical applications of Raman spectroscopy are limited due to the fact that fluorescence emission from most tissues normally overwhelms the weaker Raman signals. Even though there are several successful results reported using just a conventional Raman arrangement similar to that shown in Fig. 3.8. However, in studies of atherosclerotic lesions [39,40] and kidney stones [41,42], a significant fluorescence background have been reported. Other studies of gallstones report no or almost no fluorescence background [43,44]. Furthermore, results reported from Raman spectroscopy of human breast tissue show a very weak fluorescence background [45].

Nevertheless, fluorescence is in general a large problem, and may totally obscure weak Raman signals. Therefore, one most often have to use additional spectroscopic tricks to reduce the fluorescence contribution, among which the most common ones will be discussed in the following chapter.

3.4.4 Fluorescence reduction

Wavelength modulation or shifted excitation. The development of tuneable CW dye lasers has made it possible to modulate the excitation light. This can be used to reduce the influence due to fluorescence on the Raman spectrum [46], beacause, as the wavelength of the excitation laser light is modulated, the wavelength of the Raman signals are also modulated but the fluorescence background remains fairly constant. When viewed through a fixed monochromator this modulation of the exciting light leads to an intensity modulation of the scattered light proportional to the derivative of the spectral line intensity with respect to the wavelength. By using a scanning monochromator, or by scanning the center wavelength of the excitation light, in connection to phase sensitive detection, a simple but highly sensitive Raman spectroscopic system may be obtained [47].

A similar approach is to shift the excitation wavelength. By recording two spectra with slightly different excitation wavelengths and subtracting these two spectra, an almost fluorescence free difference spectrum is obtained. This difference spectrum is mainly a

derivative spectrum of the Raman spectrum and hence an integration of the difference spectrum yields a conventional Raman spectrum [48]. Another variant of the shifted excitation method is to choose the two used wavelengths so that one spectrum contains both the Raman lines and the fluorescence, while the other spectrum contains a pure fluorescence spectrum only [49].

Time-resolved Raman spectroscopy. Since Raman scattering and fluorescence exhibit different time characteristics (typically of the order of picoseconds for the former and nanoseconds for the latter) some kind of time-gated detection might be applicable. The principle of this technique is to excite the sample with short laser pulses and then detect the signal during the duration of the laser pulses. The long-lived fluorescence can in this way be efficiently suppressed. Another more complex time-resolved approach is to use a streak camera. In this case, one uses a picosecond laser pulse for the photo-excitation and a quasi-CW laser radiation (that is the second harmonic of a CW Q-switched laser) for probing. Raman scattering at each delay time is time-resolved and detected by the streak camera [50]. For a detailed description of time-resolved Raman spectroscopy reference [37] is warmly recommended.

UV-excitation. Another fluorescence reduction technique that may be sucessful is to excite the samples with ultra violet (UV) light. One obvious advantage with UV-excitation is an increased Raman intensity, as the Raman scattered intensity strongly increases with diminishing wavelength (c.f. Eqs. 3.28 and 3.29). The fluorescence spectrum is a broad envelope, most often without any structure, with the intensity maximum normally located anywhere in the visible region depending on the actual sample. By illuminating the sample with UV-light, which means that the excitation is outside the fluorescence envelope, it is in some cases possible to reduce the fluorescence background efficiently. On the other hand there are some important drawbacks with UV-excitation in connection to tissue measurements: The short excitation wavelength means a high energy of the illuminating light, which will increase the probability for photo-decomposition and hence the risk of cancerogenous changes of the tissue. Furthermore, there are several strongly absorbing tissue cromophores, such as adenine and hemoglobin, and some strongly fluorescent chromophores, such as tryptophan, in the UV-region. However good results have been reported on synthetic polymers with this method [51].

Near-infrared excitation. Near-infrared (NIR) excitation, as well as UV-excitation, implies an excitation outside the fluorescence envelope. Excitation in the NIR-region most often entirely eliminate the fluorescence background, since very few materials fluoresce when irradiated by NIR light. Another benefit of NIR excitation is that the low-energy NIR photons reduce photolytic or thermal damage of the sample. These advantages have a rather high cost, however, in form of a greatly reduced sensitivity for the Raman signals. Raman cross sections are, for instance, reduced by a factor of 18 when the laser wavelength is increased from 515 to 1064 nm, due to the $1/\lambda^4$ dependence of scattering cross sections. Furthermore detectors in the NIR-region have much higher noise than those in the visible, greatly affecting the signal-to-noise ratio (S/N). One remedy against the noise problem might be to use heterodyne detection. IR-detectors are usually single-channel photoconducting detectors. The sensitive wavelength domain depends on the detector material, which most often is a semiconductor material, such as Ge, InAs, InSb and InGaAs.

There are mainly three factors that determine the optimum choice of excitation wavelength: The background fluorescence, and the sensitivity and noise of the detector. During the last 5-10 years a very rapid development in especially filter technology has occurred, and a number of essential improvements in spectrometer and detector design have been done. These strong progresses in addition to the almost non-existent risk of photo-decompsition and cancerogenous changes of tissue, has made NIR Raman spectroscopy to an attractive tool in tissue diagnostics.

Fourier transform (FT) spectroscopy is a well suited detection technique for NIR Raman spectroscopy, yielding high resolution spectra with a single-channel detector. A typical FT-Raman arrangement is shown in Fig. 3.12a, and the basic principles of this type of interferometric spectrometer will be discussed in connection to infrared spectroscopy in chapter 3.5.8. The technique has been pursued actively because of some important advantages: An interferometer provides high resolution, wavelength accuracy, and relatively high throughput, in comparison to that achieved with most dispersive spectrometers. Such features are particularly useful for spectral subtraction and for spectra covering a wide wavelength range. An associated disadvantage of the FT-experiment is the distributed noise from Rayleigh-scattered light. The equivalent stray light rejection of a shot-noise limited Michelson interferometer is of the order of 10^{-3}, instead of the 10^{-9}-10^{-11} typical and necessary for other conventional Raman spectrometers. Hence an excellent laser line rejection filter must precede the interferometer in order to obtain FT-Raman spectra with an acceptable signal-to-noise ratio. However, this problem is normally easily solved with the excellent Rayleigh line rejection filter commercially available today.

In NIR-FT Raman spectroscopy it is convenient to use Nd:YAG laser excitation at 1064 nm in an effort to avoid the fluorescence background. The first successful results with NIR-FT Raman spectroscopy was reported in 1986 by Hirschfeld and Chase [52]. Nowadays NIR-FT Raman spectroscopy is a well established technique, frequently used in various applications. Fig 3.11b convincingly illustrates the potential of the NIR FT-Raman method.

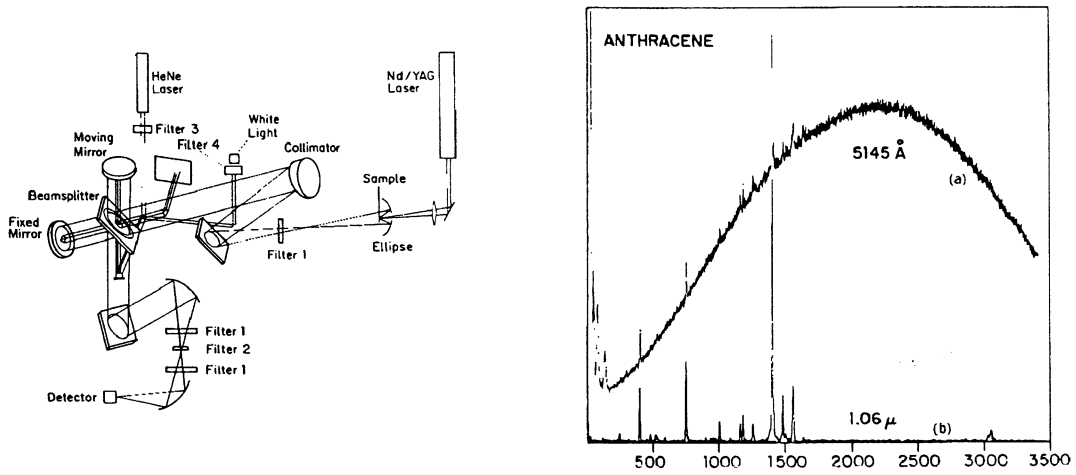

Fig 3.12 *(a) FT-Raman spectroscopy arrangement. (b) A comparisation between Raman spectra of anthracene recorded by a FT-Raman arrangement at 1064 nm excitation (lower spectrum) and with a conventional set-up at 514.5 nm excitation (upper spectrum). From Ref. [30].*

In addition to the previously mentioned disadvantages of NIR excitation, due to reduced sensitivity and detector noise, the rather high cost of the equipment and the moving mirrors of the interferometer also have to be mentioned in connection to NIR FT-Raman spectroscopy. Nevertheless NIR FT-Raman spectroscopy have been used for various tissue studies, e.g. gallstone [53], haemoglobin in blood [54], normal and atherosclerotic tissue [55,56] and normal and cancerous tissue [57].

FT spectroscopy is a scanning method, not compatible with multichannel detection. To better analyse all light, multichannel detection is to prefer. This can best be accomplished by using a grating spectrometer and a Charge Coupled Device (CCD) camera as a detector. The best sensitivity can with the presently available technology be obtained for 700-850 nm excitation, as CCD detectors have an extremely low noise level (higher S/N) and a high quantum efficiency in the 400 nm to 1050 nm spectral domain [58]. The multichannel detector may be either a one-dimensional array detector or a two-dimensional CCD detector. Most recent for NIR Raman spectroscopic operation is the CCD detector. A CCD detector consists of a matrix, commonly of the size 256×512 or 512×512, of sensitive elements (pixels), in which the photo-electrically generated charges are collected. If the pixel matrix is located in the focal plane of a spectrometer a spectrum is immediately obtained in the multichannel analyser (Optical Multichannel Analyser, OMA).

By shifting the excitation from 1064 nm to the 750-850 nm region, one can use the CCD to detect the Raman scattered signals while still avoiding fluorescence excitation in most molecules. Thus a Raman experimental set-up consisting of a CCD detector, a Rayleigh line rejection filter, and a single spectrometer in the 750-850 nm domain provides high optical throughput, high detection sensitivity and low noise, limited fluorescence background, relatively low cost, and a compact equipment without moving details. This kind of arrangement with a diode laser at 780 nm as a light source has been utilized to study Raman active samples with promising results [59,60].

The CCD/diode laser system can be modificated for use with a fibre-optic probe providing both excitation and collection of scattered light [61,62,63]. As reported by several laboratories for visible [38,64,65] and 1064 nm light [66,67], fibre-optic sampling greatly simplifies alignment, since a spectrum may be obtained merely by immersing the fibre-optic probe in the sample. Other benefits include reduced power density at the sample, due to the fact that a non-focused beam is employed, and the ability to measure signals from remote samples and in hostile environments. Hence fibre-optic sampling may paving the way for *in vivo* human applications. Fig 3.13 shows a Raman spectroscopy arrangement based on diode laser excitation, spectrometer and CCD detection.

Tuneable dye lasers or titanium sapphire lasers are other possible choices of excitation sources in the 750-850 nm region. These lasers in connection to CCD detection have been used in the study of atherosclerotic lesions [68,69], and in the resulting spectra the fluorescence background was not fully suppressed. Thus the 750-850 nm excitation is actually a compromise between fluorescence reduction and quantum efficiency of the CCD detector. A low fluorescence background is the prize one has to pay for the high sensitivity and extremely low noise when operating in this spectral region.

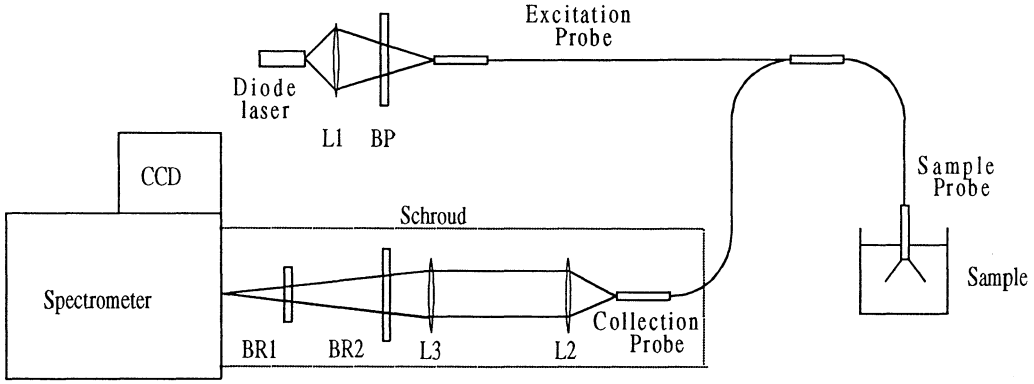

Fig 3.13 *Raman spectroscopy experimental set-up (L1, L2, and L3 are lenses and BR1, BR2, and BP are band rejection and band pass filters, respectively)*

3.4.5 The Raman spectrum

The most fundamental property of a Raman spectrum is that it contains information of the vibrational frequencies of the molecule. These vibrational frequencies is in a Raman spectrum manifested by more or less sharp spectral lines. Whether a particular line will occur in the Raman spectra or not depends on if the corresponding vibrational frequency (vibrational mode) is Raman active or not, which in turn depends on if the polarisability of the molecule changes during a vibration (c.f. chapter 3.3.2). For an asymmetric molecule it is easy to understand that the polarisability will vary for all vibrational modes, which implies that all vibrational modes are Raman active. For symmetric molecules, however, nothing generally can be said about whether the vibrational mode is Raman active or not.

In order to be able to predict which vibrational modes that may be present in a Raman spectrum, i.e. are Raman active, one has to resort to mathematical group theory. In group theory the symmetry of molecules is described by so-called point groups. Which point group a particular molecule belongs to depends on which symmetry operations that characterises the molecule. The point group may be evaluated by following a simple question-and-answer scheme. Such a scheme is displayed in fig. 3.14. A thorough description of group theory and point groups can be found in for instance Ref. [70].

However, some general conditions of molecules may be stated without any group theory involved: If a molecule has a centre of symmetry, vibrations can not be both Raman and IR active, vibrations that do not distort the molecule, i.e. symmetric vibrations, are intense in the Raman spectrum, in contrast to the conditions in the IR spectrum where the vibrations that maximise the distortion are most intense. Different types of vibrations are presented in chapter 3.2.2.

As an example of a Raman spectrum we can take a look at the Raman spectrum of water, which is shown in Fig. 3.15. The Raman spectrum of water is weak and rather featureless. This is an important fact, since water is present in almost all biological species or biochemical solutions. Therefore it is important that the contribution to the Raman signal due to water is weak and featureless. Furthermore, the Raman lines from water interferes very weakly with Raman spectrum of a solute, which is another lucky condition. The x-

axis in the Raman spectra represents an energy difference between the incoming laser light and the scattered light. From the water-spectrum in Fig. 3.14, it is obvious that more energy is required to excite the O-H stretching vibration than is required for the H-O-H bending vibration. In addition it is clear that the line due to the O-H stretch vibration are much stronger than the line due to the H-O-H bend (i.e. the O-H stretch is more probable than the H-O-H bend).

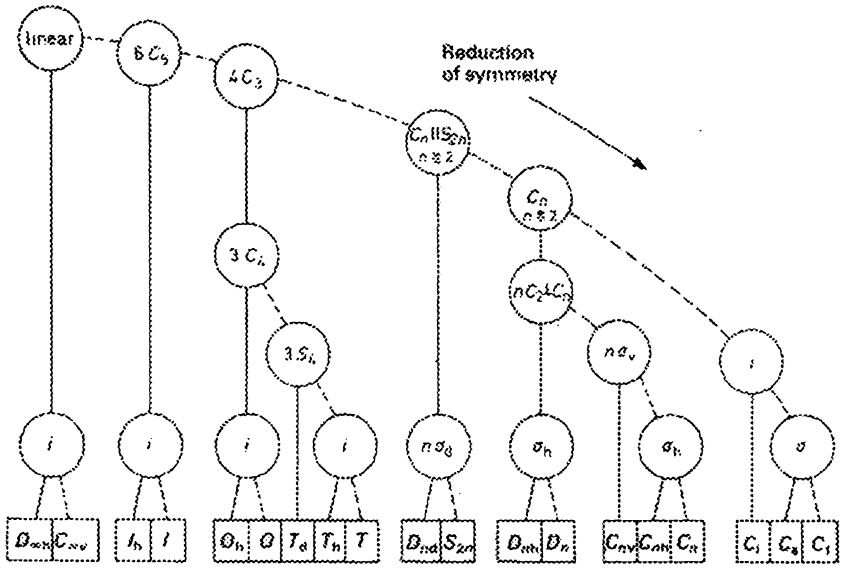

Fig 3.14 *An algorithm for determination of point groups. The correct point group is found by following a path according to the presence (straight line) or absence (dashed line) of symmetry elements.* C_n *denotes the axis of rotation of the highest order. From Ref. [22].*

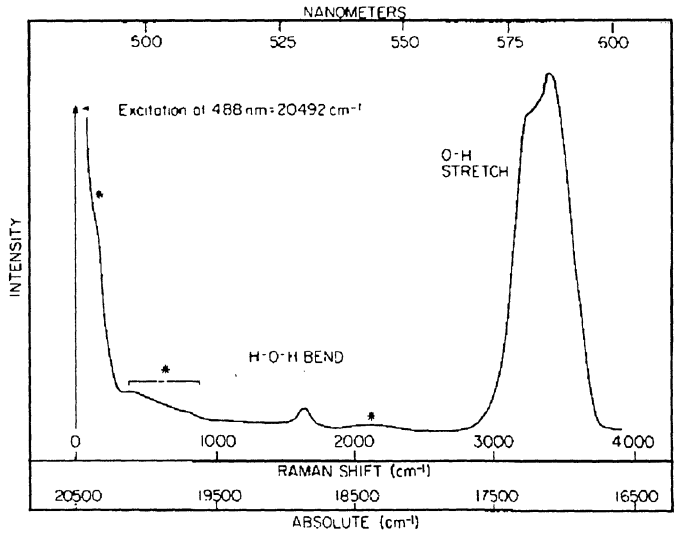

Fig 3.15 *Raman spectrum of water. The broad features marked with an asterisk are due to interactions between water molecules which are not completely understood. From Ref. [32].*

We conclude this chapter by some rules of thumb (from Refs. [71] and [72]):

1. Raman bands are generally more intense for stretching vibrations of covalent bonds than for deformation vibrations.
2. A Raman band assignable to a C=C stretching vibration is stronger than that assignable to a C-C vibration.
3. A Raman band becomes stronger with increase in atomic numbers of the atoms involved in the stretching vibration, all other things being equal.
4. If two bond-stretching motions are involved in a normal co-ordinate, the Raman bands are more intense if they take place in-phase as compared to if they take place with 180° phase difference. For a cyclic molecule, the Raman band assignable to a vibration in which all bonds forming the ring stretch and contract in-phase (ring breathing vibration) is usually the strongest one.
5. Approximative Raman intensities for some common structure elements are given in Table 3.3.

Table 3.3 *Rules of thumb for the approximation of intensities of Raman bands for some structure elements. Derived from Ref. [72].*

System	Structure element	Vibration	Intensity
X—Y	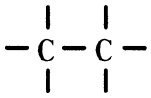	ν(C – C)	strong
	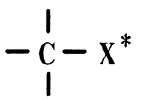	ν(C – X)	very strong
	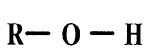	ν(O – H)	weak
X=Y	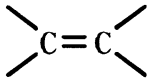	ν(C = C)	strong
	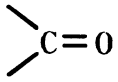	ν(C = O)	strong
X≡Y	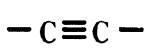	ν(C ≡ C)	strong
Y—X—Y	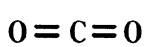	ν_s(OCO)	strong
	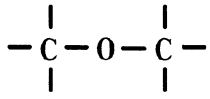	ν_{as}(COC)	weak
	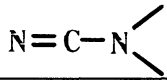	ν_{as}(NCN)	weak

* X = heavy atom

Exhaustive lists of vibrational Raman modes and their frequency range can be found in e.g. Refs. [70,72,73,74,75].

3.5 Infrared absorption spectroscopy

3.5.1 Introduction

Spectroscopy in the IR region can be used for qualitative as well as quantitative analysis. Qualitative analysis is performed by comparing a measured spectrum with a catalogued reference spectrum. Such reference spectra have been catalogued for a large number of compounds and substances. Quantitative analysis of a measured spectrum gives the possibility to identify different compounds or substances. The structures observed in the IR region are due to vibrational transitions in the molecules. These give rise to rather sharp spectral features, in comparison with those obtained for normal electronic transitions observed in the UV/Visible regions. The rotational transitions are quenched and thus normally only broadened vibrational transitions are observed. In a complicated molecule many fundamental frequencies, corresponding to different atomic groups, are obtained. This makes the identification of substances possible.

3.5.2 The vibrational bands

The simplest types, or modes, of vibrational motion in a molecule which are infrared active, i.e. give rise to IR absorptions, are the stretching and bending modes (see Sect. 3.2.2). However, other more complex types of stretching and bending can also be infrared active. In general, asymmetric stretching vibrations occur at higher frequencies than symmetric stretching vibrations. For example

CH_2 asymmetric stretch	CH_2 symmetric stretch
~ 2926 cm^{-1}	~ 2853 cm^{-1}

Also, stretching vibrations occur at higher frequencies than bending vibrations. For example

CH stretching	CH bending
~ 3000 cm^{-1}	~ 1340 cm^{-1}

If we recall Eq. (3.9) in Sect. 3.2.1 we found the natural frequency of vibration to be

$$\nu = \frac{\omega}{2\pi} = \frac{1}{2\pi}\sqrt{\frac{f}{\mu}} \tag{3.35}$$

From Eq. (3.35) we can immediately note two things. First, that a larger force constant (f) gives a higher frequency of vibration, and second that a bond between heavier atoms (which gives a larger reduced mass μ) gives a lower frequency of vibration. In general, triple bonds are stronger than double or single bonds between two atoms of the same type and will therefore have a larger force constant, and hence, a higher frequency of vibration. For example

C ≡ C	C = C	C - C
~ 2150 cm^{-1}	~ 1650 cm^{-1}	~ 1200 cm^{-1}

As the atom bonded to, for instance, a carbon atom increases in mass, the reduced mass increases and hence the frequency of vibration goes down. For example

C - H	C - O	C - Br
~ 3000 cm^{-1}	~ 1100 cm^{-1}	~ 550 cm^{-1}

Vibrations that arise from excitation from the ground state to the lowest energy excited state are called fundamental absorption frequencies. Usually the spectrum is complicated because the presence of weak overtone, combination and difference bands. Overtones result from excitation from the ground state to higher energy states which correspond to integral multiples of the frequency of the fundamental (ν). For example, one might observe weak overtone bands at 2ν, 3ν, ... When two vibrational frequencies ν_1 and ν_2 in a molecule couple to give rise to a vibration of a new frequency within the molecule, and when such a vibration is infrared active, it is called a combination band. These frequencies are the sum of the two interacting bands ($\nu_{comb} = \nu_1 + \nu_2$). Not all possible combinations occur. Selection rules exist that govern which combinations are allowed. Difference bands are similar to combination bands. The observed frequency, in this case, results from the difference between the two interacting bands ($\nu_{diff} = \nu_1 - \nu_2$). When a fundamental vibration couples with an overtone or combination band, the coupled vibration is called Fermi resonance. Again, only certain combinations are allowed. A description of the formation of infrared bands is given in Ref. [76].

3.5.3 The infrared absorption process

As with other types of energy absorption, molecules are excited to a higher energy state when they absorb infrared radiation. The absorption of infrared radiation is, like other absorption processes, a quantized process. Only certain frequencies of infrared radiation will be absorbed by a molecule. Radiation in this energy range corresponds to the range encompassing the stretching and bending vibrational frequencies of the bonds in the molecule. In the absorption process, only those frequencies of infrared radiation which match the natural vibrational frequencies of the molecule in question will be absorbed. The molecule absorbs the radiation energy by increasing its own vibrational energy, i.e. the amplitude of its vibrational motion is increased.

While the absorption frequency depends on the molecular vibrational frequency, the absorption intensity depends on how effectively the infrared photon energy can be transferred to the molecule, and this, in turn, depends on the change in the dipole moment that occurs as a result of molecular vibration. Only molecules or molecular bonds which have a dipole moment are capable of absorbing infrared radiation. The electrical dipole moment must be changing at the same frequency as the incoming radiation in order for energy to be transferred.

Since the wavelength of infrared radiation is far greater than the size of most molecules, the electrical field of the photon in the vicinity of a molecule can be considered uniform over the whole molecule. The electrical field of the photon exerts forces on the molecular charges and by definition the forces on opposite charges will be exerted in opposite directions. Therefore the oscillating electric field of the photon will exert forces tending to change the spacing between the centers of charge, thereby tending to induce the dipole moment of the molecule to oscillate at the frequency of the incoming photon. The more

the dipole moment changes during a vibration, the more easily the photon electric field can activate that vibration. If a molecular vibration should cause no change in dipole moment then a forced dipole moment oscillation cannot activate that vibration. This can be summarized in the selection rule that in order to absorb infrared radiation, a molecular vibration must cause a change in the dipole moment of the molecule. It can be shown that the intensity of an infrared absorption band is proportional to the square of the change in dipole moment, with respect to the change in the normal coordinate $(\partial\mu/\partial Q)^2$ of the molecular vibration, giving rise to the absorption band [70].

3.5.4 Applications of the infrared spectrum

Since every different type of molecule, or bond in a molecule, have a different natural frequency of vibration, and since the same type of bond in two different compounds is in a slightly different environment, no two molecules of different structure will have exactly the same infrared absorption spectrum. Although some of the frequencies absorbed in the two cases might be the same, in no case of two different molecules will their infrared spectra be identical. By comparing the infrared spectra of two substances thought to be identical, one can establish whether or not they in fact are identical. If their infrared spectra coincide peak for peak, the two substances will, in most cases, be identical.

A second and more important use of the infrared spectrum is that it gives structural information about a molecule or a substance. The absorptions of each type of bond are regularly found only in certain small portions of the vibrational infrared region. A small range of absorption can be defined for each type of bond. Outside this range, absorptions will normally be due to some other type of bond.

3.5.5 Sources of infrared radiation

All IR spectrometers have a source of infrared radiation which is usually some solid material heated to incandescence by an electric current. The Nernst Glower is a source composed mainly of oxides of rare earth metals such as zirconium, yttrium and thorium, and the Globar is a silicon carbide rod. Other materials have been used aswell. All these sources are fairly efficient emitters of infrared radiation and approach the energy distribution of a theoretical black body.

Planck´s distribution law for blackbody radiation, giving the radiant energy between the wavelengths λ and $\lambda+d\lambda$, may be expressed in the form

$$M_e d\lambda = \frac{c_1 \lambda^{-5}}{e^{c_2/\lambda T} - 1} d\lambda \qquad (3.36)$$

where λ = the wavelength
$c_1 = 2\pi c^2 h$
$c_2 = ch/k$
c = the speed of light
h = Planck´s constant
k = Boltzmann´s constant
T = the absolute temperature
$M_e d\lambda$ = radiant energy emitted per unit volume

Wien's displacement law gives the wavelength λ_m at which the energy is at a maximum at a given temperature T

$$\lambda_m = \frac{b}{T} \tag{3.37}$$

where b = Wien's displacement constant.

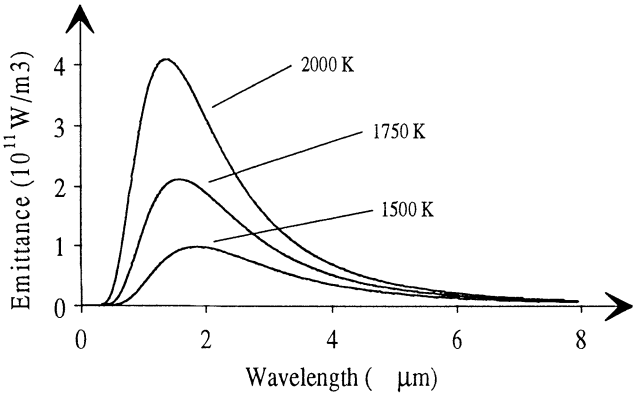

Fig 3.16 *The energy distribution of a theoretical blackbody radiator at some different temperatures.*

It is important to note that the energy output falls off rapidly at long wavelengths. If one tries to increase the long wavelength energy by increasing the temperature of the light source, a small increase in long wavelength energy will be accompanied by a huge energy increase in the unwanted short wavelengths. Most IR sources are operated at a temperature where the energy maximum is near the short wavelength limit of the spectrum. The Nernst Glower, for instance, is usually heated to 1500-2000 K.

3.5.6 Infrared detectors

The infrared detector is a device which measures the infrared energy of the source which has passed through the spectrometer. One way or another these devices change radiation energy into electrical energy which can be processed to generate a spectrum. There are two basic types, thermal detectors which measure the heating effects of radiation and respond equally well to all wavelengths, and selective detectors whose response is markedly dependent on the wavelength.

Examples of thermal detectors include thermocouples, bolometers and pyroelectric detectors. A thermocouple has a junction of two dissimilar metals. When incident radiation is absorbed at the junction, the temperature rise causes an increase in the electromotive potential developed across the junction leads. A bolometer is a resistance thermometer with a platinum wire or a thermistor as a sensor. It detects the change of resistance with temperature.

The pyroelectric detector consists of a thin pyroelectric crystal such as lithium niobate. A pyroelectric crystal give rise to an electrical potential between opposite surfaces when heated. Pyroelectric detectors are well suited for Fourier Transform Infrared (FTIR) spectrometers.

The most important type of selective detector is the photoconductive cell which has a very rapid response and high sensitivity. These cells show an increase in electrical conductivity when illuminated by infrared light. Especially common is the lead sulphide (PbS) cell, which operates at room temperature. Detectors made of indium arsenide (InAs) or indium antimonide (InSb) are, however, considerably faster than the PbS cell but are frequently cooled to liquid nitrogen temperatures (77 K). Further down in the IR region cooled mercury cadmium telluride (HgCdTe) detectors are used. More about IR detectors can be found in e.g. Ref. [77].

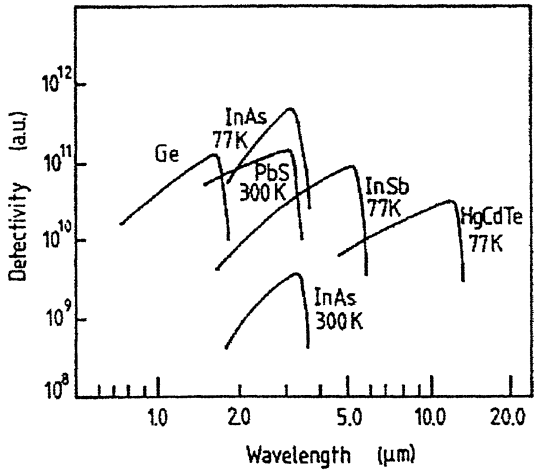

Fig. 3.17 *Sensitivity curves for some different infrared detector materials. From Ref. [28].*

3.5.7 Monochromators

Between the source and detector, there must be some kind of device to analyze the radiation so that an intensity can be evaluated for each wavelength resolution element. There are two basic types, namely, monochromators, used in dispersive instruments, and interferometers used in Fourier transform instruments.

In a monochromator, a prism or grating is used which separates the components of polychromatic radiation by bending the radiation by an amount that varies with wavelength. The radiation enters the monochromator through an entrance slit and the radiation beam is made parallel by a suitable mirror or lens. The parallel undispersed radiation approaches the prism or grating at one angle and leaves at angels that vary with the wavelength of the dispersed radiation. The dispersed spectrum is then focused by a mirror or a lens onto an exit slit. In the prism monochromator the exit slit allows only one wavelength element to pass through and reach the detector while blocking other wavelengths. Then, the spectrum (which is focused on the exit slit) is shifted slightly so that a different wavelength element passes through to the detector. The whole spectrum is thus measured one wavelength at a time. In the grating monochromator the same steps happen, except that the exit slit allows one wavelength, and also multiples of that wavelength, to pass through. The unwanted wavelength multiples are removed, usually by a selective filter, before the radiation reaches the detector. By rotating the grating slightly, the path length difference for adjacent grooves will be changed slightly and a slightly different wavelength will reach the detector. The spectrum is recorded one wavelength

resolution element at a time. Usually for the whole spectral range, more than one grating is used, and more than one grating order may also be used.

The monochromator generates a singlebeam spectrum where the vertical coordinate is radiation energy as a function of wavelength or wavenumber reaching the detector. In doublebeam spectrometers, the monochromator alternately measures source radiation intensity with and without sample absorption for each wavelength or wavenumber resolution element of the spectrum. From this, the instrument generates a percent transmission spectrum.

Grating instruments have better resolution than those with prisms. A potential disadvantage of a grating for infrared instrumentation is that the grating, unlike the prism, distributes energy into unused orders. However, this disadvantage can be largely overcome by controlling the shape of the grooves to a specific blaze angle, which can concentrate the energy in the desired region of the spectrum for a given order.

3.5.8 The Michelson interferometer

The Fourier transform spectrometer is a dual-beam interferometer, which is most frequently of the Michelson type. As shown in Fig. 3.17 the Michelson interferometer consists of two plane mirrors, one fixed and one moveable, and a beam splitter. One type of beam splitter is a thin layer of germanium on an IR transmitting support. The radiation from the source is made parallel and as seen in Fig. 3.17 then strikes the beam splitter at 45°. The beam splitter has the characteristic that it transmits half of the radiation and reflects the other half. The transmitted and reflected beams from the beam splitter strikes the two mirrors oriented perpendicular to each beam, and are reflected back to the beam splitter. Interference occurs at the beam splitter where the radiation from the two mirrors combine. While the monochromator described earlier generates a spectrum, an interferometer produces an interferogram from which a spectrum is generated by a Fourier transform.

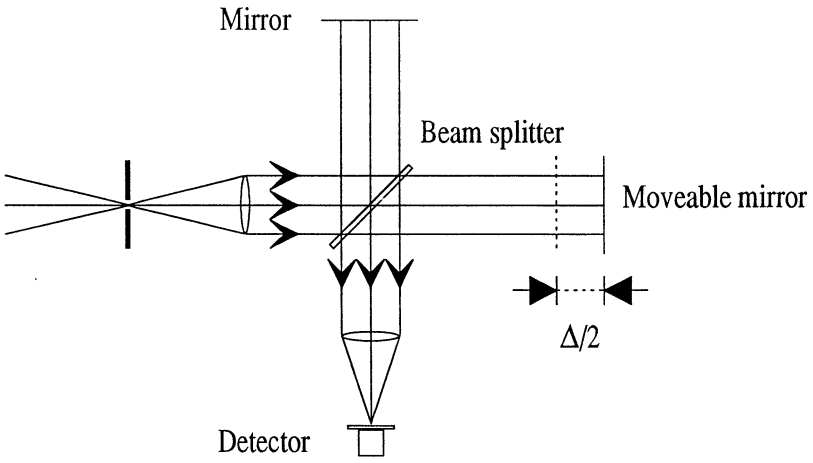

Fig.3.17 *A Fourier transform spectrometer of the Michelson type.*

If the arms of the interferometer have equal lengths the path difference between the two interfering beams would be zero. If the movable mirror is moved Δ/2 an optical path

difference of Δ is introduced. For the case of monochromatic radiation and equally intense beams the intensity at the detector will be

$$I(\Delta) = I_0 \cos^2(\frac{\Delta}{c}\pi\nu) \tag{3.38}$$

If the light source emits a spectrum $B(\nu)$ we then obtain

$$I(\Delta) = \int_0^\infty B(\nu)\cos^2(\frac{\Delta}{c}\pi\nu)d\nu = \frac{1}{2}\int_0^\infty B(\nu)\left[1+\cos(\frac{\Delta}{c}2\pi\nu)\right]d\nu \tag{3.39}$$

The Δ-dependent part of Eq. (3.39) is called the interferogram

$$J(\Delta) = \frac{1}{2}\int_0^\infty B(\nu)\cos(\frac{\Delta}{c}2\pi\nu)d\nu \tag{3.40}$$

The spectrum $B(\nu)$ can be calculated from the interferogram $J(\Delta)$ as its Fourier cosine transform

$$B(\nu) \propto \int_0^\infty J(\Delta)\cos(\frac{\Delta}{c}2\pi\nu)d\Delta \tag{3.41}$$

Such a calculation is conveniently performed on a computer and special, very fast processors have been constructed. In practice, the moveable mirror can only be moved a limited distance and therfore the integration must be performed over a finite interval. Such a limited integration gives rise to side maxima on the spectral lines. By using a mathematical trick, which involves the multiplication of the integrand in eq. (3.40) by a particular function, the unwanted side maxima can be suppressed. However, this procedure, which is called apodization, gives rise to broader spectral lines.

One of the great advantages of Fourier transform spectroscopy is that all spectral lines are recorded at the same time (the multiplex or Felgett advantage). Further, a Fourier transform spectrometer has a comparatively high light collecting efficiency, since it does not require narrow slits to separate and collect information at a particular wavelength at a particular time (the Jaquinot advantage).

The sample is normally placed between the interferometer and the detector. The spectrum generated is a singlebeam spectrum where the vertical coordinate is the radiation intensity from the source after sample absorption, measured as a function of radiation wavelength or wavenumber. In order to generate a percent transmission spectrum, the sample singlebeam spectrum is stored in the computer and is later ratiod with a reference singlebeam spectrum generated without the sample present. A single scan of the moveable mirror produces a complete singlebeam spectrum. However, usually a number of scans are taken and averaged by the computer, which reduces the noice by the square root of the number of scans. The evolution of Fourier transform infrared spectroscopy is given in Ref. [78].

4 Material and methods

4.1 The Raman experiment

4.1.1 The experimental setup

The experimental arrangement is shown in Fig. 4.1. The setup consisted of five components: an excitation source, a fibre-optic sampler, collection optics, a spectrometer, and a CCD detector system.

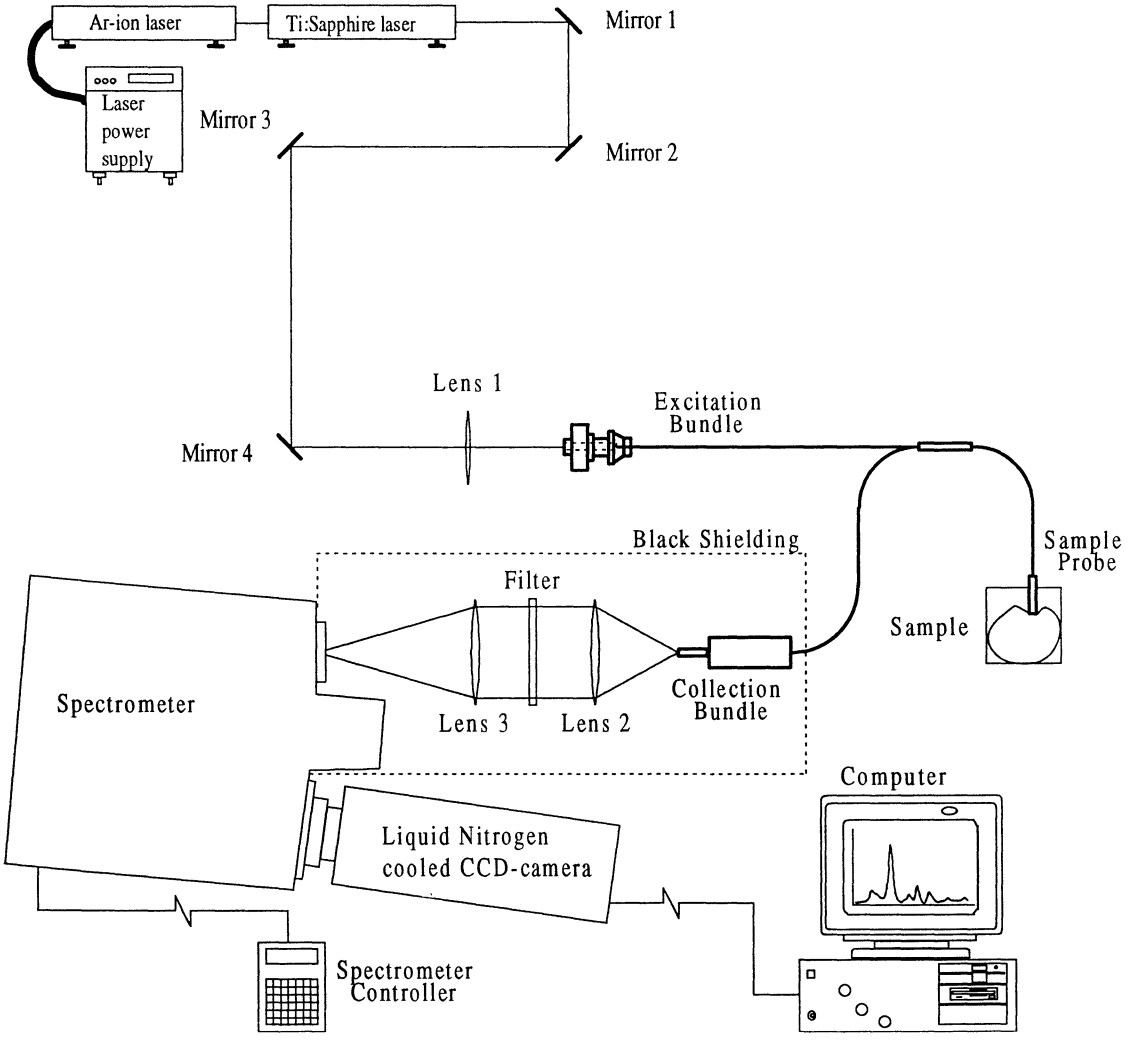

Fig 4.1 *The experimental setup was based on continous wave excitation using a Ti:Sapphire laser and a fibre-optic sampler. Mirrors 1-3 were gold coated, while Mirror 4 was of aluminum. Lens 1 was a ∅ 50 mm f/1.66 plano-convex collimating and focusing lens, Lens 2 was a ∅ 25.4 mm f/2 plano-convex collimating lens, and Lens 3 was a ∅ 20.0 f/2 plano-convex lens. The filter was a notch plus filter.*

The excitation source. The light source was a Ti:Al_2O_3 (Ti:Sapphire) laser pumped by an Ar^+ laser. The Ti:Sapphire laser was a Coherent Mira 900, while the pump laser was a Coherent Innova 400. The Mira is a laser oscillator normally used in order to generate ultra short mode-locked high-power pulses. The mode-locking device in Mira is based on a Kerr cell requiring two components: one non-linear Kerr cell which decreases the laser beam diameter if the laser intensity is high enough, i.e. during the mode-locked pulses, and a slit which introduces losses for beams with larger diameters. Roughly one may say that a large beam diameter corresponds to continous wave (CW) operation, while the beam diameter is reduced for mode-locked operation. In order to get a CW beam, the slit was open during operation. The excitation wavelengths used were 792.5 nm and 794.0 nm. The excitation wavelength was easily changed since the Mira light was tunable. The output power of the Mira laser was measured to be 1.0 W.

The fibre-optic probe. The fibre-optic probe was manufactured by C-technologies (772 Bloomfield Avenue, Verona, New Jersey 07044), and primarily designed for fluorescence measurements. However, it has shown to be useful for Raman spectroscopy as well. The probe model was SFA 371-541L-1-01, which stands for a fluorescence assembly probe composed of 37 100 μm excitation fibres in a cirkular array, surrounded by 54 other 100 μm core fibres in the sample probe, with a linear array at the detection end towards the spectrometer slit, and that the fibre is 1 meter long and operates in the UV-visible region. The excitation light was focused on the excitation fibres with a collimating and focusing lens, made of Suprasil (Lens 1 in Fig. 4.1). The laser light power, measured just in front of the focusing lens (Lens 1 in Fig. 4.1), was 650 mW, of which 110 mW reached the sample. The main power losses occurred in the aluminum mirror (Mirror 4 in Fig. 4.1) and in the coupling to the excitation probe.

The collection optics. The collection optics was composed of two lenses (Lens 2 and 3 in Fig 4.1) and a filter. Lens 2 was aimed to collimate the scattered light, while Lens 3 was used to focus the light onto the entrance slit of the spectrometer. Lens 2 was a ∅25.4 mm f/2 plano-convex lens, while Lens 3 was a ∅20.0 mm f/2 plano-convex lens. Both lenses were made of Suprasil. The Rayleigh scattered light was suppressed with a Raman holographic notch plus filter (HNPF-795-1.0) manufactured by Kaiser Optical Systems Inc. Before entering the spectrometer this notch plus filter provided a very efficient Rayleigh line rejection, with an optical density, OD larger than 6.0 at 795 nm, a bandwidth less than 20 nm between the 50% transmission points, and a transmission larger than 80% outside the notch plus filter. It is possible to use holographic notch plus filters at other laser wavelength than the one specified, since they have a tilt and tune capability. Since the excitation wavelengths were 792.5 nm and 794.0 nm, which is very close to 795 nm, it should not be necessary to tilt the filter. However some minor tilting was required for optimization. Furthermore it was important to collimate the light in front of the filter, because otherwise the light will pass the filter in different angles and hence with different attenuation.

The spectrometer. The spectrometer was a Spex 270M single-stage imaging spectrometer with a focal length of 270 mm and f/4. Two different gratings were available in the spectrometer: a 150 g/mm grating blazed at 500 nm, and a 1200 g/mm grating blazed at 750 nm, with a dispersion of 24.8 nm/mm and 3.1 nm/mm at the focal plane, respectively. The width of the entrance slit of the spectrometer could be set in steps of 6.25 μm

between 0 μm and 7000 μm. All moving parts of the spectrometer were controlled remotely by a hand controller.

The CCD detector system. The CCD detector was an OMA-Vision CCD detecor manufactured by EG&G Princeton Applied Research. The entire detector system was composed of a CCD camera (Thomson CSF THX-31159 A), an OMA-Vision controller board, an OMA-Vision power block, and a personal computer (PC). The wavelength range of detector operation was 400 nm - 1100 nm. The image sensor device of the CCD camera was composed of a matrix array of 512 columns by 512 horizontal rows (512×512) of charge-coupled pixels. The entire CCD array size was 9.7 mm×9.7 mm and each pixel size was 19 μm×19 μm. Each pixel column was electronically "binned", which means that they were summed before readout, forming a multichannel detector with 512 channels of 9.7 mm height. Since the dispersions were 24.8 nm/mm for the 150 g/mm grating and 3.1 nm/mm for the 1200 g/mm grating, the corresponding spectral coverage obtained were about 240 nm and 30 nm, respectively. Thus, the spectral coverage counted in wavenumbers from the 792.5 nm laser line was about 2900 cm^{-1} for the 150 g/mm grating and 460 cm^{-1} for the 1200 g/mm grating. The CCD camera was cryogenically cooled with liquid nitrogen. The CCD camera could be cooled in the temperature range from -80 °C to -140 °C. Since the dark current decreases with temperature, it is of great importance to keep the temperature as low as possible. The lowest possible temperature should be -140 °C, according to the manufacturer specifications, but the CCD detector could actually not lock at this temperature at all. However, there was no problem to keep the detector at -130 °C. Hence, all Raman spectra recorded were measured with the CCD held at -130 °C. The temperature hold time at this temperature was more than 5 hours and the dark current should, according to the detector manual, be below 10 photoelectrons per pixel and hour. The CCD camera was controlled by an acquisition and data handling software (OMA Spec 4000 Applications Software).

4.1.2 Data analysis

Raman spectra were typically measured between 350 cm^{-1} and 1800 cm^{-1} below the laser excitation frequency. Both the 150 g/mm and 1200 g/mm grating were utilized. The actual grating is indicated in each presented spectrum. Because of the limited spectral coverage of the 1200 g/mm grating the spectra recorded with this grating were composed of 5 succesively recorded spectra.

Each spectrum was background subtracted but not corrected for the wavelength dependent response of the filter, spectrometer, and CCD detector.

The entrance slit width of the spectrometer was constantly 50 μm and the Raman signals were accumulated for 30 seconds and 150 seconds, respectively, in all measurements except one, in wich spectra were recorded with the integration times 10 ms, 100 ms, 1 s, 10 s, and 30 s. The actual integration time is indicated in each presented spectrum. Raman frequencies were calibrated with the spectrum of an argon lamp.

In order to remove the fluorescence emission background of the highly fluorescent tissue sample and thereby extract the much weaker Raman signals, a shifted excitation difference technique was utilized. This technique utilizes the fact that the Raman band positions vary directly with the excitation frequency, while the fluorescence emission

remains fairly constant with small changes in excitation frequency. In contrast with mathematical filters, this operation requires no assumptions about the emission line shape. To implement this approach, we recorded the Raman spectrum with excitation wavelengths of 792.5 nm and 794.0 nm. The Raman bands then were shifted with the excitation wavelength by 1.5 nm or about 25 cm^{-1}, which corresponded approximately to the width of the tissue Raman bands, while the fluorescence emission remained fairly constant. In order to compensate for changes in laser power and scattering intensity between the two recordings, the two spectra were scaled to the same total area before subtraction. Then the spectrum recorded with 794.0 nm excitation was subtracted from the spectrum recorded with 792.5 nm excitation, which yielded an almost fluorescence free difference spectrum with much more readily observed Raman bands. Eventually the difference spectrum was integrated to form a conventional Raman spectrum. The operation of this method was mathematically analogous to taking the derivative of the Raman spectrum and then by integrating the difference spectrum the original Raman spectrum could be recovered. The accurancy of this method primarily depended upon the high linearity and stability of the CCD detector.

4.2 The near infrared absorption experiment

The experimental arrangement was very compact and consisted of a Bomem DA8 Fourier Transform Infrared (FTIR) spectrometer, with an InSb detector, completed with a fitting software (Bomem Research Analytical Software) for instrumental control, accessory set up, data collection, data archiving, data interpretation, and plotting of results. The optical configuration of the FTIR spectrometer is shown in Fig. 4.2.

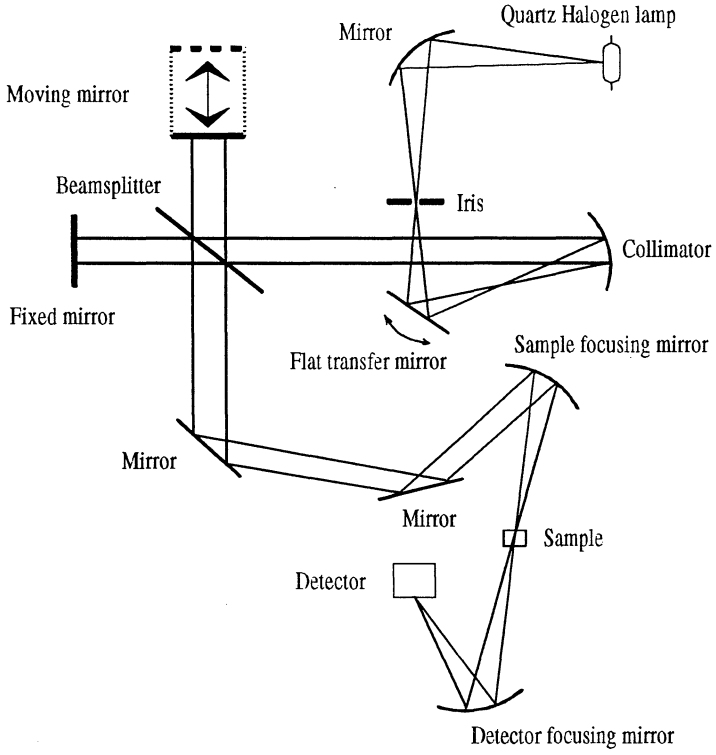

Fig 4.2 *The optical configuration of the FTIR spectrometer.*

The Bomem DA8 FTIR spectrometer. This spectrometer is a commercial instrument manufactured by Hartmann and Braun (450 St-Jean-Baptiste, Québec, Canada G2E5S5). DA stands for dynamic alignment of the interferometer fixed mirror. The interferometer is a flat mirror Michelson type with a maximum unapodized resolution of 0.026 cm^{-1}, a wavelength range between 4 cm^{-1} and 55000 cm^{-1}, and a resolving power of 10^6 at any frequency. The optical layout is along a vertical axis, providing a small "footprint" for the instrument and good access for several experimental setups. Three water-cooled light sources, two focused sample positions, and three collimated outputs are available by computer-controlled selection mirrors. The optical configuration displayed in Fig. 4.2 is thus a modified picture containing just the optical components actually utilized in our experiment. Other notable features include a 30 degree incidence beamsplitter (which reduces the beamsplitter size and cost, and reduces polarization effects, but slightly narrows the usable spectral range), an aperture of the size range 0.5 mm to 10 mm in diameter in 8 computer selectable steps. Further data that have to be mentioned are that the absolute frequency accuracy at 2000 cm^{-1} is ± 0.004 cm^{-1}, the frequency repeatability at 2000 cm^{-1} is ± 0.0002 cm^{-1}, and the scanning speed of the movable mirror in the interferometer can be set in 11 steps from 0.04 cm/s to 2 cm/s.

The hardware. The DA8's overall controll is achieved by a built-in 80286 (Intel) based controller which includes a standard ThinWire Ethernet interface, a serial port interface for interferometer control, a coading memory, and an array processor. The controller interprets the commands, controls acquisition and numerical processing, and transfers the spectral data to the network. The numerical processing implies Fourier transforming and digital filtering. The digital filtering of incomming interferograms can significantly reduce the number of data points to be stored when the spectral range of interest is narrow. A VAX 3100 workstation is used as a host computer.

In our experimental setup the light source was a quartz halogen lamp emitting in the spectral region from about 4000 cm^{-1} to 20000 cm^{-1}, that is the near infrared (NIR) region. The spectral irradiance as a function of the wavenumber for the quartz halogen lamp is displayed in Fig 4.3 (the middle curve).The beamsplitter utilized was TiO_2-coated. The beamsplitter of a Michelson interferometer is of crucial importance, since it determines the wavelength region. The quartz TiO_2-coated beamsplitter provided good reflectivity and low absorption in the spectral region from 4000 cm^{-1} to 20000 cm^{-1}, which can be seen in the lower curve of Fig. 4.3. The detector was an InSb detector. This detector provided high detectivity in the region from 2000 cm^{-1} to 20000 cm^{-1}, illustrated by the upper curve in Fig. 4.3.

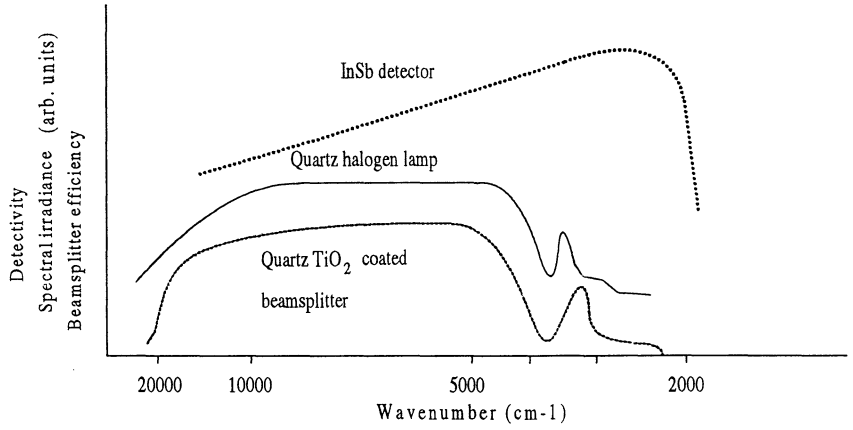

Fig 4.3 *Efficiency curves for the detector, light source, and beamsplitter.*

With the previously mentioned choises of light source, beamsplitter, and detector, spectra in the NIR region were recorded. In order to obtain a good signal-to-noise ratio, all spectra were collected at 2 cm^{-1} resolution with 500 scans. 500 scans implied a collection time of 5 minutes. The spectra were typically recorded between 4000 cm^{-1} and 10000 cm^{-1}.

4.3 The samples

Solvents.. In order to explore the ability of the experimental arrangement and to optimize it, four different solvents were used as samples in the initial Raman measurements. The solvents used were: nitrobenzol ($C_6H_5NO_2$), 1,2-dichlorbenzol ($C_6H_4Cl_2$), 1,4-dioxane ($C_4H_8O_2$), and toluene (methylbenzene C_7H_8). Nitrobenzol and toluene are both monosubstituted benzenes, while 1,2-dichlorbenzol and 1,4-dioxane are disubstituted benzenes. Monosubstituted benzene means that one atom, either a hydrogen or a carbon atom, of the benzene ring is substituted, and hence disubstituted benzene means that two atoms are substituted. The structure formulas of the four solvents are shown in Fig 4.4.

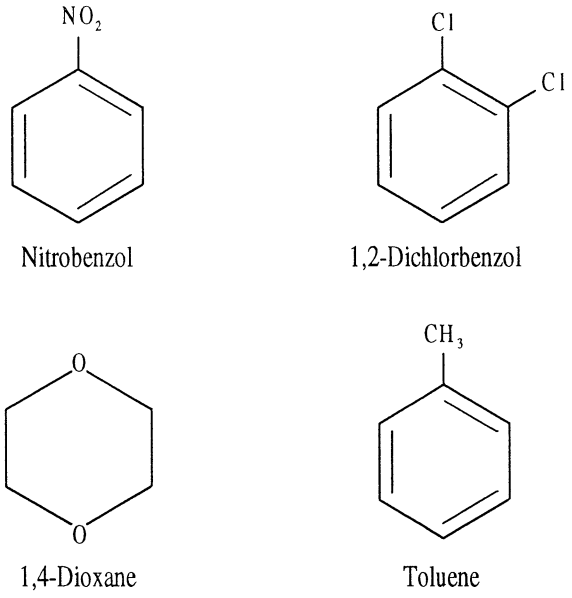

Fig. 4.4 *The structures of nitrobenzol, 1,2-dichlorbenzol, 1,4-dioxane, and toluene.*

The samples of collagen, elastin, cholesterol, and NADH, were all delivered by Sigma Chemical Company (P.O. Box 14508, St.Louis, MO 63178, USA). The number in prenthesis after each sample is the product number.

Collagen. Since the collagens are the most abundant protein of the body it was quite obvious to record spectra of a collagen sample. The sample chosen for this purpose was a collagen I powder from bovine achilles tendon (C 9879).

Elastin. Elastin is also a very abundant protein of human tissue. Spectra of elastin was recorded with a sample of elastin from bovine neck ligament (E 1625).

Cholesterol. Cholesterol ($C_{27}H_{46}O$) was one of the samples that was probed, and the reason for investigating that was the fact that free cholesterol occurs in biological tissues under pathological conditions, e.g. in advanced *atherosclerotic plaques*. The cholesterol sample used was a pure solid cholesterol powder (C 8667).

NADH. The NADH (nicotineamide adenine dinucleotide in reduced form, $C_{21}H_{27}N_7O_{14}P_2Na_2$) sample was a β-NADH powder (N 6005). Malignant tissue with an elevated growth rate has a shifted balance between NAD^+ and NADH and may therefore contain a different amount of NADH compared to normal tissue. Thus it was interesting to study NADH.

Tissue samples. Samples of biological tissue were taken from a pig heart and other cured meats, bought at a local supermarket and butchery. The samples were cooled and kept at $+8^oC$ not longer than two days after sacrifice. We selected specimens of aorta from the pig heart, and fat and muscle from the other meats. All samples were probed at room temperature.

5 Results

5.1 The Raman experiment

5.1.1 Solvents

To examine the ability of the experimental arrangement the first measurements were done on comparatively highly Raman active liquids with distinct spectral lines. Appropriate specimens were nitrobenzol, 1,2-dichlorbenzol, 1,4-dioxane, and toluene. In the first measurements the 150 g/mm grating was utilized and the integration time was 30 seconds. The Raman spectra recorded are shown in Fig. 5.1 and 5.2.

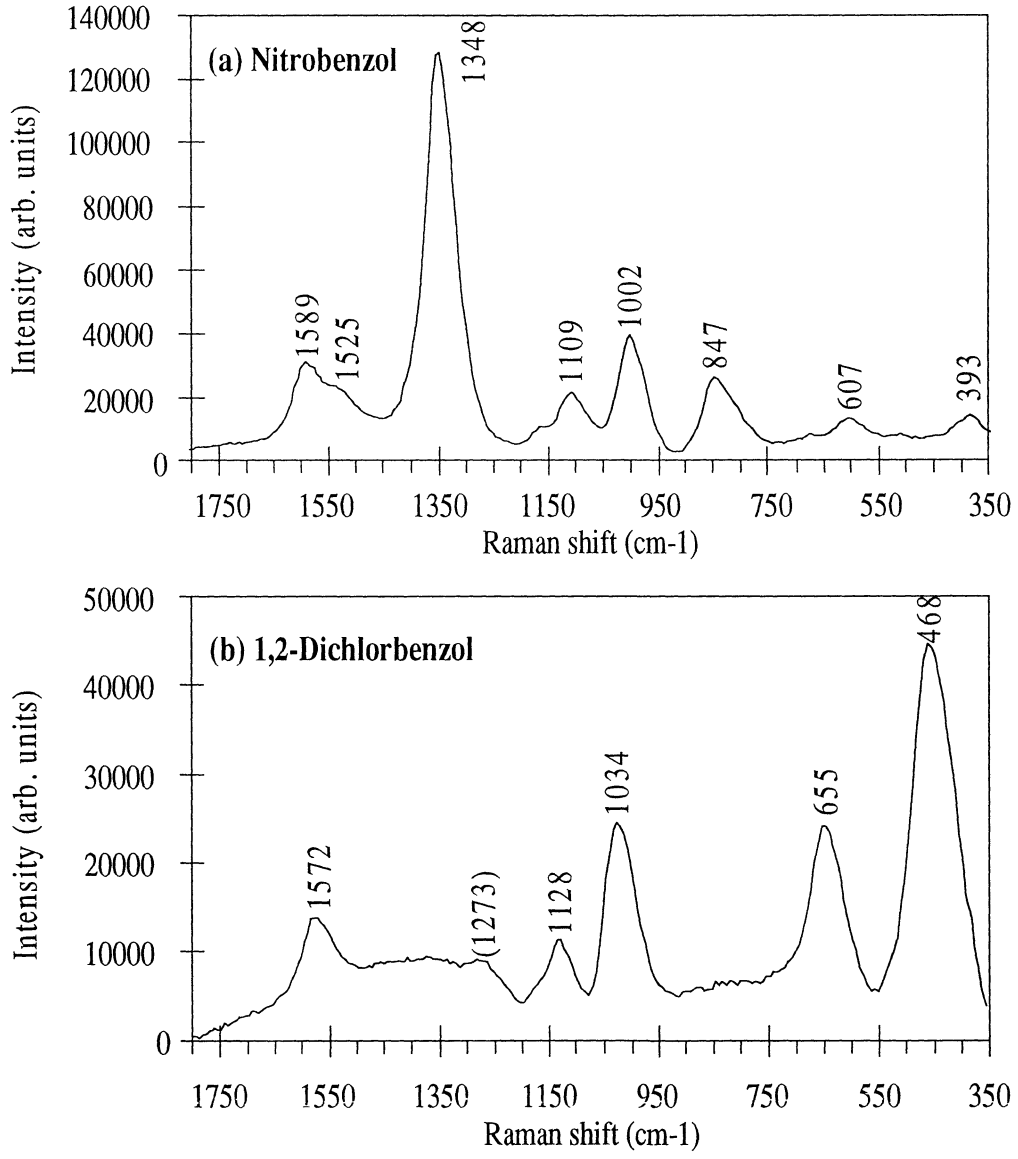

Fig 5.1 *Raman spectrum of (a) nitrobenzol and (b) 1,2-dichlorbenzol with 792.5 nm excitation, 50 μm slit width, and 30 seconds integration time.*

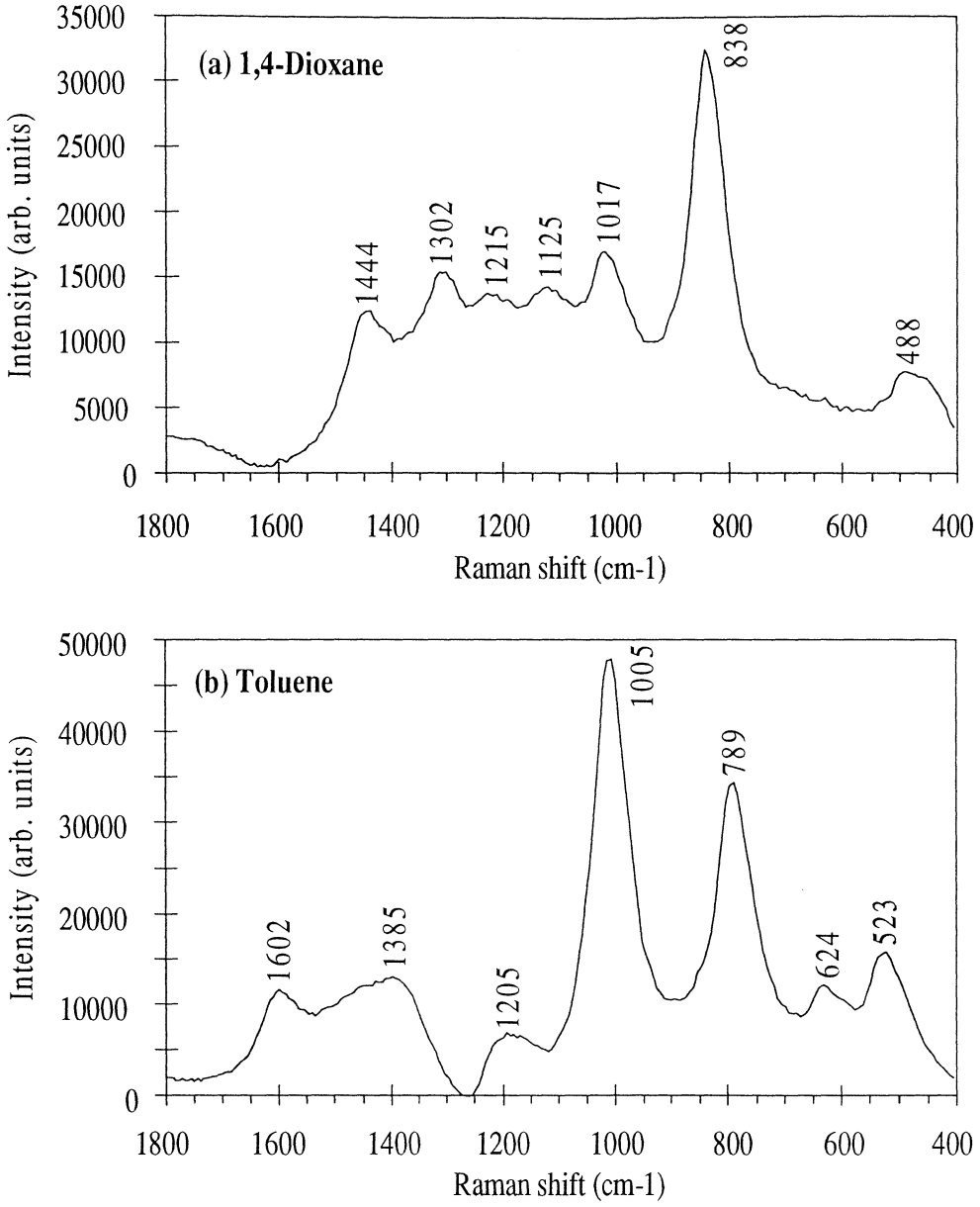

Fig 5.2 *Raman spectra of (a) 1,4-dioxane and (b) toluene with 792.5 nm excitation, 50 μm slit width, 150 g/mm grating, and 30 seconds integration time.*

It is obvious from these first results that the experimental setup actually worked very well. However, it is also apparent that the resolution of the grating is not sufficiently high to resolve all Raman lines, resulting in broad spectral lines and hence a significant uncertainty in the determination of Raman frequencies. Nevertheless most of the vibration modes are represented in these spectra. The observed Raman shifts are partly marked in the figures and partly listed in Table 5.1 and 5.2. As mentioned above all spectra were recorded with 30 seconds integration time, and because the integrationtime should be as short as possible with an acceptable signal-to-noise ratio, it would be of great interest to investigate how much the integration time could be lowered. Therefore spectra of nitrobenzol with 10 ms, 100 ms, 1 s, 10 s, and 30 s integration time, but still the same illuminating power, were recorded. These spectra are displayed in Fig. 5.3.

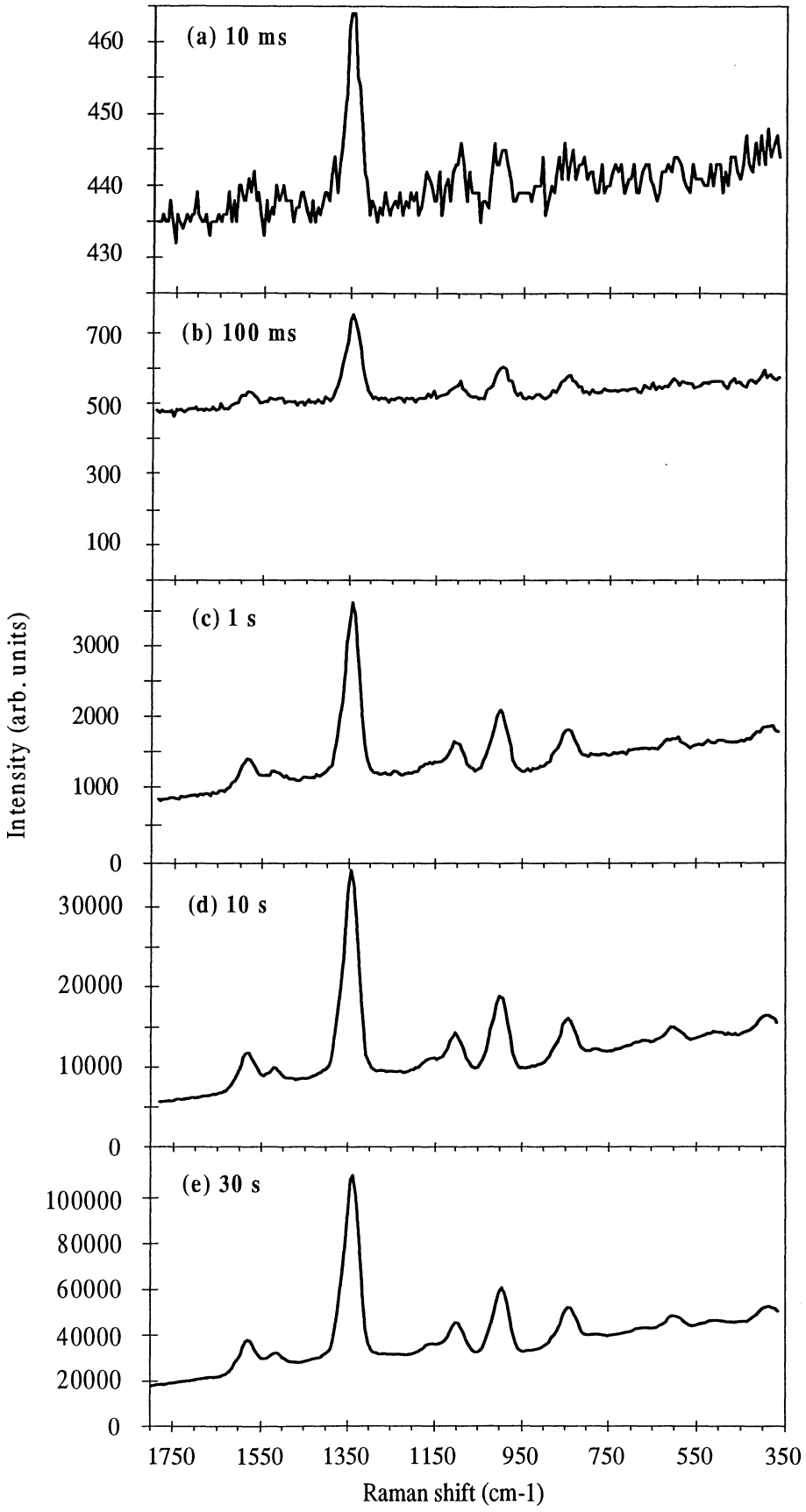

Fig 5.3 *Raman spectra of nitrbenzol with 792.5 nm excitation, 50 μm slit width, 150 g/mm grating, and integration times (a) 10 ms, (b) 100 ms, (c) 1 s, (d) 10s, and (e) 30 s.*

These recorded spectra clearly shows that, as expected, the signal-to-noise ratio drops when the integration time is shortened. Nevertheless, the spectrum recorded with 1 second integration time exhibits as many peaks, that is vibrational modes, as the spectrum recorded with 30 seconds integration time, though the former spectrum contains slightly more noise. Furthermore, the spectrum recorded with 100 milliseconds integration time still shows the major peaks, but with a largely deteriorated signal-to-noise ratio. Remarkably enough, the spectrum recorded with such an extremely short integration time as 10 milliseconds (!) still apparently exhibits the major peak and an intimation of several other peaks as well.

In order to improve the resolution, the grating was changed to a grating with 1200 g/mm, and spectra of the same samples were recorded with otherwise the same conditions as before. The recorded spectra are shown in Fig. 5.4 and 5.5.

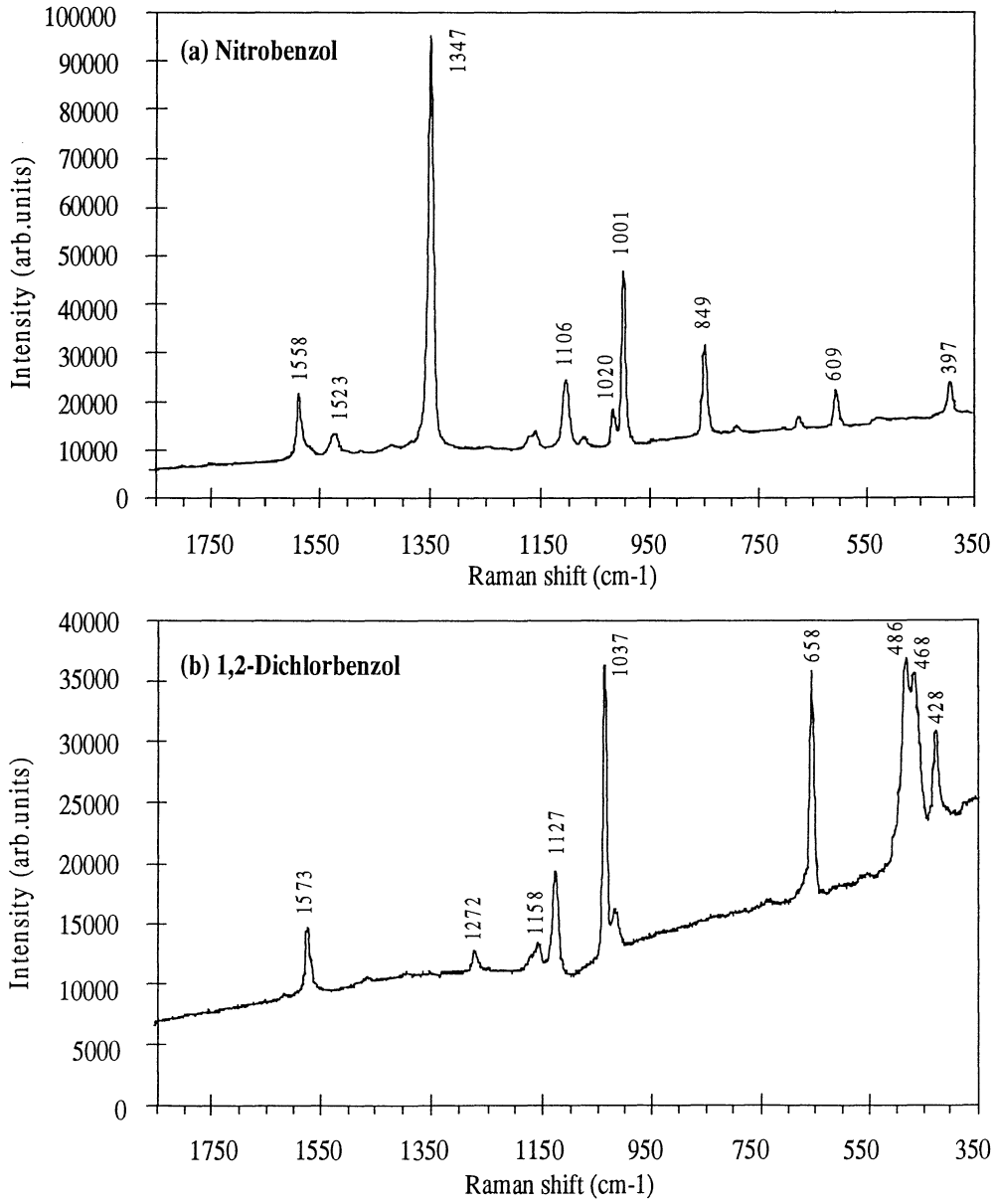

Fig 5.4 *Raman spectra of (a) nitrobenzol and (b) 1,2-dichlorbenzol with 792.5 nm excitation, 50 μm slit width, 1200 g/mm grating, and 30 seconds integration time.*

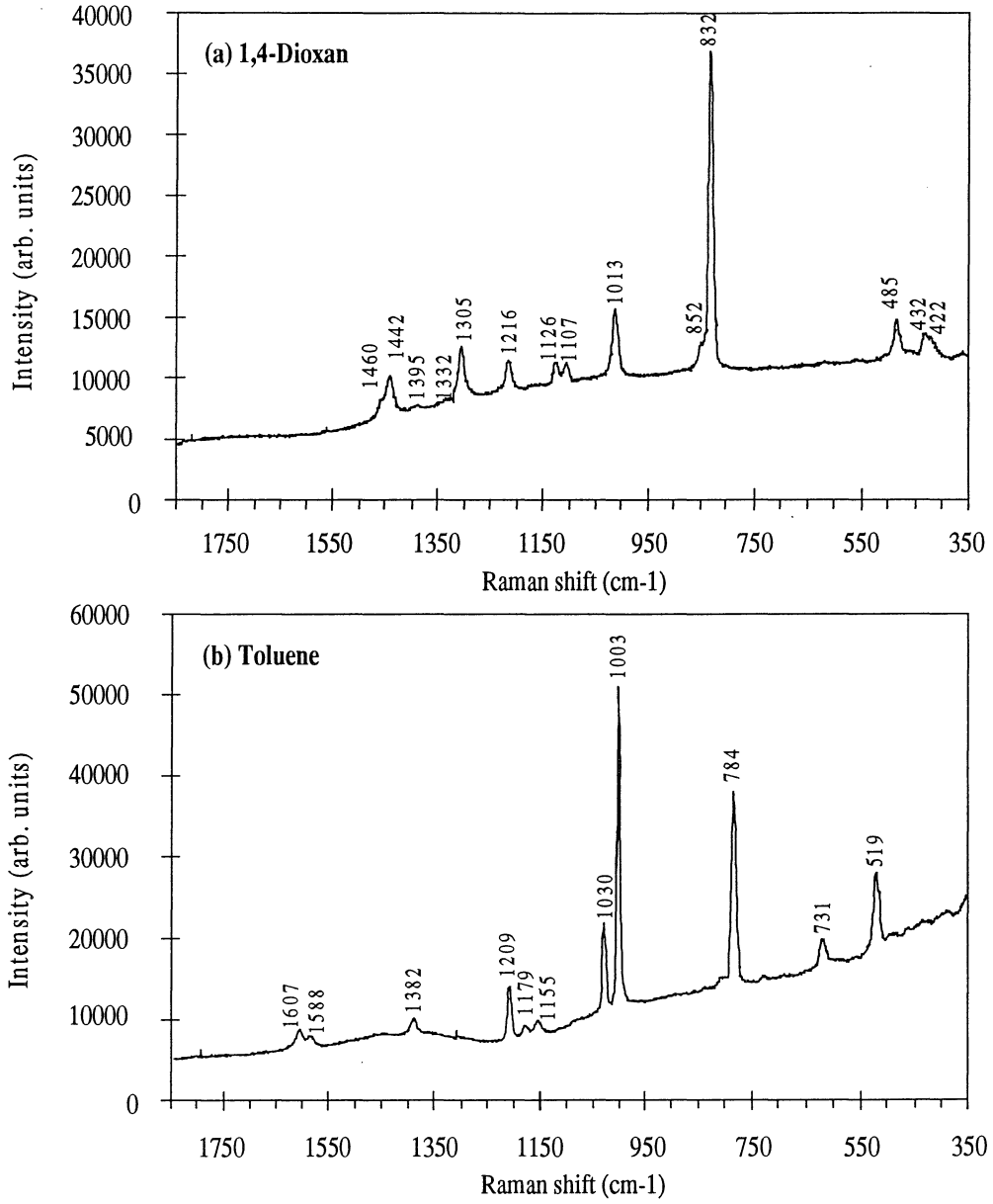

Fig 5.5 *Raman spectra of (a) 1,4-dioxane and (b) tolouene with 792.5 nm excitation, 50 μm slit width, 1200 g/mm grating, and 30 seconds integration time.*

These measurements, displayed in Fig 5.4 and 5.5, with the 1200 g/mm shows very obviously that the resolution is significantly improved compared to the results recorded with the 150 g/mm grating (Fig 4.1 and 4.2). About twice as many peaks can be observed with this grating. Moreover the double peaks is now completely resolved. One important disadvantage with the 1200 g/mm is however that the spectral coverage is limited, and in order to cover the whole spectral region from 350 to 1800 cm^{-1} five succesive spectra has to be recorded.

Considering the four different spectra in Fig. 5.4 and 5.5, they all exhibit a similar overall spectral structure with distinct Raman peaks. The Raman spectra are readily distinguishable and show that differences in molecular structure are manifested in the Raman spectra. The observed Raman peaks, their relative intensities, and their

corresponding vibrational modes are summarized in Table 5.1 and 5.2, where references to tabulated Raman frequencies and the vibration assignments (Table 5.2) also are listed.

Table 5.1 *Observed Raman band frequencies and Raman band intensities, and tabulated Raman band frequencies and Raman band intensities for nitrobenzol and 1,2-dichlorbenzol.*

Nitrobenzol

Observed Raman shift[a] (cm^{-1})	Observed Raman shift[b] (cm^{-1})	Relative band intensity[b] (%)	Tabulated Raman shift[c] (cm^{-1})	Relative band intensity[c] (%)
			179	8
393	397	7	398	3
607	609	9	610	7
847	849	22	850	18
1002	1001	42	1001	46
	1020	9	1020	8
1109	1106	16	1106	14
1348	1347	100	1345	100
1525	1523	5	1523	4
1589	1588	16	1588	17
			3081	8

1,2-Dichlorbenzol

Observed Raman shift[a] (cm^{-1})	Observed Raman shift[b] (cm^{-1})	Relative band intensity[b] (%)	Tabulated Raman shift[c] (cm^{-1})	Relative band intensity[c] (%)
			153	46
			243	11
	428	28	428	18
468	468	50		
	486	60	486	24
655	658	80	658	50
1034	1037	100	1036	100
1128	1127	34	1127	28
	1158	8		
(1273)	1272	6	1272	8
	1458	1	1458	1
1572	1573	1	1573	20
		22	3067	30

[a]150 g/mm grating and 30 seconds integration time.
[b]1200 g/mm grating and 30 seconds integration time. The band intensities are expressed in percent relative to the strongest band.
[c]From Ref. [75]. The band intensities are expressed in percent relative to the strongest band.

Table 5.2 *Observed Raman band frequencies, tabulated Raman band frequencies, Raman band intensities, and band assignment for 1,4-dioxane and toluene.*

1,4-Dioxane

Observed Raman shift[a] (cm^{-1})	Observed Raman shift[b] (cm^{-1})	Relative band intensity[b] (%)	Tabulated Raman shift[c] (cm^{-1})	Band intensity	Vibration assignment[c]
	422	5			
	432	6	427	m	Ring deformation
488	485	10	486	m	Ring deformation
838	832	100	834	vs	Ring stretch
	852	8	852	w	CH_2 rock
1017	1013	21	1015	s	Ring stretch
	1107	5	1109	m	Ring stretch
1125	1126	6	1127	m	CH_2 rock
1215	1216	9	1216	s	CH_2 twist
1302	1305	16	1303	vs	CH_2 twist
	1332	1	1334	m	CH_2 wag
	1395	1	1396	w	CH_2 wag
1444	1442	10	1443	vs	CH_2 deformation
	1460	4	1461	m	CH_2 deformation
			2854	vs	Symmetric
			2966	vs	Anti-symmetric

Toluene

Observed Raman shift[a] (cm^{-1})	Observed Raman shift[b] (cm^{-1})	Relative band intensity[b] (%)	Tabulated Raman shift[d] (cm^{-1})	Relative band intensity[d] (%)	Vibration assignment[e]
523	519	21	521		Ring deformation
624					
	731	9			C_6H_5-C vibration
789	784	59	788	51	Ring stretch
	806	2			CH deformation
1005	1003	100	1001	100	Ring "breathing"
	1030	27	1028	24	CH deformation i-p
	1155	3			CH deformation i-p
	1179	2			CH deformation i-p
1205	1209	16	1210	17	C_6H_5-C
1385	1382	3	1380	5	CH_3 symmetric
	1588	2			Ring stretch
1602	1607	4	1605	6	Ring stretch

[a]150 g/mm grating and 30 seconds integration time.
[b]1200 g/mm grating and 30 seconds integration time. The band intensities are expressed in percent relative to the strongest band.
[c]From Ref. [74]. Abbrevations: vs=very strong, m=medium, and w=weak.
[d]From Ref [75]. The band intensities are expressed in percent relative to the strongest band.
[e]From Ref [70,72,73,74]]

5.1.2 Cholesterol and NADH

The Raman spectra of purified cholesterol and NADH, recorded with 792.5 nm excitation, 1200 g/mm grating, and 150 seconds integration time, are shown in Fig. 5.6 (a) and (b).

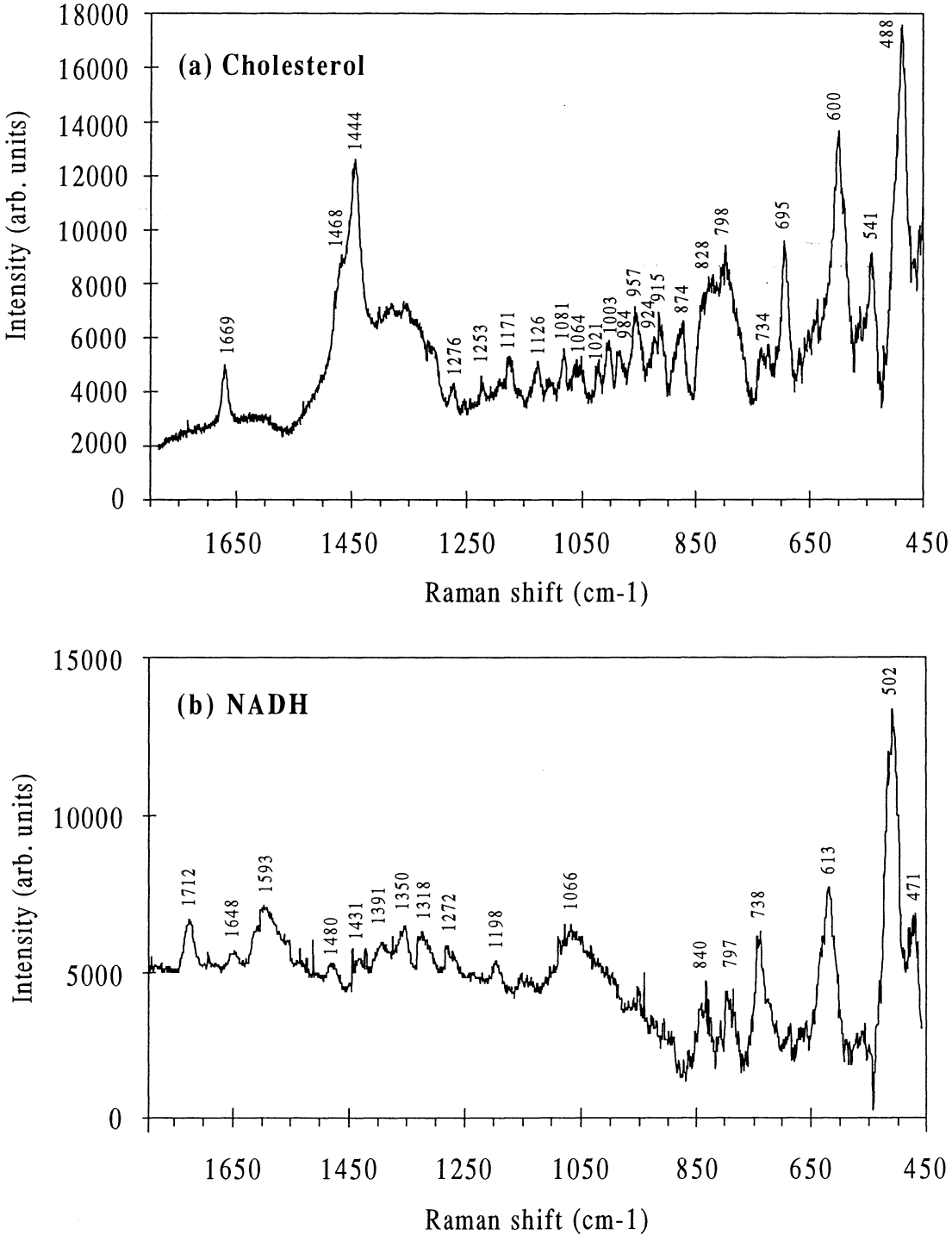

Fig 5.6 *Raman spectrum of (a) cholesterol and (b) NADH with 792.5 nm excitation, 50 μm slit width, 1200 g/mm grating, and 150 seconds integration time.*

The larger complexity of the cholesterol molecule, compared to the solvents previously treated, appears clearly from the large number of Raman peaks in the spectra recorded (Fig 5.6a). All the observed vibrational bands are listed in Table 5.3., where the corresponding bands, in this spectral region, for cholesterol and cholesterol monohydrate reported from the Lipid Chemistry Laboratory at the University of Gothenburg, Sweden, [79] are listed as well.

Table 5.3. *Observed Raman band frequencies of the cholesterol sample and observed Raman band freqeuncies reported in Ref. [79] for cholesterol and cholesterol monohydrate.*

Observed Raman shift of cholesterol (cm^{-1})	Raman shift of cholesterol[a] (cm^{-1})	Raman shift of cholesterol monohydrate[b] (cm^{-1})
	465	455
488	496	490
541	550	545
	570	570
600	600	603
	620	627-640
695	693	700
734	732	
		745
798	798	803
	812	815
828	830	846
874		885
915		
924		925
950	950	960
	975	960
984	992	990
1003	1010	
1021	1020	1020
	1050	1050
1064	1068	1088
1081	1090	
	1116	
1126	1125	1132
	1156	
1171	1162	1178
		1194
	1200	1220
	1235	
1253	1252	1258
1276	1280	1272
	1300	1300
	1328	1326
1350	1358	
	1364	1390
1444	1444	1448
1468	1468	1456
		1580
1669	1668	1673

[a]From Ref [79]. The spectrum was recorded with Spex 1401 double monochromator with slit widths of 3-5 cm^{-1} and excited with the 4880 Å line of a Spectra Physics Argon ion laser of 300 mW radiation.

[b]From Ref [79]. The spectrum was recorded on Cary 82 triple monochromator with slit width of 8 cm^{-1} and excited with the 4880 Å line of a Coherent Radiation Model 52B Argon ion laser at 300 mW radiation.

Normally the entire cholesterol spectrum is divided in three different spectral regions. They are (1) the low frequency region below 300 cm^{-1}, giving information of the inter- and intramolecular vibrations, (2) the methylene rocking/deformation region between 1400 and 1500 cm^{-1} giving information on chain packing in the crystalline state, and (3) the C-H stretching region between 2700 and 3100 cm^{-1} which appears to indicate that there is correlation between branching in the side chains of cholesterols. In the spectrum recorded (Fig 5.6a) it can be seen that region (2) is obviously represented by an intense, broad band envelope with a major peak at 1444 cm^{-1} and a faint shoulder band at 1468 cm^{-1}. The spectral coverage was not sufficiently wide to record region (1) and (3). However, it can be seen in Table 5.3 that most of the Raman bands recorded are in accordance with the bands reported in [76]. Nevertheless some of the frequencies measured are in better accordance with the bands of cholesterol monohydrate. This may be due to any water contamination in the sample container or due to water in the air.

Also the spectrum recorded of NADH (Fig. 5.6b) contains quite a large number of peaks, but the fluorescence background was significantly higher compared to the cholesterol spectrum, yielding weaker Raman peaks. For instance the peak due to the amide I vibration at 1648 cm^{-1} is very faint.

5.1.3 Tissue from pig heart

In order to test the ability of the experimental arrangement on biological tissue, a spectrum was recorded on a piece of aorta from a pig heart. One might expect that the fluorescence background should be considerably strong, and so it was. The Raman peaks are in this case very faint and hard to distinguish from the fluorescence background. Therefore the excitation difference technique was implemented. The excitation wavelengths utilized were 792.5 nm and 794.0 nm, 50 μm slitwidth, 1200 g/mm grating, and 150 seconds integration time. Fig 5.7 displays (a) the 792.5 nm excited Raman spectrum, (b) the difference Raman spectrum, and (c) the integrated Raman spectrum of aorta tissue from pig heart. The power of the excitation dfference technique is clearly shown in Fig. 5.7a and 5.7c. It is also obvious that the technique smoothes the Raman spectrum and causes the spectral line widths to be about twice as broad compared to the original spectrum.

The spectrum recorded (Fig 5.7c) covers the spectral region from 800 cm^{-1} to 1800 cm^{-1} and is dominated by bands due to proteins. In particular, the bands observed at 1650 cm^{-1} can be assigned to the amide I vibration of the polypeptid chain, the 1458 cm^{-1} band to a C-H bending mode of proteins, and the 1256 cm^{-1} band to the amide III vibration. The weak band at 1342 cm^{-1} appears to be specifik to elastin, and the band at 1012 cm^{-1} is likely due to phenylalanine residues. It is more difficult to say anything certain about the bands at 950 cm^{-1}, 1065 cm^{-1}, 1400 cm^{-1}, and 1700 cm^{-1}, since no pre-histological examination was done. Nevertheless, one may suspect that the 950 cm^{-1} band is assigned to the symmetric stretching vibration of phosphate groups, which are present if the tissue is calcified. The weaker phosphate anti-symmetric stretch is also present at 1065 cm^{-1}. The remaining three bands at 1210 cm^{-1}, 1400 cm^{-1}, and 1700 cm^{-1}, appear to be mainly due to lipids.

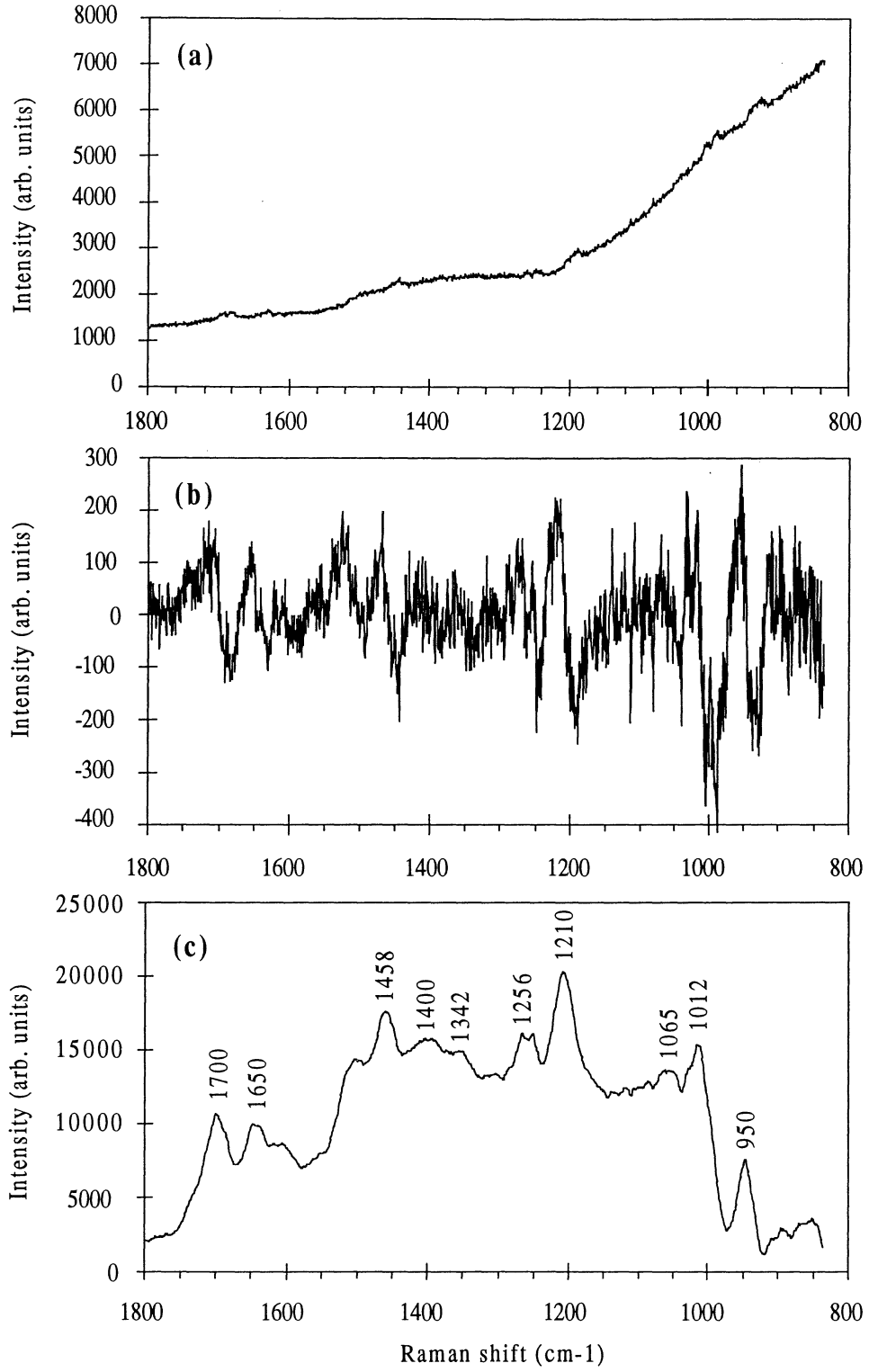

Fig 5.7 *(a) Raman spectrum of aorta tissue from pig heart with 792.5 nm excitation, 50 μm slit width, 1200 g/mm grating, and 150 seconds integration time. (b) Difference spectrum of Raman spectra of aorta tissue from pigheart excited with 792.5 nm and 794.0 nm (c) Integrated difference spectrum.*

5.2 The near infrared absorption experiment

5.2.1 Pure tissue constituents

Fig. 5.8 depicts the recorded Fourier transform-near infrared (FT-NIR) absorption spectra of collagen I (a) and elastin (b), while Fig. 5.9 shows the recorded FT-NIR absorption spectra of cholesterol (a) and NADH (b). The ordinate axis of the spectra represents the transmitted light intensity in arbitrary units, while the abscissa axis represents the wavenumbers in cm^{-1}. Since the absorption bands are broad it is difficult to estimate the vibrational frequencies with high accuracy.

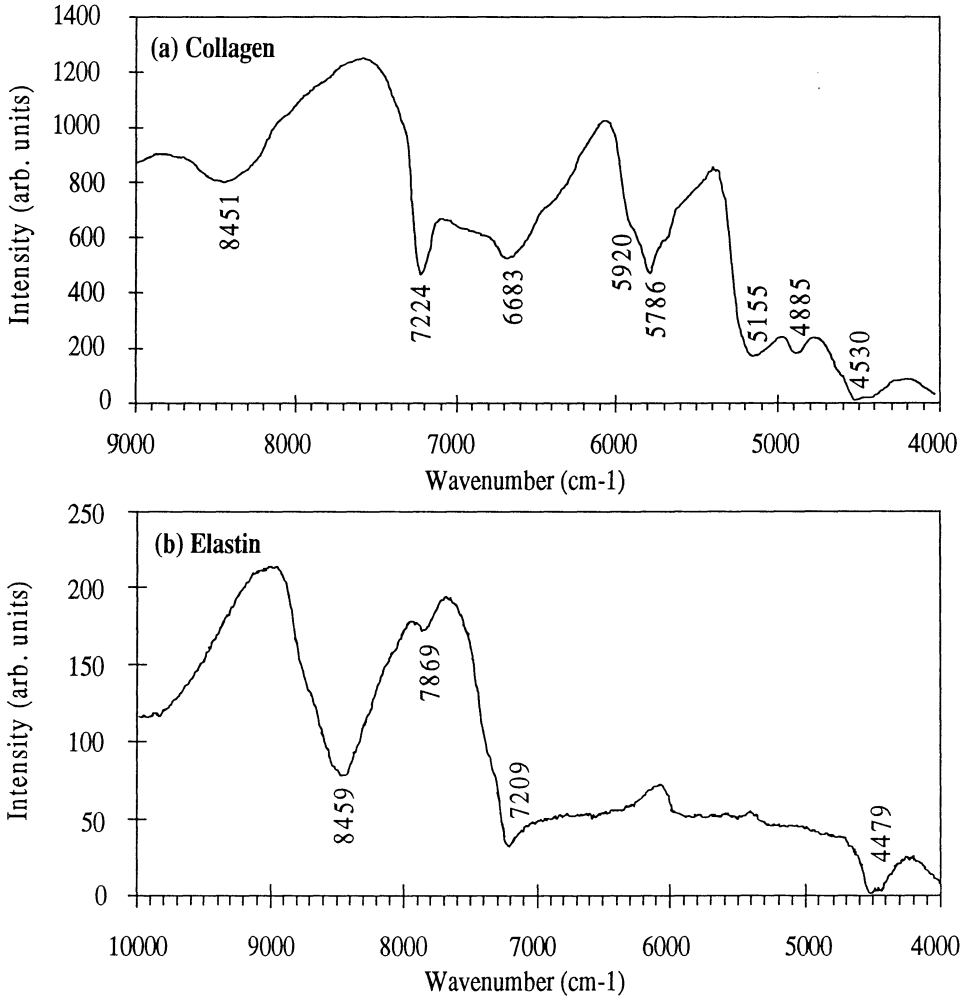

Fig 5.8 *FT-NIR absorption spectra of (a) collagen I and (b) elastin.*

However, the spectrum of collagen (Fig. 5.8a) exhibits a couple of strong bands at 5786 cm^{-1}, 6683 cm^{-1}, and 7224 cm^{-1}. Since photons in the NIR region interact with molecules via overtone and combination vibrations, band assignments of the NIR spectra have not been well established [80]. Nevertheless, quite recently, Wang et al. [81] gave the rationale for the assignments in the 9000-4000 cm^{-1} region of the NIR spectra of homo-polypeptides. According to these authers [81], bands near 4850 and 4600 cm^{-1} were assigned to combinations of amide A and amide II, and amide B and amide II, respectively. In the following we identify these bands as amide A/II and amide B/II.

According to the foregoing, the band at 4885 cm^{-1} in the spectrum of collagen (Fig 5.8a) can be assigned to amide A/II vibration, and the broad band at 4530 cm^{-1} is probably an amide B/II vibration. The other band frequencies, indicated in Fig. 5.8a, are not assigned to any particular combination in this context.

The spectrum of elastin (Fig. 5.8b) exhibits even broader absorption bands. The strong band at 8459 cm^{-1} dominates the spectrum. As in the collagen spectrum, the elastin spectrum contains a band due to amide B/II vibration, but at 4520 cm^{-1}, a slightly lower frequency than in collagen. The band at 7209 cm^{-1} is in all probabillity due to the same vibration as the band at 7224 cm^{-1} in the collagen spectra (Fig. 5.8a).

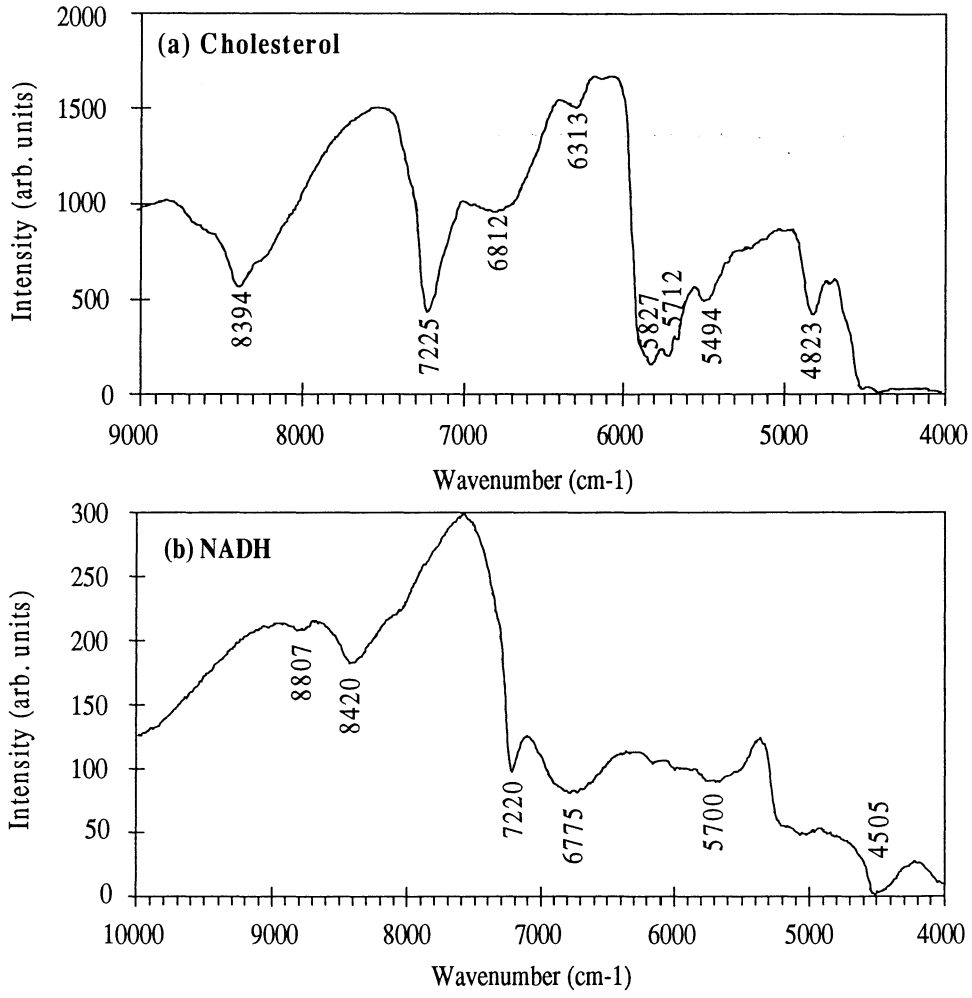

Fig. 5.9 *FT-NIR absorption spectra of (a) cholesterol and (b) NADH.*

The recorded spectrum of cholesterol, shown in Fig. 5.9a, exhibits quite intense absorption bands. The band at 7225 cm^{-1} is the strongest one. Since the purpose of this project not is to evaluate combinations and overtones but rather to characterize tissue, i.e. to find markers significant for various tissue constituents, no band assignments are estimated for the cholesterol and NADH spectra (Fig. 5.9). The NADH spectrum, displayed in Fig. 5.9b, exhibits broader and less intense absorption bands compared to the cholesterol spectrum. However there is a sharp dip at 7220 cm^{-1}. It is also interesting to note that the NADH spectrum has a very similar structure to the cholesterol spectrum. The band frequencies of cholesterol and NADH are listed in Table 5.4.

Table 5.4 *Near infrared band frequencies of cholesterol and NADH.*

Observed band frequencies (cm^{-1})	
Cholesterol	**NADH**
	4505
4823	
5494	
5712	5700
5827	
6313	
6812	6775
7225	7220
8394	8420
	8807

5.2.2 Tissue samples

The tissue samples were specimens of fat and muscle, both taken from a pork, and an aorta specimen from a pig heart. The recorded NIR-FT absorption spectra of the fat and muscle specimens are displayed in Fig. 5.10.

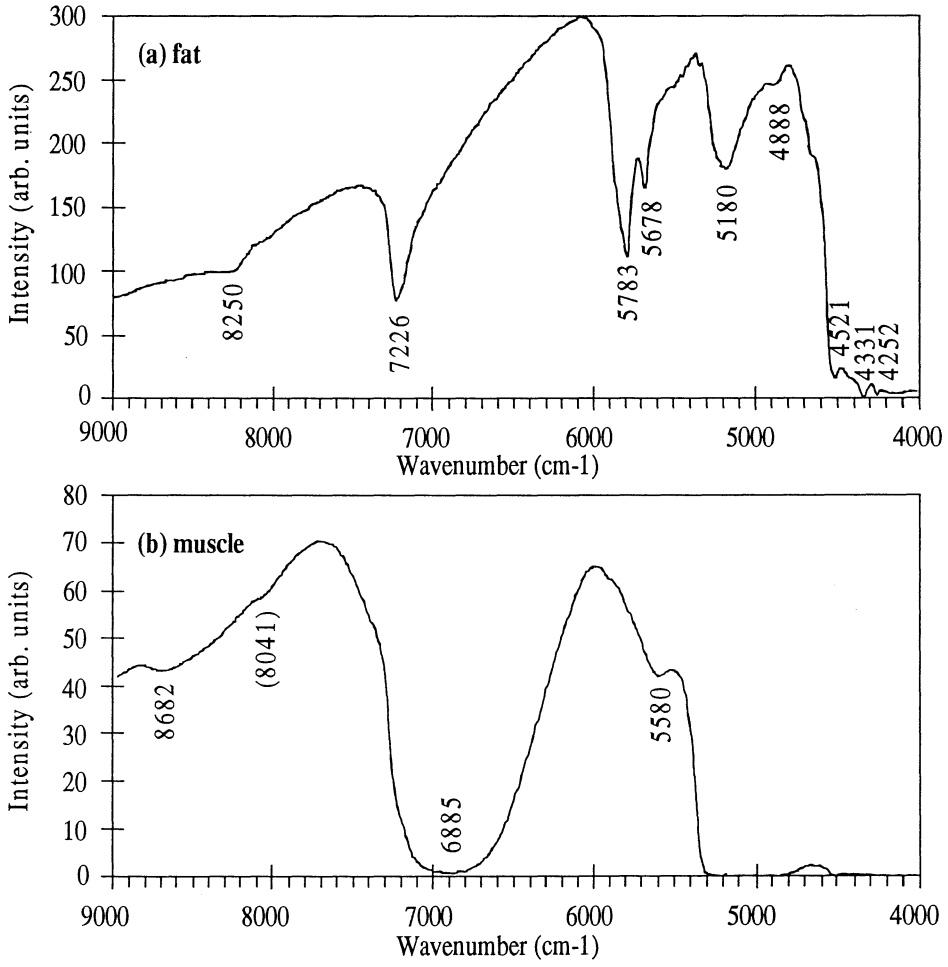

Fig 5.10 *FT-NIR spectra of (a) fat tissue and (b) muscle tissue from a pork.*

The recorded spectrum of fat tissue (Fig 5.10a) contains four quite apparent vibrational bands at 5180 cm^{-1}, 5678 cm^{-1}, 5783 cm^{-1}, and 7226 cm^{-1}, and a number of fainter bands. If one compares the spectra of fat with the previously shown spectrum of cholesterol (see Fig. 5.9a) obviously the band at 7226 cm^{-1} is due to cholesterol, since the cholesterol spectrum exhibits a dominating band at 7225 cm^{-1}. This is not very surprising since tissue of fat is rich of cholesterol. Futhermore the band at 5783 cm^{-1} might be due to collagen, according to the fact that the spectrum of collagen (see Fig. 5.8a) contains a band at 5786 cm^{-1}.

The recorded spectrum of the muscle specimen (Fig. 5.10b) is dominated of a very broad band at about 6885 cm^{-1}, with three much fainter bands at 5580 cm^{-1}, 8041 cm^{-1}, and 8682 cm^{-1}. The strong band at 6885 cm^{-1} might be due to interference between the bands at 6683 cm^{-1} and 7224 cm^{-1} of collagen, according to the recorded collagen spectrum displayed in Fig. 5.8a.

Fig. 5.11 displays the near-infrared spectrum recorded of the aorta specimen.

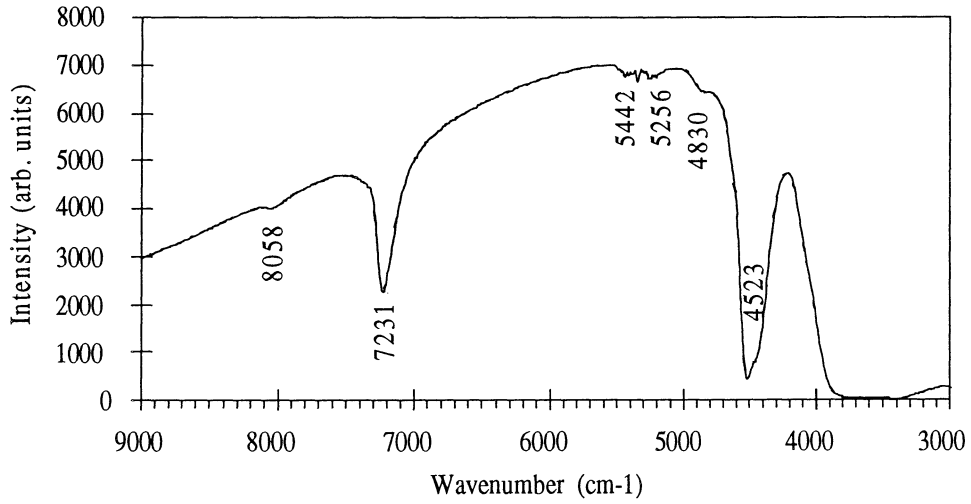

Fig. 5.11 *FT-NIR spectrum of an aorta specimen from a pig heart.*

The spectrum of the aorta specimen exhibits two strong bands at 4523 cm^{-1} and 7231 cm^{-1}, and four weaker bands at 4830 cm^{-1}, 5256 cm^{-1}, 5415 cm^{-1}, and 8058 cm^{-1}. The strong absorption for wavenumbers lower than about 3800 cm^{-1} is due to water absorption, since water absorption becomes significant at about 6500 cm^{-1} (1500 nm) and increases with decreasing wavenumber from that limit.

6 Discussion and conclusion

6.1 Raman spectroscopy

Our results with an experimental set-up based on a Ti:Sapphire laser, a single stage spectrometer, and a cooled CCD detector show that high quality Raman spectra of pure liquid and powder samples, but also from more complex molecular systems such as tissue samples, can be obtained.

Our results from measurements on solvents such as nitrobenzol clearly shows that the integration time can be decreased to about 1 s without loosing any essential information or without any particular loss in resolving power. This is illustrated by Fig. 4.3. Notable is that the major peaks still can be resolved with such a short integration time as 100 ms. It is also important to note the great difference between spectra recorded with the 150 g/mm grating and the 1200 g/mm grating. A comparison between e.g. Fig. 4.1 and Fig. 4.4 shows that nearly twice as many peaks can be resolved with the 1200 g/mm grating. However, to cover the same spectral range with this higher resolution, one has to record five succesive spectra. Hence, the total collection time becomes at least five times as long.

Regarding measurements on complex molecules such as cholesterol and NADH, significantly longer integration times were required (150 s). However, a very large number of peaks were resolved. The situation regarding our measurements on aorta from pig is similar. This indicates that Raman spectroscopy as a method for tissue chacterization or to discriminate between healthy and diseased tissue should be possible. A determining factor of whether this could be clinically feasible or not, is the requirements of resolution and spectral coverage for such a measurement. The equipment used by us would, however, require too long integration times for practical use.

Generally, our recorded spectra exhibited broad flanks on both the Stokes and Anti-Stokes side of the suppressed laser line. This phenomenon is illustrated by Fig. 6.1.

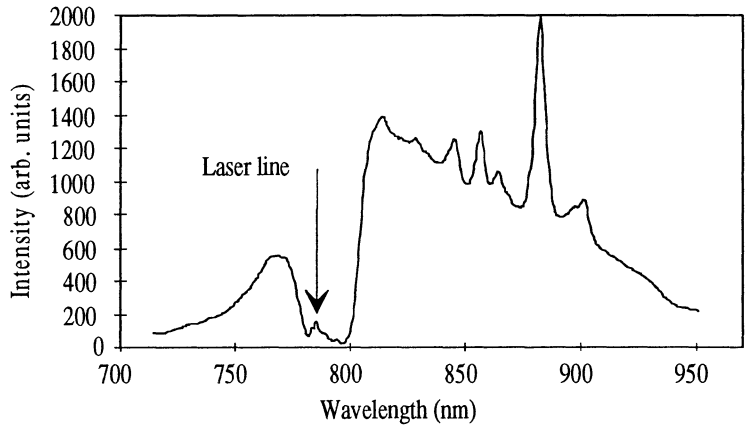

Fig. 6.1 *A recorded spectrum of nitrobenzol with 792.5 nm excitation, 50 μm slit width, and 30 s integration time, clearly showing the broad banded flanks mentioned in the text.*

Obviously these flanks are not due to fluorescence. Our suggestion is that these broad band features in fact are the flanks of the laser line itself. They just become more apparent when the laser line is strongly suppressed. As illustrated in Fig. 6.1 the Raman signals are superimposed on the flanks. In order to eliminate the flanks and thereby increase the signal-to-background ratio we tried to diminish the laser linewidth by two different techniques: by using a dispersive prism in combination with a narrow slit; and by using an interference filter. However, none of these approaches gave any improved result. The flanks remained unaffected, indicating that they were not due to the laser line after all.

6.2 Fourier transform infrared absorption spectroscopy

Our results from measurements on different tissue constituents with a Bomem DA8 FTIR spectrometer show apparent absorption bands. Generally, these absorption bands are significantly broader than the obtained Raman bands. This implies a difficulty in exact identification of vibrational frequencies. However spectra of different substances and tissues exhibit major differences. It is, for instance, no difficulty to discriminate between fat, muscle, and aorta tissue samples. This indicates that also FTIR spectroscopy could be a possible method for tissue characterization.

As comes to absorption spectroscopy the medical usage would be limited to *in vitro* measurements. In this case integration times of 5 minutes would not be of any obstacle. For conceivable *in vivo* measurements reflection spectroscopy in combination with a fiber optic collecting system must be used. A problem here is the lack of IR transmitting fibres.

A direct comparison between infrared spectroscopy and Raman spectroscopy was not possible, as we did not have the equipment for measurements in the same wavelength region. Our absorption spectroscopic measurements were exclusively performed in the near infrared wavelength region, where observable bands are due to overtones and combinations.

6.3 The future

A suitable continuation of this project would be to perform further measurements on different types of tissue and to investigate and to ensure the differences between healthy and diseased tissue. For this purpose a spectrometer with a higher light collecting ability, for instance, a spectrometer based on transmission grating instead of reflection grating, probably is required. With a better spectrometer it should be possible to use a less powerful laser than the Ti:Sapphire laser used by us. A compact diode laser would be desirable for clinical measurements.

It would also be of interest to procure suitable technical equipment for absorption spectroscopy in the region 300-2000 cm^{-1}. In order to achieve a clinically applicable set-up, reflection spectroscopic measurements should initially be performed.

6.4 Conclusion

With a 1.0 W Ti:Sapphire laser, conventional lens and fiber optics, a single stage spectrometer, and a CCD detector it is possible to obtain high quality Raman spectra of nitrobenzol, 1,2-dichlorbenzol, 1,4-dioxane, and toluene with an integration time less than 1s. It is also possible to obtain high quality Raman spectra of cholesterol, NADH, and aorta tissue from pig with an integration time of 150 s.

With a Bomem DA8 FTIR spectrometer and an integration time of 5 minutes it is possible to obtain absorption spectra from collagen, elastin, cholesterol, and NADH and to distinguish between tissue samples of fat, muscle, and aorta from pig.

These results suggests that Raman and infrared absorption spectroscopy might be used for tissue characterization.

7 Acknowledgements

First of all, we would like to express our appreciation to our supervisors Stefan Andersson-Engels and Jonas Johansson for guiding us through this project.

Thank you, Ingrid Rokahr, for helping us getting started.

We would like to thank Ulf Gustafsson for his constant encouragement and for sharing his skills in Raman spectroscopy with us.

Claes af Klinteberg has been of great help and support when struggling with computers.

We are very grateful to Anders Persson for always finding the time to help us.

We would also like to thank Janos Olajos for letting us put meat in his FTIR spectrometer.

Finally, Sune Svanberg is greatly acknowledged for his dynamic lectures which have made us interested in medical applications of laser physics.

8 List of references

1. R.R. Alfano, B.T. Darayash, J. Cordeo, P. Tomashefsky, F.W. Longo, and M.A. Alfano, *Laser induced fluorescence spectroscopy from native cancerous and normal tissue*. IEEE Jornal of Quantum Electronics **20**, 1507-1511 (1984).

2. Y.M. Ye, Y.L. Yang, Y.F. Li, and F.M. Li, *Characteristic autofluorescence for cancer diagnosis and the exploration of its origin*, Proc. CLEO´85 (Baltimore, MD) (1985).

3. P.S. Andersson, E. Kjellén, S. Montán, K. Svanberg, and S. Svanberg, *Autofluorescence of various rodent tissues and human skin tumour samples*, Lasers in Medical Science **2**, 41-49 (1987).

4. R.R. Alfano, W. Lam, H.J. Zarrabi, M.A. Alfano, J. Cordeo, D.B. Tata, and C.E. Swenberg, *Human teeth with and without caries studied by laser scattering, fluorescence and absorption spectroscopy*, IEEE Jornal of Quantum Electronics **20**, 1512-1516 (1984).

5. F. Sundström, K. Fredriksson, S. Montán, U. Hafström-Björkman, and J. Ström, *Laser-induced fluorescence from sound and carious tooth substance: Spectroscopic studies*, Swedish Dental Journal **9**, 71-80 (1985).

6. P.S. Andersson, A. Gustafsson, U. Stenram, K. Svanberg, and S. Svanberg, *Diagnosis of arterial atherosclerosis using laser-induced fluorescence,* Lasers in Medical Science **2**, 261-266 (1987).

7. S. Andersson-Engels, A. Gustafsson, J. Johansson, U. Stenram, K. Svanberg, and S. Svanberg, *Laser-induced fluorescence used in localizing atherosclerotic lesions,* Lasers in Medical Science **4**, 171-181 (1989).

8. S. Andersson-Engels, J. Johansson, D. Killander, E. Kjellén, M. Olivio, and L.O. Svaasand, *Photodynamic therapy alone or in conjunction with near-infrared ligth-induced hyperthermia in human malignant tumours, a methodological case study*, Proc. SPIE **908**, 116-125 (1988).

9. T. Andersson, S. Andersson-Engels, R. Berg, J. Johansson, D. Killander, U. Stenram, K. Svanberg, S. Svanberg, and I. Wang, *Photodynamic therapy of non-melanoma malignant tumours of the skin utilizing topical δ-amino levulinic acid sensitization and laser irradiation*, Brittish Journal of Dermatology **130**, 743 (1994)

10. *Laser picosecond spectroscopy and photochemistry of biomolecules*, V.S. Letokhov (ed.), Hilger, Bristol (1987).

11. S. Andersson-Engels, J. Johansson, U. Stenram, K. Svanberg, and S. Svanberg, *Time-resolved laser-induced fluorescence spectroscopy for enhanced demarcation of human atherosclerotic plaque*, Journal of Photochemistry and Pathobiology. B: Biology **4**, 363-369 (1990).

12. S. Andersson-Engels, J. Johansson, and S. Svanberg, *The use of time-resolved fluorescence for diagnosis of atherosclerotic plaque and malignant tumours*, Spectrochimica Acta **46A**, 1203-1210 (1990).

13. S. Andersson-Engels, R. Berg, O. Jarlman, and S. Svanberg, *Time-resolved transillumination for medical diagnostics*, Proc. SPIE **1431**, 110-119 (1991).

14. S. Andersson-Engels, R. Berg, and S. Svanberg, *Effects of optical constants on time-gated transillumination of tissue and tissue-like media*, Journal of Photochemistry and Pathobiology. B: Biology **16**, 155-167 (1992).

15. R. Berg, O. Jarlman, and S. Svanberg, *Medical transillumination imaging using short-pulse diode lasers*, Applied Optics **32**, 574-579 (1993).

16. S.L. Wolfe, *Molecular and cellular biology*, Wadsworth Publishing Company, Belmont, California (1993).

17. B. Alberts, D. Bray, J. Lewis, M. Raff, K. Roberts, and J.D. Watson, *Molecular biology of the cell* (third edition), Garland publishing, New York & London (1994).

18. B. Sonesson and G. Sonesson, *Människans anatomi och fysiologi*, Almqvist & Wiksell, Falköping (1993).

19. M.H. Ross and L.J. Romrell, *Histology*, Williams & Wilkins, Baltimore (1989).

20. U. Gustafsson, *Near-infrared Raman spectroscopy using a diode laser and CCD detector for tissue diagnostics,* Diploma Paper, Lund Reports on Atomic Physics **LRAP-138** (1993).

21. E. Merzbacher, *Quantum mechanics*, John Wiley & Sons, New York (1970).

22. A. Fadini and F-M. Schnepel, *Vibrational Spectroscopy, methods and applications*, Wiley, New York (1989).

23. C.J.H. Schutte, *The theory of molecular spectroscopy*, North-Holland Publishing Company, Amsterdam (1976).

24. J.D. Graybeal, *Molecular spectroscopy*, McGraw-Hill, New York (1988).

25. C.V. Raman and K.S. Krishnan, *A new type of secondary radiation*, Nature **121**, 501-502 (1928).

26. C.V. Raman, *A change of wave-length in light scattering*, Nature **121**, 619 (1928).

27. C.V. Raman and K.S. Krishnan, *The optical analogue of the Compton effect*, Nature **121**, 711 (1928).

28. S. Svanberg, *Atomic and molecular spectroscopy. Basic aspects and practical applications*, Springer Verlag, Berlin (1991).

29. G. Landsberg and L. Mandelstam, *Eine neue erscheinung bei der Lichtzerstreuung in Krystallen*, Die Naturwissenschaften **16**, 557-558 (1928).

30. *Analytical Raman spectroscopy*, J.G. Grasselli and B.J. Bulkin (eds.), Wiley, New York (1991).

31. *Practical Raman spectroscopy*, D.J. Gardiner and P.R. Graves (eds.), Springer-Verlag, Berlin (1989).

32. P.R. Carey, *Biochemical applications of Raman and resonance Raman spectroscopies*, Academic Press, New York (1982).

33. J.G. Grasselli, M. Snavely, and B.J. Bulkin, *Chemical applications of Raman spectroscopy*, Wiley, New York (1981).

34. E. Hecht, *Optics* (second edition), Addison-Wesley Publishing Company, Reading, Massachusetts (1987)

35. F. Parker, *Applications of infrared, Raman and resonance Raman spectroscopy in biochemistry*, Plenum, New York (1983).

36. *Time-resolved vibration spectroscopy*, G.H. Atkinson (ed.), Wiley, New York (1983).

37. *Time-resolved vibrational spectroscopy*, A. Lauberau and M. Stockburger (eds.), Springer-Verlag, Berlin (1985).

38. S.D. Schwab and R.L. McCreery, *Versatile, efficient Raman sampling with fiber optics*, Analytical Chemistry **56,** 2199 (1984).

39. R.H. Clarke, E.B. Hanlon, J.M. Isner, and H. Brody, *Laser Raman Spectroscopy of Calcified Atherosclerotic Lesions in Cardiovascular Tissue*, Applied Optics **26**, 3175-3177 (1987).

40. R.H. Clarke, Q. Wang, and J.M. Isner, *Laser Raman spectroscopy of atherosclerotic lesions in human coronary artery segments*, Applied Optics **27**, 4799-4800 (1988).

41. V.R. Kodati and A.T. Tu, *Raman spectroscopic identification of cysteine-type kidney stone*, Applied Spectroscopy **44**, 837-839 (1990).

42. V.R. Kodati, A.T. Tu, and J.L. Turumin, *Raman spectroscopic identification of uric-acid-type kidney stone*, Applied Spectroscopy **44**, 1134-1136 (1990).

43. S. Zheng and A.T. Tu, *Raman spectroscopic identification of bilirubin-type gallstone*, Applied Spectroscopy **40**, 1099-1103 (1986).

44. S. Zheng and A.T. Tu, *Spectroscopic identification of gallstone*, Applied Spectroscopy **41**, 696-697 (1987).

45. D.C.B. Redd, Z.C. Feng, K.T. Yue, and T.S. Gansler, *Raman spectroscopic characterisation of human breast tissues: implications for breast cancer diagnosis*, Applied Spectroscopy **47**, 787-791 (1993).

46. J. Funfschilling and D.F. Williams, *CW laser wavelength modulation in Raman and site selection fluorescence spectroscopy*, Applied Spectroscopy **30**, 443-446 (1976).

47. K.H. Levin and C.L. Tang, *Wavelength modulation Raman spectroscopy*, Applied Physics **33**, 817-819 (1978).

48. A.P. Shreve, N.J. Cherepy, and R.A. Mathies, *Effective rejection of fluorescence interference in Raman spectroscopy using a shifted excitation difference technique*, Applied Spectroscopy **46**, 707-711 (1992).

49. K. Kamagowa, T. Fujii, and T. Kitagawa, *Improved fluorescence rejection in measurements of Raman spectra of fluorescent compounds*, Applied Spectroscopy **42,** 248-254 (1988)]

50. T. Tahara and H-O. Hamaguchi, *Picosecond Raman spectroscopy using a streak camera*, Applied Spectroscopy **47**, 391-398 (1993).

51. S. Chadha, E. Ghiamati, R. Manoharan, and W. Nelson, *UV-excited Raman and resonance Raman spectra of synthetic polymers*, Applied Spectroscopy **46**, 1176-1181 (1992).

52. T. Hirschfeld and B. Chase, *FT-Raman spectroscopy: development and justification*, Applied Spectroscopy **40**, 133-137 (1986).

53. H. Ishida, R. Kamoto, S. Uchida, A. Ishitani, Y. Ozaki, K. Iriyama, E. Tsukie, K. Shibata, F. Ishihara, and H. Kameda, *Raman microprobe and Fourier transform-infrared microsampling studies of the microstructrure of gallstones*, Applied Spectroscopy **41**, 407-412 (1987).

54. Y. Ozaki, A. Mizuno, H. Sato, K. Kawauchi, and S. Muraishi, *Biomedical application of near-infrared Fourier transform Raman spectroscopy. Part I: the l064-nm excited Raman spectra of blood and met hemoglobin*, Applied Spectroscopy **46**, 533-536 (1992).

55. J.J. Baraga, M.S. Feld, and R.P. Rava, *In situ optical histochemistry of human artery using near infrared Fourier transform Raman spectroscopy*, Proceedings of the National Academy of Sciences of the USA **89**, 3473-3477 (1992).

56. R. Manoharan, J.J. Baraga, M.S. Feld, and R.P. Rava, *Quantitative histochemical analysis of human artery using Raman spectroscopy*, Journal of Photochemistry and Photobiology B: Biology **16**, 211-233 (1992).

57. R.R. Alfano, C.H. Liu, W.L. Sha, H.R. Zhu, D.L. Akins, J. Cleary, R. Prudente, and E. Cellmer, *Human breast tissues studied by IR Fourier transform Raman spectroscopy*, Lasers in Life Sciences **4**, 23-28 (1991).

58. R.D. Billhorn, J.V. Sweedler, P.M. Epperson, and M.B. Denton, *Charge transfer device detectors for analytical optical spectroscopy - operation and characteristics*, Applied Spectroscopy **41**, 1114-1125 (1987).

59. Y. Wang and R.L. McCreery, *Evaluation of a diode laser / charge coupled device spectrometer for near-infrared Raman spectroscopy*, Analytical Chemistry **61**, 2647-2651 (1989).

60. J.M. Williamson, R.J. Bowling, and R.L. McCreery, *Near-infrared spectroscopy with a 783-nm diode laser and CCD array detector*, Applied Spectroscopy **43**, 372-375 (1989).

61. C.D. Newman, G.G. Bret, and R.L. McCreery, *Fiber-optic sampling combined with an imaging spectrograph for routine Raman spectroscopy*, Applied Spectroscopy **46**, 262-265 (1992).

62. T.M. Niemczyk, M. Delgado-Lopez, and C.D. Newman, *Multichannel Raman spectroscopy tackles industrial problems*, Laser Focus World (November), 85-98 (1993).

63. C.D. Allred and R.L. McCreery, *Near-infrared Raman spectroscopy of liquids and solids with a fiber-optic sampler, diode laser, and CCD detectorer*, Applied Spectroscopy **44**, 1229-1231 (1990).

64. S.D. Schwab, R.L. McCreery, and F.T. Gamble, *Normal and resonance Raman spectroelectrochemistry with fiber optic light collection*, Analytical Chemistry **58**, 2486-2492 (1986).

65. S.D. Schwab and R.L. McCreery,Remote, *Long-pathlength cell for high-sensitivity Raman spectroscopy*, Applied Spectroscopy **41**, 126 (1987).

66. E.N. Lewis, V.F. Kalasinsky, and I.W. Levin, *Near-infrared Fourier transform Raman spectroscopy using fiber-optic assemblies*, Analytical Chemistry **60**, 2658-2661 (1988).

67. D.D. Archibald, L.T. Lin, and D.E. Honigs, *Raman spectroscopy over optical fibers with the use of a near-IR FT spectrometer*, Applied Spectroscopy **42**, 1558-1563 (1988).

68. J.J. Baraga, M.S. Feld, and R.P. Rava, *Rapid near-infrared Raman spectroscopy of human tissue with a spectrograph and CCD detector*, Applied Spectroscopy **46**, 187-190 (1992).

69. D.D. Klug, D.L. Singleton, and V.M. Walley, *Laser Raman spectrum of calcified human aorta*, Lasers in Surgery and Medicine **12**, 13-17 (1992).

70. N.B. Colthup, L.H. Daily, and S.E. Wiberly, *Introduction to infrared and Raman spectroscopy*, Academic Press, San Diego (1990).

71. Y. Nishimura, A.Y. Mirakawa, and M. Tsuboi, *Resonance Raman studies of nucleic acids*, Advances in Infrared and Raman Spectroscopy **5**, 217-275 (1978).

72. M.C. Tobin, *Laser Raman spectroscopy*, Wiley, New York (1971).

73. Schrader, *Chemische anwendungen der Raman-spectroscopie*, Angewandte Chemie **85**, 925-950 (1973).

74. F.R. Dollish, W.G. Fateley, and F.F. Bentley, *Characteristic Raman frequencies of organic compounds*, Wiley, New York (1974).

75. B. Schraeder, *Raman / infrared atlas of organic compounds,* VCH Verlagsgesellschaft, Weinheim (1989).

76. D.L. Pavia, G.M. Lampman, and G.S. Kriz Jr., *Introduction to spectroscopy*, Saunders Golden Sunburst Series, Philadelphia (1979).

77. J.E. Stewart, *Infrared spectroscopy*, Marcel Dekker, New York (1970).

78. S.F. Johnston, *Fourier transform infrared*, Ellis Horwood, New York (1991).

79. R. Fairman, *Raman spectroscopic studies of different forms of cholesterol and its derivatives in the crystalline state*, Chemistry and Physics of Lipds **18**, 84-104 (1977).

80. *Handbook of near-infrared analysis*, D.A. Burnes and E.W. Ciurczck (eds.), Marcel Dekker, New York (1992).

81. J. Wang, M.G. Sowa, M.K. Ahmed, and H.H. Mantasch, *Photoacoustic near-infrared investigation of homo-polypeptides*, Journal of Physical Chemistry **98**, 4748-4755 (1994).